104 pages

FINAL REPORT

CORRELATION OF TRANSONIC-CONE PRESTON-TUBE DATA AND SKIN FRICTION

(RESEARCH GRANT NUMBER NAG 2-76)

(Nov. 80 - May 84)

Principal Investigator

T. D. Reed

Prepared by

A. S. Abu-Mostafa and T. D. Reed

May 1984

School of Mechanical and Aerospace Engineering
Oklahoma State University
Stillwater, Oklahoma 74078

The NASA Technical Officer for this Grant is:

F. W. Steinle, Jr.
Experimental Investigators Branch, 227-5
NASA Ames Research Center
Moffett Field, California 94035

ABSTRACT

Preston-tube measurements obtained on the Arnold Engineering Development Center (AEDC) Transition Cone have been correlated with theoretical skin friction coefficient in transitional and turbulent flow. This has been done for the NASA Ames 11-Ft Transonic Wind Tunnel (11 TWT) and flight tests. During analyses of the data, errors were discovered in the Preston-tube measurements. The errors in the 11 TWT data are minor and were easily corrected. The errors in the flight data, however, are much larger and random. The source(s) of these errors are unknown. We suspect they are due, at least in part, to twisting of the probe during a traverse. A procedure has been developed to correct for these errors and has been successfully applied to the flight data.

The developed semi-empirical correlations of Preston-tube data have been used to derive a calibration procedure for the 11 TWT flow quality. This procedure has been applied to the corrected laminar data, and an effective freestream unit Reynolds number is defined by requiring a matching of the average Preston-tube pressure in flight and in the tunnel. In contrast to previous studies of the effect of tunnel noise on boundary layer transition, this study finds that the operating Reynolds number is below the effective value required for a match in laminar Preston-tube data. The distribution of this effective Reynolds number with Mach number correlates well with freestream noise level in this tunnel. Analyses of transitional and turbulent data, however, did not result in effective Reynolds numbers that can be correlated with background noise. This is a result of the fact that vorticity fluctuations present in transitional and turbulent boundary layers dominate Preston-tube pressure fluctuations and, therefore, mask the tunnel noise effects. So, in order to calibrate the effects of noise on transonic wind

tunnel tests only laminar data should be used, preferably at flow conditions similar to those in flight tests. To calibrate the effects of transonic wind-tunnel noise on drag measurements, however, the Preston-tube data must be supplemented with direct measurements of skin friction. Such data could be used in the subject procedure to define an equivalent flight unit Reynolds number for a given tunnel setting which would result in a matching of the average, laminar skin friction.

ACKNOWLEDGMENTS

The authors gratefully acknowledge the support of this work by the NASA Ames Research Center via Research grant No. NAG 2-76.

Thanks are due to Mr. E. Hardy for the illustrations and Mrs. N. Lock for typing services.

TABLE OF CONTENTS

LIST OF FIGURES

LIST OF TABLES

NOMENCLATURE

A^+	Effective sublayer thickness, Eqn. (43)
A, B, C	General correlation coefficients, Eqn. (23)
A_1, B_1, D_1	Correlation coefficients for flight data, Eqn. (25a)
A_2, B_2, D_2	Correlation coefficients for wind tunnel data, Eqn. (25b)
C	Constant of Eqn. (52)
C_f	Skin friction coefficient, $\tau_w/(\frac{1}{2}\rho_e u_e^2)$
$\bar{C}_f$	$= (C_{f,fit} - C_{f,\ theoretical})/C_{f,theoretical}$
$\bar{C}_{f,rms}$	R.M.S. error in $\bar{C}_f$
$C_{p,rms}$	R.M.S. fluctuating freestream pressure coefficient, $(\overline{p'^2}/q_\infty)^{0.5}$
D	Pipe internal diameter, or van Driest damping coefficient
d	Outer Diameter of circular Preston tube
F	Function defined in Eqn. (27)
h	Preston-tube height
K_{eff}	Normalized, effective Preston-tube height, $2\ y_{eff}/h$
L	Characteristic length of a pipe, or cone length
M	Mach number
P	Static pressure
P'	Fluctuating freestream pressure
P_p	Preston-tube pressure
q_∞	Freestream dynamic pressure, $\frac{1}{2}\rho_\infty U_\infty^2$
R	Gas constant, $= 0.2234 \times 10^6$ J/Kg ^oK for air
Re_D	Reynolds number based on pipe internal diameter
Re_m	Freestream unit Reynolds number, U_∞/ν_∞
$Re_{m,eff}$	Effective freestream unit Reynolds number
Re_x	Length Reynolds number, $U_e x/\nu_e$

Re_θ	Momentum-thickness Reynolds number, $U_e\theta/\nu_e$
R_τ	$= U_\tau h/\nu_w$
S	Compressibility factor, $(\rho_e/\rho')^{.5}$
T	Static temperature
T_o	Total temperature
TF	Turbulence factor, $Re_{m,eff}/Re_m$
U_e	Velocity at edge of boundary layer
U_p	Velocity at Y_{eff}
U^+	$= U/U_\tau$
U_τ	Shear velocity, $(\tau_w/\rho_w)^{0.5}$
w	External width of Preston-tube face
x	Local surface distance from cone apex
x*	Dimensionless parameter, $\log_{10}\left(\frac{U_p Y_{eff}}{\nu_w}\right)^2$
x_1^*	Dimensionless parameter, Eqn. (6a)
x_2^*	Dimensionless parameter, Eqn. (15a)
Y	Distance normal to cone surface
Y^+	$= Y U_\tau/\nu_w$
Y_{eff}	Effective Preston-tube height
y*	Dimensionless parameter, $\log_{10}\left(\frac{\tau_w Y_{eff}^2}{\rho_w \nu_w^2}\right)$
y_1^*	Dimensionless parameter, Eqn. (6b)
y_2^*	Dimensionless parameter, Eqn. (15a)

Greek Letters:

α	Angle of attack
β	Angle of yaw
γ	Dhawan-Narasimha's intermittency function, Eqn. (19), or ratio of specific heats (= 1.4 for air)
δ	Boundary layer thickness

ΔP_p	Pressure increment used to correct experimental data
ΔR_{eff}	$= (Re_{m,eff} - Re_m)/Re_m$
Δx	Location of virtual origin of turbulent boundary layer
ε	Turbulent eddy diffusivity
θ	Momentum thickness
κ	Von Karman's constant, = 0.41
λ	Dhawan-Narasimha's fit factor, Eqn. (21)
μ	Molecular viscosity
ν	Kinematic viscosity
ρ	Density
ξ	$= (x - x_B)/\lambda$
τ	Shear stress

Subscripts:

B	Beginning of boundary layer transition
E	End of boundary layer transition
e	At the outer edge of the boundary layer
eff	At the effective Preston-tube height
FD	Flight Data
g	At the geometric center of the probe
i	At the edge of Couette-flow region
ℓ	Fully laminar flow
P	Associated with the Preston-tube measurement
ref	At the reference point used for transition calculations
T	Position of maximum transitional Preston-tube pressure, or denotes fully turbulent flow properties
t	Position of minimum Preston-tube pressure near beginning of transition

v	Measured from the virtual origin of turbulent boundary layer
WT	Wind-tunnel data
w	At the wall (cone surface)
o	Total property
∞	Freestream property

Superscripts:

$\overline{\quad}$	At Summer and Short's average temperature, Eqn. (16)

CHAPTER I

DEFINITION OF THE PROBLEM

Since the transonic wind tunnel became operational at NASA Langley in the late 1940's, there has been a need for a procedure to calibrate the effects of wall-generated noise on the tunnel flow quality. As noted by Dougherty and Steinle (1), the primary indicators of flow quality in a wind tunnel are variations of: (1) Mach number, (2) flow angularity within the empty test section, and (3) the Reynolds number at which transition from laminar to turbulent flow occurs on models. Variations in Mach number and flow angularity can be calibrated with conventional Pitot-static probes and yaw meters, e.g. see Reed, et al. (2) And in the case of low-speed wind tunnels, the Reynolds number at which the drag coefficient of a sphere equals 0.30 can be used to define a turbulence factor (TF), as described by Pope and Harper (3). An "effective" unit Reynolds number for a given low-speed tunnel can then be defined by

$$Re_{m,eff} = (TF)\, Re_m$$

However, when Mach number exceeds about 0.35, compressibility effects cause the classical turbulence factor to become increasingly erroneous and therefore not useful. Recently, Miller and Bailey (4) have reviewed the status of knowledge concerning the drag of a sphere at transonic speeds. Even today, the precise variation of sphere drag with Mach number and Reynolds number is not well defined. Thus, the classical turbulence-sphere method is not applicable to the calibration of transonic wind tunnels.

In recognition of the non-applicability of a sphere for defining a turbulence factor for tests in transonic wind tunnels, NASA, as part of the C-5A wind tunnel correlation program (Treon, et al.(5)) employed what is now known as the AEDC 10^{0} Transition Cone as a means of defining an adjustment to Reynolds numbers on a tunnel-to-tunnel basis. The cone was initially developed in the mid-sixties by engineers at Arnold Engineering Development Center (AEDC). It has a traversing Pitot probe resting on its surface to directly detect boundary-layer transition.† The cone geometry has the advantage that no shock is generated along the surface at transonic speeds, and thereby avoids shock/boundary-layer interactions such as occur on airfoils, wings and blunt-nose bodies. A schematic of this cone and some of the associated instrumentation are shown in Fig. 1. Since the cone was designed to calibrate the effects of tunnel noise on boundary-layer transition, it also has two miniature microphones imbedded in the surface at 45.7 and 66 cm aft of the nose for noise measurements. Additional description of this cone can be found in the papers by Dougherty and Steinle (1) and Dougherty and Fisher (7).

The need for such a calibration device was emphasized when discrepancies between numerous transonic wind-tunnel tests of models at ostensibly identical flow conditions were observed. A particularly well-documented study of differences in static aerodynamic data has been obtained with the same model of a Lockheed C-5A transport aircraft in three major transonic wind tunnels. The results have been reported by Treon, et al. (5) The differences between the three different sets of wind-tunnel data were reduced by accounting for

---

† This, of course, is not a new measurement technique. In fact, the first Wright brothers' lecture by Jones (6) in 1937 describes the utility of this technique for flight tests.

NOTE: CS = Cone Station = Distance in inches aft of the nose

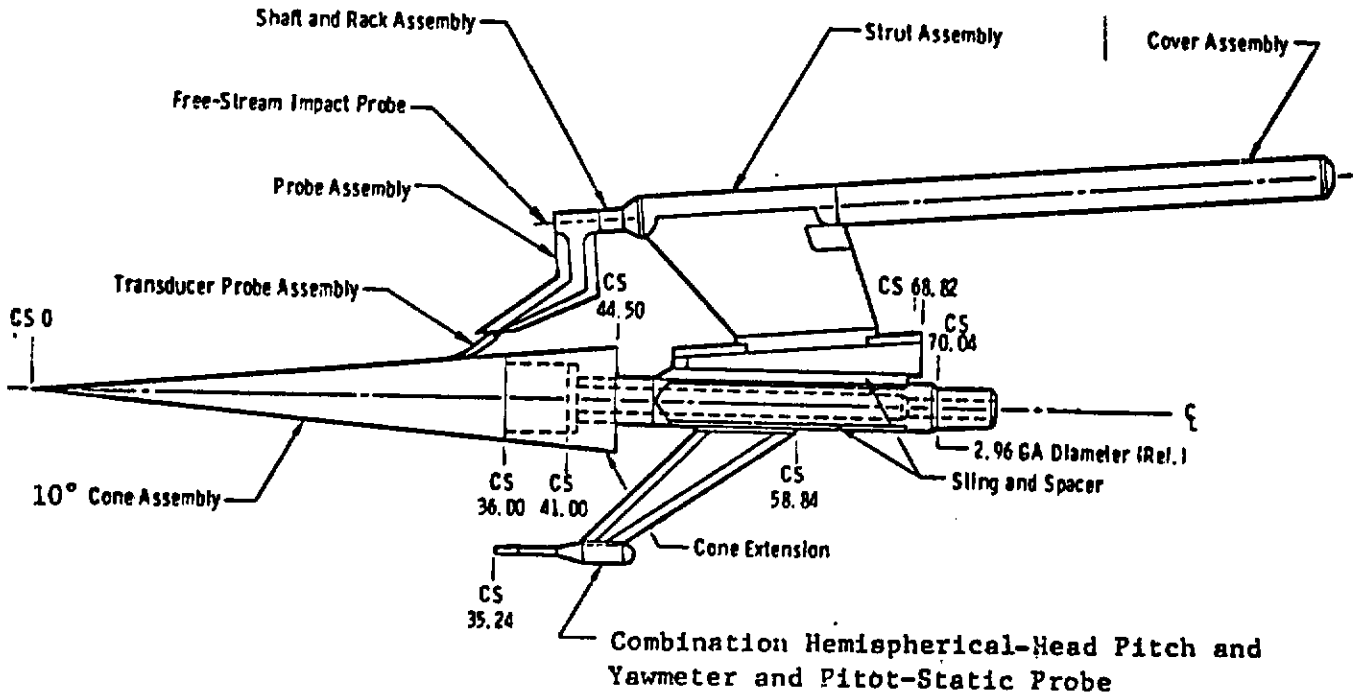

Figure 1. AEDC Boundary Layer Transition Cone

"relative" Reynolds number effects between facilities. The AEDC Transition Cone was used to define the differences in "relative" Reynolds number.

As observed by Dougherty and Steinle (2): "These results substantiated the need for developing a method for predicting these corrections to Reynolds number to improve extrapolation of wind-tunnel test results to full-scale conditions, i.e., a "turbulence factor for transonic tunnels."

Subsequent to the C-5A correlation program, the cone was tested in transonic wind tunnels both in the U.S. and in Europe. At the completion of the wind tunnel tour, the cone was tested in flight, Dougherty and Fisher (6). Parallel with the planning of the flight program, NASA focused on using the data from the cone in flight, in conjunction with the wind tunnel data, to develop a means for defining an adjustment (transonic turbulence factor) to Reynolds number on a tunnel-to-flight basis.

Such a Reynolds number will calibrate noise effects on the onset of transition, so that by increasing the flight Reynolds number to that value, transition will occur at the same location as in the tunnel. However, matching of transition onset is not sufficient practical use, since other useful parameters like Preston-tube pressure and skin friction measurements are not necessarily matched by that procedure.

The objective of this work, on the other hand, is to infer skin friction along the AEDC cone using the Preston-tube impact pressure measurements in both wind-tunnel and flight tests and, in analogy with the turbulence sphere method, define a procedure whereby an "effective" freestream unit Reynolds number can be calculated for a given tunnel setting, but this number now represents the freestream unit Reynolds number at which the model tested in the tunnel will experience the same average, theoretical skin friction as in flight, or, equivalently, will give the same measured values of average

Preston-tube pressure.

The importance of this work lies not only in the calibration of wind tunnel flow quality, but also in the general and systematic way of relating wind-tunnel flow conditions to actual flight. Thus, the prediction of flight level drag will be improved and the results obtained from wind tunnel tests can be directly applied towards the design and development of prototypes.

The basic approach used in this study to achieve the above-mentioned objective is as follows:

1. Preston-tube measurements are correlated with theoretical skin friction along the surface of the AEDC Cone in laminar, transitional and turbulent portions of the boundary-layer flow. This is done for the wind tunnel tests as well as the flight tests.

2. With the two sets of correlations (one set of three correlations for the wind tunnel tests, and a second set for the flight tests), the skin friction coefficient is equated as well as all other variables and parameters, except the freestream unit Reynolds number, Re_m. The two sets of correlations are expected to have different empirical coefficients since noise and freestream turbulence effects, which are not modeled in the theoretical computations, are different. This means that substituting wind tunnel data, which includes C_f but excludes Re_m, into the flight correlation results in a freestream unit Reynolds number that is different from the measured one in the tunnel. This derived Reynolds number is therefore the noise-free "effective" Reynolds number the tunnel should operate at to get the same P_p measurements as in flight.

3. Since correlations for the laminar portion of the boundary layer are expected to be different from those in the transitional and turbulent portions, the resulting $Re_{m,eff}$'s may be different in general for each

portion. Analysis of these results should reveal the best measure of tunnel flow quality.

An earlier report by the authors (8) presented the results obtained from the analysis of laminar data. The adjustments to freestream unit Reynolds numbers, ΔR_{eff}, were found to range between 3.0 and 6.5%. The findings of that report are summarized at the beginning of Chapter IV. The present report focuses on the analysis of transitional and turbulent data.

CHAPTER II

SURVEY OF RELATED LITERATURE

Since Preston-tube pressures are by definition total pressures near the wall, the classical law-of-the-wall can be used to relate these pressures with wall shear stress. The law-of-the-wall can be expressed in the following general form:

$$U^+ = F_1 (Y^+). \tag{1}$$

Using the definitions of U^+ and Y^+, Eqn. (1) can be written as

$$\frac{U}{U_\tau} = F_1 \left(\frac{U_\tau Y}{\nu_w} \right), \tag{2}$$

where U is the velocity parallel to the wall at the normal distance Y. Associated with the Preston-tube measurement of total pressure, P_p, is a velocity, U_p, at a height Y_{eff}. In other words, there exists a streamline entering the probe face, Y_{eff} units above the wall, at which the theoretical total pressure in the undisturbed boundary layer flow equals the total pressure measured by the probe, P_p, Fig. 2. This "effective" probe center or height concept was introduced by Preston (9) in 1953. The corresponding theoretical velocity at this height is denoted by U_p.

Thus, at the effective height, Eqn. (2) is written as follows

$$\frac{U_p}{U_\tau} = F_1 \left(\frac{U_\tau Y_{eff}}{\nu_w} \right) \tag{3}$$

Multiplying both sides by $U_\tau Y_{eff}/\nu_w$ gives

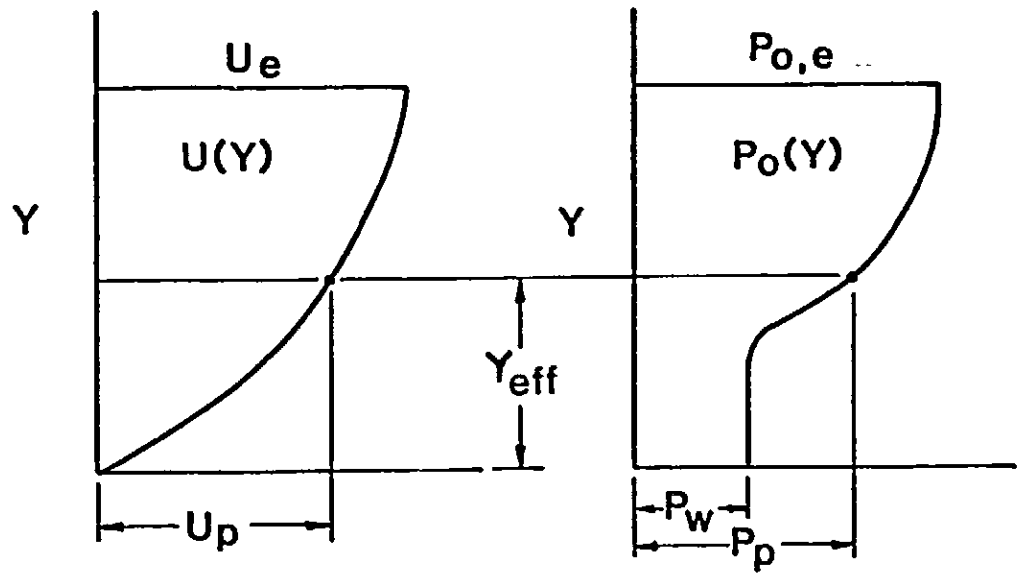

Figure 2. Definition of the Effective Probe Center

$$\frac{U_p Y_{eff}}{\nu_w} = \frac{U_\tau Y_{eff}}{\nu_w} \; F_1 \left(\frac{U_\tau \; Y_{eff}}{\nu_w} \right) = F_2 \left(\frac{U_\tau \; Y_{eff}}{\nu_w} \right),$$

or, alternatively,

$$\frac{U_\tau Y_{eff}}{\nu_w} = F_3 \left(\frac{U_p \; Y_{eff}}{\nu_w} \right). \qquad (4)$$

Eqn. (4) is the general form of the correlation between Preston-tube measurements and skin friction.

Incompressible-Flow Correlations

According to Preston (9), the British engineers Stephens and Haslam (10) suggested in 1938 that it should be possible to use the data from a Pitot tube traversed along a surface to infer skin friction. Apparently, this idea was not pursued until Preston's work during the early 1950's. He developed a correlation between skin friction and the total pressure as measured with circular Pitot tubes resting on the inside wall of a pipe. In order to develop his correlation, Preston used a simplified version of Eqn. (4) by making two assumptions:

1. The flow is incompressible and Bernoulli's equation is valid, thus U_p can be easily related to P_p as follows:

$$P_p = P_w + \frac{1}{2} \rho_w U_p^2 .$$

2. The effective center of the circular tube is fixed and coincides with its geometric center, i.e. $Y_{eff} = d/2$.

These two assumptions lead to the following relation.

$$\frac{\tau_w d^2}{4 \rho_w \nu_w^2} = F \left[\frac{(P_p - P_w) d^2}{4 \rho_w \nu_w^2} \right] \tag{5}$$

Using Eqn. (5) as a guide, Preston obtained measurements inside a pipe flow with circular Pitot tubes having four different external diameters but a nearly constant ratio of internal to external diameter of 0.6. Pipe Reynolds number was varied over the range $10^4 < Re_D < 10^5$. Skin friction was determined via measurements of pressure drop over a known length of constant diameter pipe, viz., $\tau_w = (P_1 - P_2)D/4L$. An empirical fit of the data led to the following correlation.

$$y_1^* = - 1.396 + 0.875\, x_1^* \tag{6}$$

Where the variables are defined as

$$x_1^* = \log_{10} \left[\frac{(P_p - P_w) d^2}{4 \rho \nu^2} \right], \tag{6a}$$

$$y_1^* = \log_{10} \left[\frac{\tau_w d^2}{4 \rho \nu^2} \right]. \tag{6b}$$

In 1964, Patel (11) published the results of an extensive set of tests with fourteen circular Pitot probes and three different pipe diameters. He obtained a more accurate calibration for Preston tubes and established limits on the pressure gradient conditions within which his calibration can be used with prescribed accuracy. Patel obtained empirical equations for $y_1^* = f(x_1^*)$ over three regions of y_1^*. These regions correspond to the fully-turbulent, the buffer or transition zone, and the viscous-sublayer regions of the classical law-of-the-wall. The normal Reynolds number range of Preston-tube

measurements in incompressible flow correspond to the buffer zone, and for this region Patel obtained

$$y_1^* = 0.8287 - 0.1381x_1^* + 0.1437(x_1^*)^2 - 0.0060(x_1^*)^3, \quad (7)$$

where $1.5 < y_1^* < 3.5$ or $5.6 < U_\tau d/\nu_w < 55$. Patel reported this correlates his data to within $\pm$ 1.5% of τ_w.

In the viscous sublayer region, Patel found his data were correlated by

$$y_1^* = 0.5\ x_1^* + 0.037, \quad (8)$$

when $y_1^* < 1.5$ or $U_\tau\ d/\nu_w < 5.6$. In this near-wall region, the classical law-of-the-wall exhibits the linear relation

$$U^+ = Y^+. \quad (9)$$

In order to relate (8), (9), Patel introduced K_{eff} as the normalized effective center of a round Pitot tube defined by

$$K_{eff} = 2\ Y_{eff}/d\ . \quad (10)$$

Substituting into (9) and using the definitions of x_1^* and y_1^* result in the following equation.

$$y_1^* = 0.5x_1^* - 0.5\ \log_{10}\ (0.5\ K_{eff}^2) \quad (11)$$

When this equation is equated with Eqn. (8) and solved for K_{eff}, the result is $K_{eff} = 1.3$.

The traversing Pitot probes, used during wind-tunnel tests with the AEDC transition Cone, are of the flattened or oval-shaped type. Since Patel's correlations are for circular Preston tubes, they cannot be applied directly to the AEDC Cone tests. In addition, these tests were conducted at transonic speeds, and compressibility effects are expected. With regard to the flattened Preston tubes, Quarmby and Das (12) conducted an experimental study and calibration of six oval-shaped Preston tubes. When $x_1^* > 4.6$, they found these probes gave exactly the same calibration relation between y_1^* and x_1^* as was obtained by Patel (Eqn. 7) if the external height of the probe face is used in place of d. At lower values of x_1^*, the negative displacement of effective center caused by wall proximity was larger ($\simeq$ 5%) for the flattened probes with aspect ratios between 1.5 and 1.9.† The following calibration equation correlated the measurements of Quarmby and Das within 1.5% of τ_w.

$$y_1^* = 0.5152 + 0.1693x_1^* + 0.0651(x_1^*)^2, \quad 3.38 < x_1^* < 6 . \tag{12}$$

The two correlations, Eqns. (11) and (12) make the assumption that the effective center of the probe is fixed. Preston showed that it is a function of $U_\tau d/\nu_w$ but did not attempt to define this function.

McMillan (13) pursued this point and found for circular tubes that the displacement of the effective center is 0.15d (K_{eff} = 1.3) when the probe is more than two diameters away from the wall and is affected by shear flow alone. As the probe gets closer to the wall, K_{eff} decreases. McMillan confirmed, therefore, that K_{eff} is a function of $U_\tau h/\nu_w$. One can understand

† This is consistent with the idea that flow about the face becomes more two-dimensional as aspect ratio increases and more of the flow passes up and over the face rather than around the sides.

this wall proximity effect by considering that a greater portion of the flow, blocked by the probe, will have to lift upward and move over and around the probe face as less passes underneath between the probe and the wall. McMillan proposed a single curve, independent of Reynolds number, to correct for wall proximity effects on the measured velocity.

The work done by Patel (11), McMillan (13) and Quarmby and Das (12) leads to the conclusion that, in general, K_{eff} is a function of $U_\tau h/\nu_w$, Y_g/h and w/h (aspect ratio). Since we are talking about a Pitot tube resting on the wall, $Y_g/h = 0.5$, and since the same probe is used in all the tests, w/h is constant. Therefore, the relation

$$K_{eff} = \text{Fn.} \left(\frac{U_\tau h}{\nu_w} \right) \tag{13}$$

seems to describe the actual variation in K_{eff} for incompressible-flow conditions. If this relation is incorporated in Eqn. (4), it can be shown that K_{eff} can be eliminated while Eqn. (4) remains in the same form. This explains why the assumption of fixed effective probe height has worked well for incompressible-flow correlations.

For compressible-flow correlations, however, Eqn. (13) is expected to be different. It will perhaps have the form

$$K_{eff} = \text{Fn.} \left(\frac{U_\tau h}{\nu_w}, M_\infty \right). \tag{14}$$

In this case, any attempt to neglect the variation of K_{eff} must show up in a greater scatter of data about the developed correlation.

Compressible-Flow Correlations

Allen (14) has performed a comprehensive analysis of Preston tubes in supersonic boundary layers. He developed a correlation using three independent sets of simultaneous measurements of Preston-tube pressures and skin friction via floating-element force balance. These data were obtained within flat-plate, turbulent boundary layers and with freestream Mach numbers in the range: $1.6 < M_\infty < 4.6$. Allen selected the same basic parameters as Patel; except, he chose to evaluate the fluid properties at a reference temperature developed by Sommer and Short (15), and the velocity U_p was calculated from P_p and the wall pressure P_w ($=P_e$) using standard compressible flow relations.†

$$x_2^* = \log_{10}\left(\frac{U_p\, d}{\nu'}\right)$$
$$y_2^* = \log_{10}\left(\sqrt{2}\,\frac{U_\tau\, d}{\nu'}\right) \qquad (15a)$$

The primes denote properties evaluated at the Sommer and Short reference temperature, viz.,

$$\frac{T'}{T_e} = 0.55 + 0.035\, M_e^2 + 0.45\,\frac{T_w}{T_e}\,. \qquad (16)$$

The correlation derived by Allen is

$$y_2^* = -0.4723 + 0.74814\, x_2^* + 0.01239\,(x_2^*)^2\,. \qquad (17)$$

† The details can be found in a report by Allen (16).

Allen found that the majority of the skin-friction-coefficient data were within +15% to -12% of Eqn. (17). This rather large scatter, compared to the incompressible pipe-flow calibrations of Patel and Quarmby and Das, is at least partly associated with the much greater sensitivity and vulnerability of floating-element balances to extraneous errors.†

Obviously, the parameters used by Allen are logical candidates in any attempt to correlate the transonic cone data. However, the basic purpose of a reference temperature is to permit use of skin-friction formulas for incompressible flow to estimate compressible skin friction by evaluating fluid properties at the reference temperature. Thus, the resulting reference properties represent "average" values across a boundary layer. Whereas, small Preston tubes encounter only the flow near the wall. Therefore, it appeared to the authors that properties based simply on the wall temperature would be more appropriate.

Laminar Preston-Tube Correlations

A survey of the literature uncovered only one paper, published by Prozorov (19) which addresses the problem of using Preston-tube measurements to deduce skin friction in a laminar boundary layer. He obtained surface Pitot-probe measurements within low-speed, flat-plate, laminar boundary layers. He used several circular and rectangular probes with different aspect ratios. Though his data exhibited considerable scatter, he concluded that K_{eff} is a function of $U_p d/\nu_w$ for both laminar and turbulent portions of the

---

† Allen (17) discussed the various error sources in floating-element balances. He has recently suggested an improved design for this type of instrumentation, Allen (18).

boundary layer irrespective of the aspect ratio, which is inconsistent with the results of McMillan (13) and Quarmby and Das (12). He also found $\tau_w d^2/\rho_w \nu_w^2$ (the square of $U_\tau d/\nu_w$) to be a different function of $U_p d/\nu_w$ compared to what Preston (9) found.

His deduction of the laminar correlation is based on a McLaurin series expansion of U_p near the wall (since the probe height was small relative to the boundary layer thickness) and the conservation equations of mass and momentum for steady, two-dimensional, incompressible flow. The result is the following equation.

$$\tau_w = \frac{\mu_w U_p}{Y_{eff}} - \frac{1}{2}\frac{dP_e}{dx} Y_{eff} \qquad (18)$$

Prozorov's correlation takes into account the pressure gradient. The theoretical calculations of inviscid static-pressure distribution by Wu and Lock (20) for the wind tunnel cases, and the measurements of surface pressures in the flight tests show that the pressure gradient in this study is negligible. Prozorov claims that his correlation is valid in laminar, transitional and turbulent flows provided that the probe is always within the viscous sublayer; a condition which was found to be invalid in this study.

It can be shown that Prozorov's correlation is equivalent to the calibration model used in this study when $dP_e/dx = 0$ and K_{eff} is small.

Boundary-Layer Transition Computation

Dhawan and Narasimha (21) developed a method of calculating the properties of a boundary layer undergoing transition by preserving the essential intermittency of the flow. Narasimha (22) modified Emmons's (23) original function to obtain an intermittency function described by

$$\gamma(x) = 1 - e^{-A\xi^2(x)}, \quad A = 0.41 , \tag{19}$$

where

$$\xi(x) = \frac{x - x_B}{\lambda} . \tag{20}$$

Here x_B is the transition point defined as the location where the Pitot-tube measurements depart from the laminar ones and λ is defined by

$$\lambda = x_{\gamma=.75} - x_{\gamma=.25} . \tag{21}$$

By comparison with numerous other data, including supersonic data, Eqn. (19) was shown to be a good approximation to a universal intermittency function for boundary layer transition. Therefore, this function is adopted in this study to model boundary layer transition, and its use is as will be described in detail in Chapter IV. Fig. 3 illustrates a typical γ distribution and how it changes with λ.

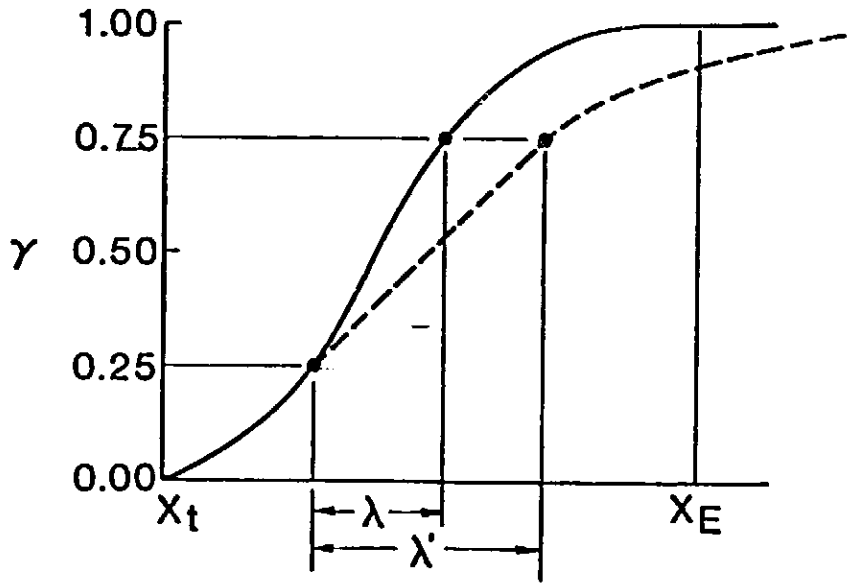

Figure 3. Distribution of γ-Intermittency Function

Calibration of Wind-Tunnel Flow Quality

With the establishment of the fact that freestream disturbances can significantly affect transonic wind-tunnel data, an extensive test program was begun at the NASA Ames research center in 1971. The AEDC Cone was tested in twenty-three tunnels between 1971 and 1977. Finally in 1978, it was flight-tested on the nose of a McDonnel-Douglas F-15 aircraft. A summary of the resulting noise and transition data has been reported by Dougherty and Fisher (7). In this concluding report, Dougherty and Fisher found, for the range of $C_{p,rms}$ observed, that the data for transition Reynolds number, based on the product of local unit Reynolds number and distance from the nose to end-of transition , x_T[†], appear to correlate with $C_{p,rms}$ by the following equation.

$$Re_T \sim (C_{p,rms})^{-.25} \tag{22}$$

This relation, with the value of the proportionality constant suggested by Whitfield and Dougherty (24), is compared in Fig. 4 with some transition data obtained with the AEDC Cone in seven different tunnels (Dougherty and Steinle (1) and Mabey (25)) and a flight test at $M_\infty = 0.80$.

The Dougherty-Fisher correlation indicates that the end-of-transition location, x_T, is decreased by either increasing the tunnel noise or increasing the freestream unit Reynolds number. In order words, the effects of noise and Re_m on x_T are equivalent. However, their effects on measurements of C_f or P_p are not equivalent. Becker and Brown (26) have discussed the effects of turbulence on time-averaged pressures measured with Pitot probes. Since

---

† As will be shown in this study, the end-of-transition location is actually different from x_T, the location of maximum P_p in transition.

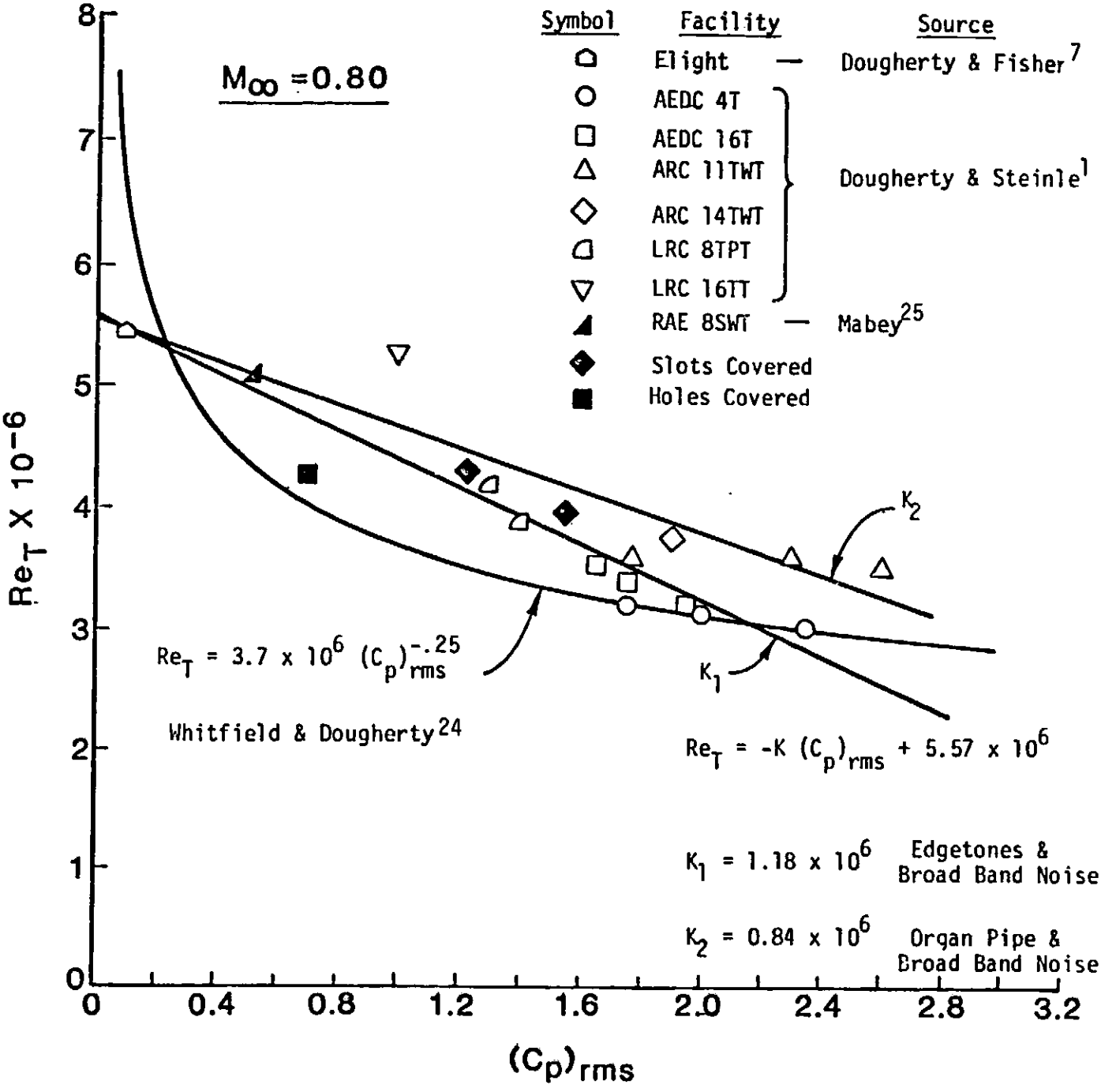

Figure 4. Effect of Noise on Boundary Layer Transition.

turbulence causes fluctuations in the direction of the flow with respect to the probe's axis, the time-averaged pressure is reduced below the true total pressure.† Similarly, we have found that the tunnel noise, in the case of laminar boundary layers, also causes P_p fluctuations and reduces P_p measurements. This is equivalent to decreasing Re_m. It is important to distinguish between the effects of noise on x_T (which is the purpose of Dougherty, Steinle and Fisher's work) and noise effects on theoretical C_f, or measured P_p (which is the purpose of this work). The two effects are actually opposite, Fig. 5.

† This effect decreases as a wall is approached, since turbulence is damped at an impermeable wall.

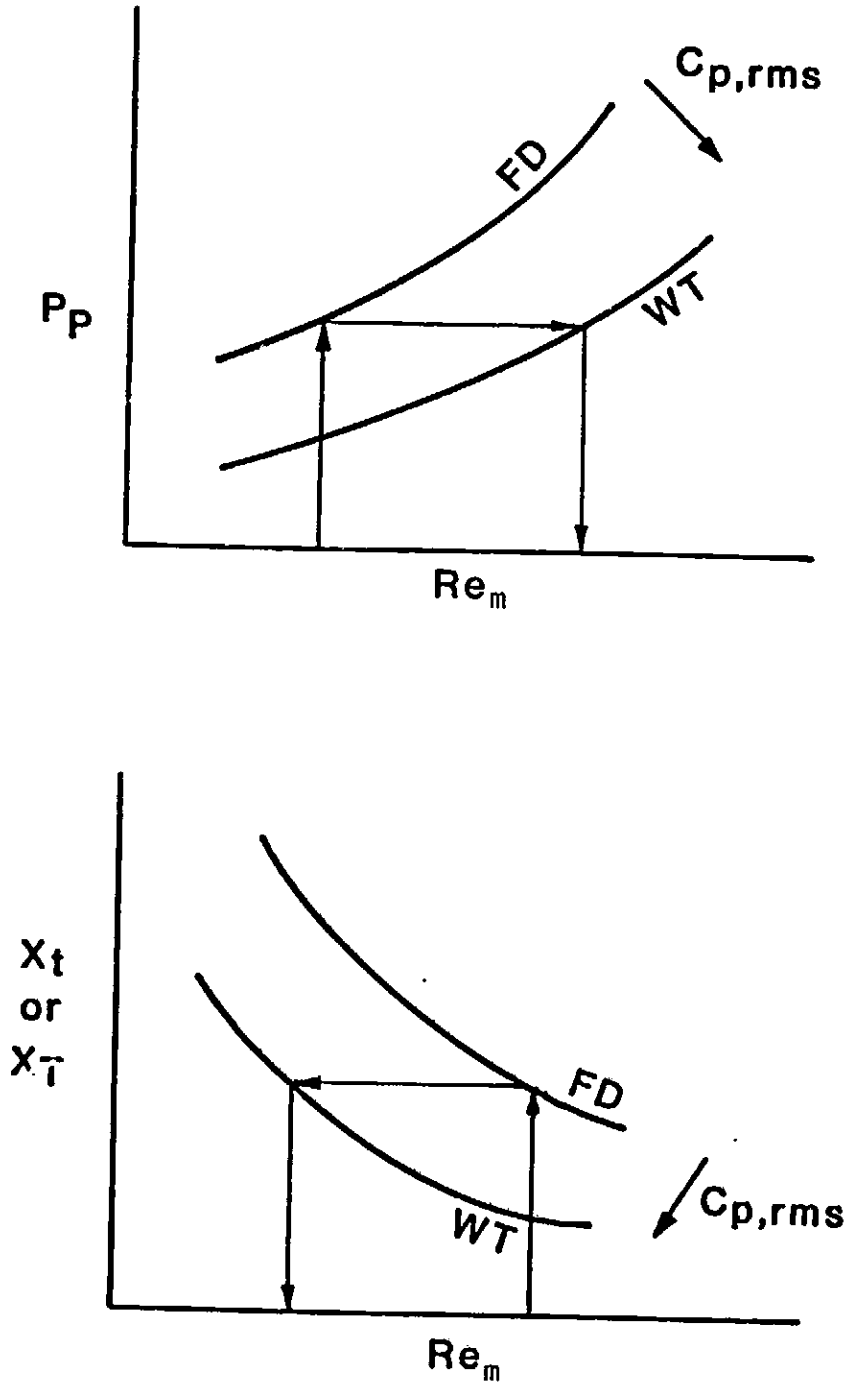

Figure 5. Effect of Tunnel Noise on Preston-Tube Measurements and Transition Onset

CHAPTER III

ANALYSIS PROCEDURE

Experimental Data

Although the AEDC Cone was tested in twenty-three different tunnels, only the data from the NASA Ames 11-Ft Transonic Wind Tunnel (27), 11-TWT for brevity, was considered for analysis in this study to develop subsonic wind-tunnel correlations. Table I lists nineteen subsonic wind-tunnel tests, and Table II lists nine subsonic flight tests which were selected for analysis in this study. The criteria for choosing a case for analysis are:

1. The Preston-tube survey covers all three portions of the boundary layer.
2. The flow angles α, β are very small.†
3. The freestream Mach number is less than unity.

The distribution of static pressure along the surface of the sharp cone was measured only in flight. For wind-tunnel analysis, this pressure distribution is assumed to be defined by the inviscid-flow theory of Wu and Lock (20). Wu and Lock's predictions for the pressure coefficient along the surface of a 10-degree cone are shown in Fig. 6 as a function of freestream Mach number. Measurements of pressure coefficients together with linear curve fits from two typical flights are shown in Figs. 7 and 8. With this information and the known freestream conditions, the flow conditions at the outer edge of the boundary layer can be calculated. (For details see Ref. 8).

---

† This criterion is necessary since the boundary-layer code used in this study, STAN-5 (28), was found to be insensitive to changes in α, β. Also, values of $\alpha > 0.5^{\circ}$ and/or $\beta > 0.25^{\circ}$ have been shown to affect the beginning of transition, x_B. Notice that the values tabulated in Table II for α and β have an experimental uncertainty of $\sim \pm 0.25^{\circ}$.

Table I

WIND TUNNEL TEST CASES

RUN NO.	M_∞	$Re_m \times 10^{-6}$	q_∞ (kPa)	α^o	β^o
15.231	0.95	13.1	33.2	-0.05	0.02
19.289	0.8	13.1	29.6	-0.00	-0.02
21.318	0.7	13.1	26.3	-0.01	-0.03
23.346	0.6	13.1	22.8	-0.00	-0.03
29.440	0.3	13.1	11.0	-0.01	-0.03
40.547	0.6	16.4	28.1	0.02	0.02
41.548	0.7	16.4	32.6	0.02	0.02
42.549	0.8	16.4	36.4	0.01	0.02
43.550	0.9	16.4	40.3	0.01	0.02
44.551	0.95	16.4	41.8	0.01	0.02
56.631	0.9	9.8	23.6	0.06	0.01
57.632	0.8	9.8	21.7	0.07	0.01
58.633	0.7	9.8	19.5	0.07	0.02
59.634	0.6	9.8	17.1	0.08	0.01
60.635	0.5	9.8	14.5	0.07	0.01
61.636	0.4	9.8	11.8	0.07	0.01
70.726	0.7	13.1	25.8	0.04	0.02
72.748	0.8	13.1	29.0	0.03	0.02

TABLE II

FLIGHT TEST CASES

FLIGHT NUMBER	M_∞	$Re_m \times 10^{-6}$	q_∞ (kPa)	α^o	β^o
327.0907	0.86	7.2	14.6	-0.03	0.30
327.0918	0.66	7.9	14.3	0.04	0.48
329.1028	0.85	6.9	13.8	-0.16	0.30
329.1036	0.74	7.2	13.3	0.19	0.25
329.1042	0.67	8.2	14.7	-0.05	0.47
332.1020	0.93	9.2	21.6	-0.44	-0.20
333.1351	0.94	9.2	21.9	-0.50	-0.16
333.1354	0.88	9.2	21.0	-0.04	0.30
349.1400	0.75	7.5	13.6	0.17	0.27

Note: α and β are time-averaged during a traverse.

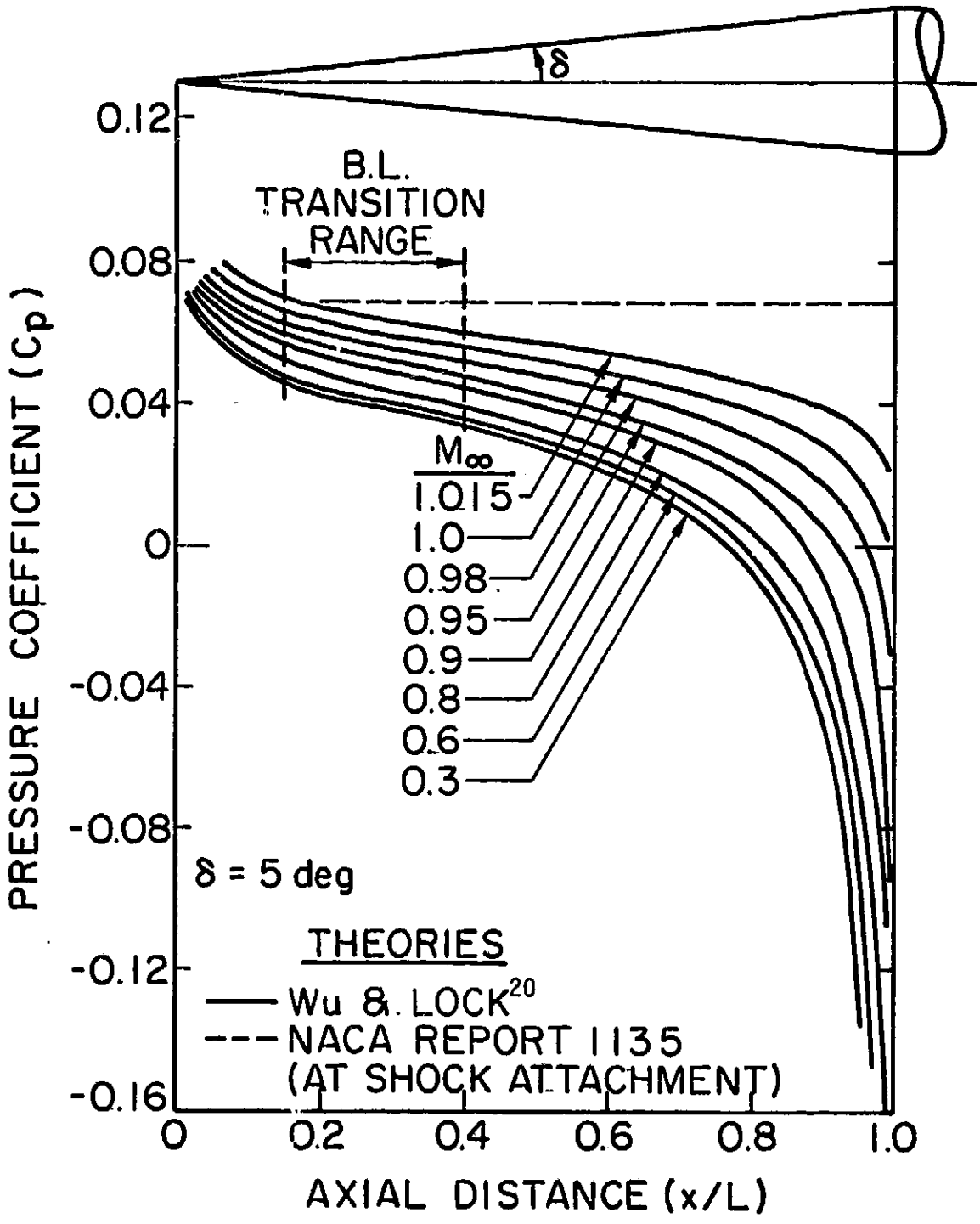

Figure 6. Inviscid Pressure Distribution on a 10^{0} Cone (Wu & Lock).

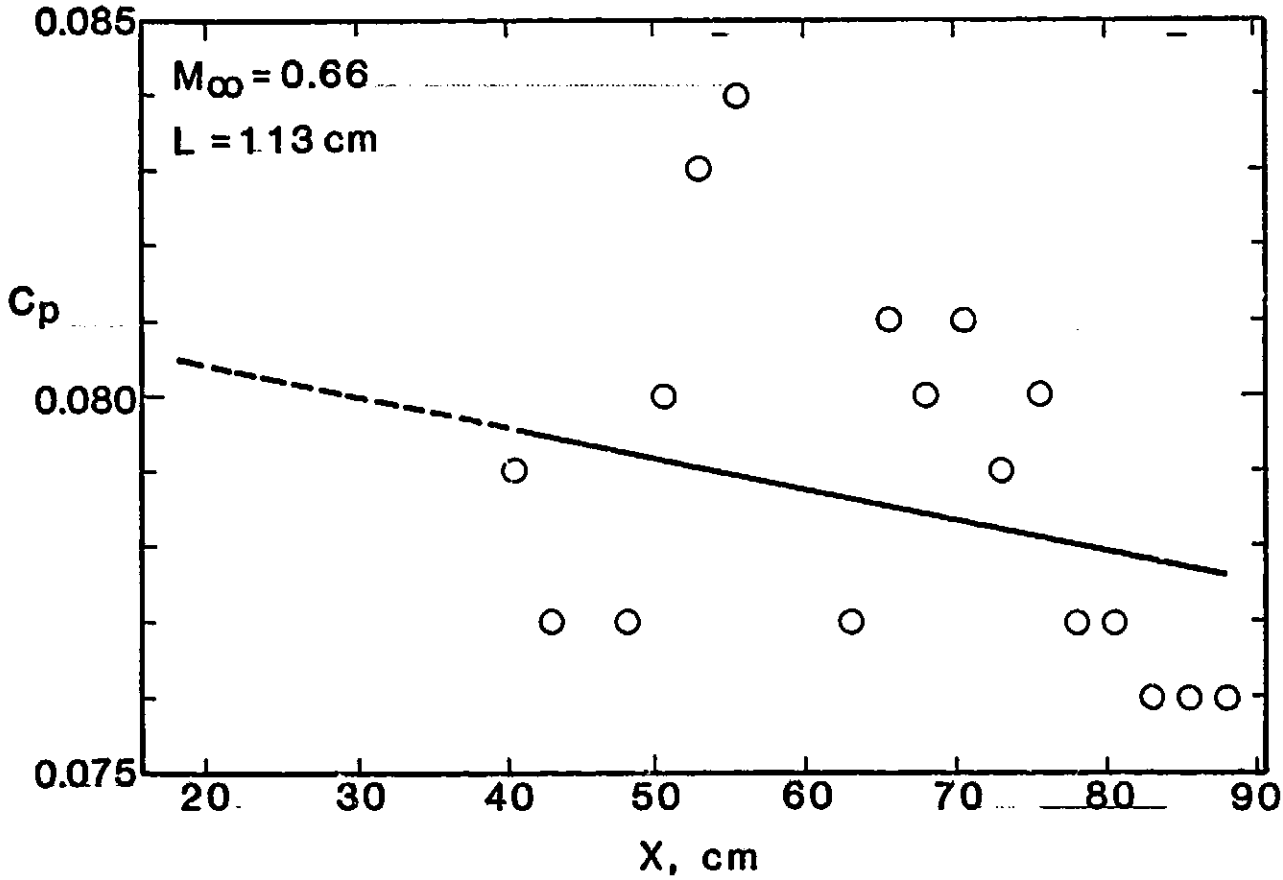

Figure 7. A Favorable Surface Pressure Distribution Measured During Flight.

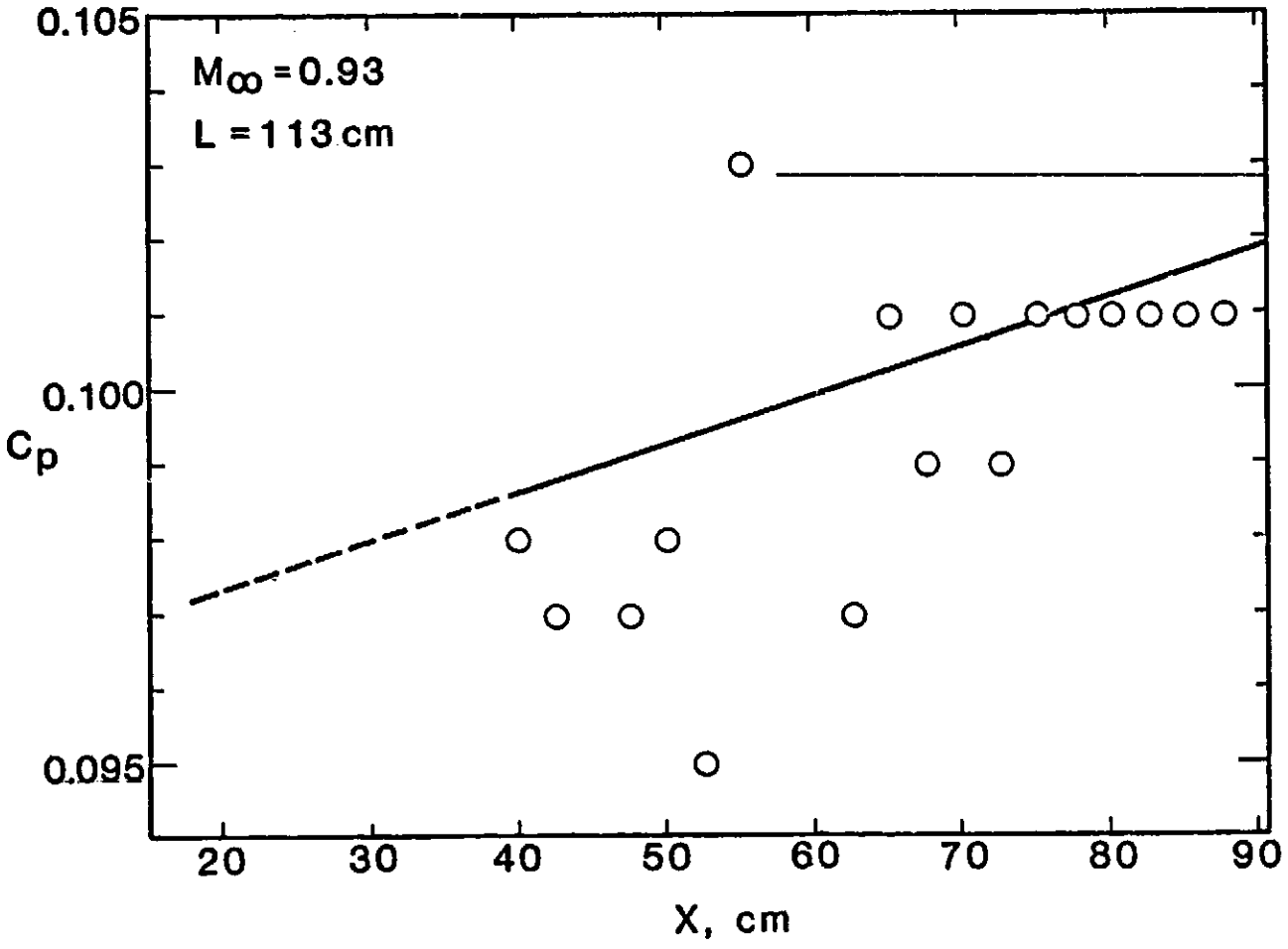

Figure 8. An Adverse Surface Pressure Distribution Measured During Flight.

Correlation of the Data

The fully-laminar and fully-turbulent boundary layer computations are done using a computer program developed by Crawford and Kays (28) which they labeled STAN-5. The resulting distribution of skin friction and boundary layer properties are then correlated with the Preston-tube pressures.

The form of the correlation equation is derived from Eqn. (4) using the parameters of Patel (11) and Quarmby and Das (12) but allowing the effective center of the probe to vary, i.e.,

$$y^* = A(x^*)^2 + Bx^* + C \tag{23}$$

where

$$x^* = \log_{10} (U_p Y_{eff}/\nu_w)^2 \tag{24a}$$

and

$$y^* = \log_{10} (U_\tau Y_{eff}/\nu_w)^2 \ . \tag{24b}$$

U_p and Y_{eff} are defined as the longitudinal velocity and the height at which the theoretical total pressure (calculated by STAN-5) is equal to the measured Preston-tube pressure at a given location on the cone surface. The coefficients A, B, and C are determined by a least-squares curve fit of the data. The results are presented and discussed in the next chapter. Fig. 9 outlines the steps followed in the data analysis to obtain Preston-tube correlations.

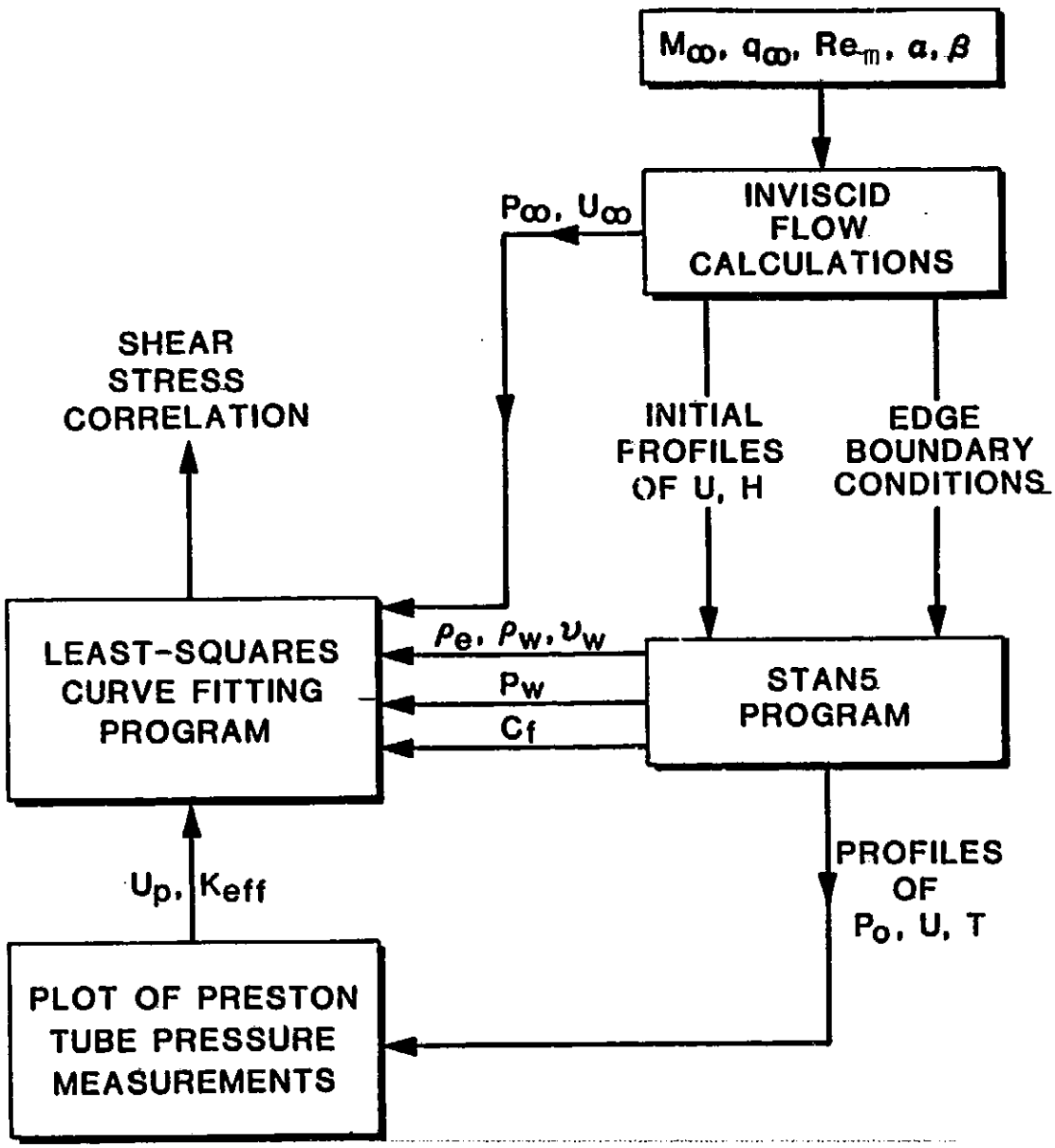

Figure 9. Flow Chart for the Analysis Procedure

Effective Reynolds Number Derivation

Given the flight correlation in the form

$$y^* = A_1(x^*)^2 + B_1\, x^* + C_1 \tag{25a}$$

and the wind-tunnel correlation in the form

$$y^* = A_2\,(x^*)^2 + B_2\, x^* + C_2 \tag{25b}$$

it is desired to derive an expression for the freestream unit Reynolds number in the wind tunnel when all other properties and parameters are equated between the two Eqns. (25a) and (25b) and the skin-friction coefficient predicted by the flight correlation is used. In other words, substitute the wind tunnel data into the flight correlation, solve for C_f in flight, then use this value of C_f together with the same wind tunnel data, except Re_m, to solve for Re_m, which is therefore the effective wind-tunnel unit Reynolds number, $Re_{m,eff}$.

The following identity relates the freestream conditions and can be derived using simple algebra, Abu-Mostafa (29).

$$\frac{1.5881 \times 10^{-3}\ M_\infty\, Re_m}{q_\infty}\ T_\infty^2 - T_\infty - 110.3 = 0 \tag{26}$$

Thus, if only M_∞ and q_∞ are to be equated between wind-tunnel and flight correlations, then T_∞ must be allowed to change. This means that T_0 also will change. Since it is desired to equate the values of the local Mach number, M_e, between the two correlations so that the static pressure may also be equated, T_e must therefore be allowed to change, and hence U_e, ρ_e, T' and

U_p. It can be shown that all variables other than T_∞, T_o, T_e, ρ_e, T', U_p and U_e can be kept unchanged without fixing Re_m. Notice that T_o is assumed constant, $T_{o,2}$, along the cone for a given wind-tunnel case, but equals a different constant, $T_{o,1}$, for the flight case.

Now, by substituting the definitions of x* and y* to both equations (25a,b) and subtracting one from the other to eliminate C_f, the following equation is obtained.

$$A_2 \log_{10}^2 T_2' + (4 A_2 + B_2) \log_{10} T_2' - [4 F^2 (A_1 - A_2) +$$
$$+ 2F (B_1 - B_2) + (D_1 - D_2 + A_1 \log_{10}^2 T_1' + (4 FA_1 + B_1) \log_{10} T_1'] = 0,$$

where $F = \log_{10}(M_p(\gamma R)^{.5} Y_{eff}/\nu_w)$. (27)

This is a quadratic equation that can be solved for $\log_{10}(T_2')$, hence T_2', the effective local reference temperature in the wind-tunnel. $T_{e,2}$ follows from the definition of reference temperature by Sommer and Short (15):

$$\frac{T_2'}{T_{e,2}} = 0.55 + 0.035M_e^2 + 0.45 \frac{T_w}{T_{e,2}} .$$

Then $T_{\infty,2}$ can be evaluated using the isentropic relation

$$\frac{T_{\infty,2}}{T_{e,2}} = \frac{1 + 0.2 M_e^2}{1 + 0.2 M_\infty^2} . \quad (28)$$

And finally $Re_{m,2}$ ($= Re_{m,eff}$) can be calculated using Eqn. (26).

This procedure is graphically outlined in Fig. 10, and the results of its application are shown in the next chapter.

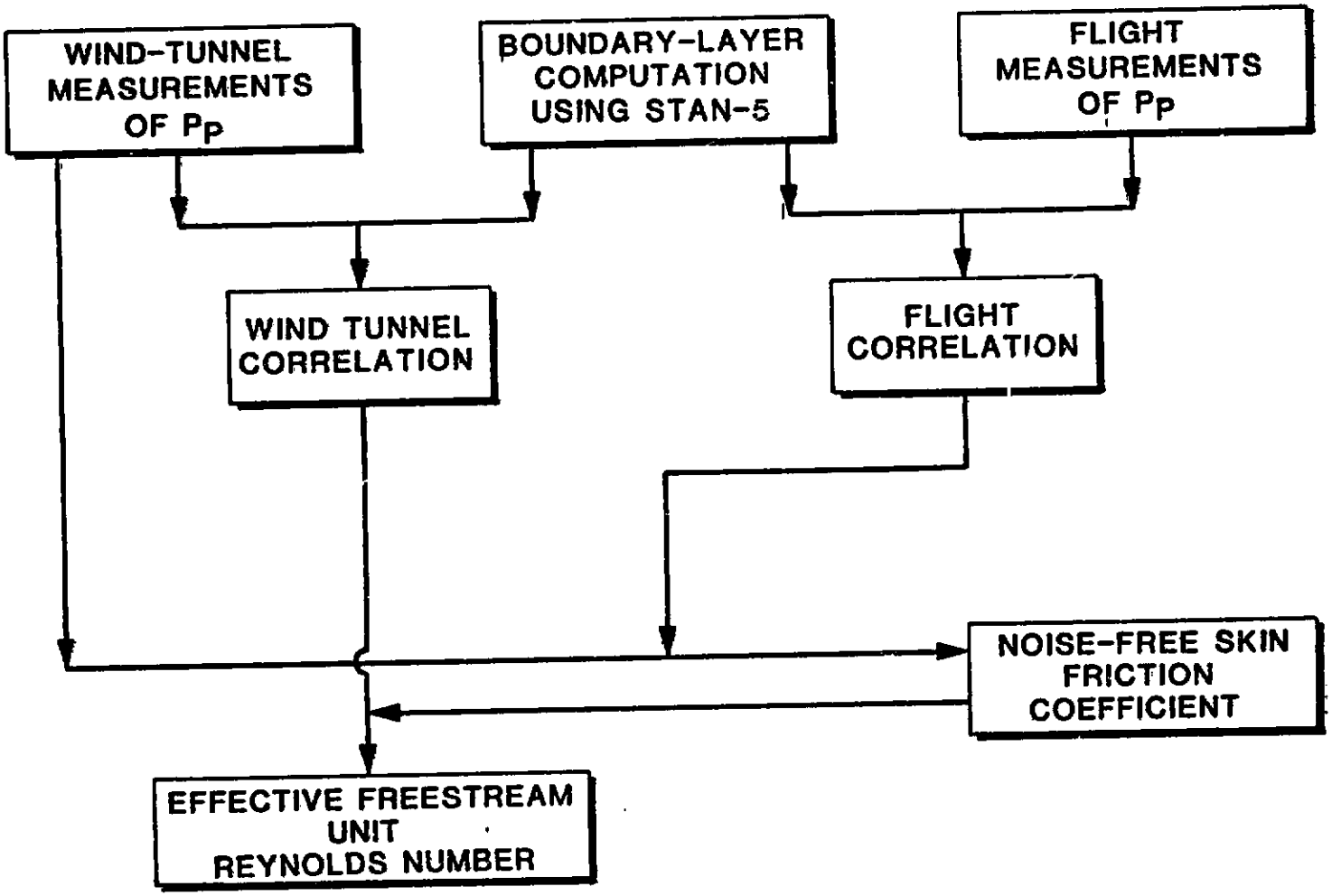

Figure 10. Flow Chart for Effective Reynolds Number Calculation.

CHAPTER IV

RESULTS AND DISCUSSIONS

Laminar Wind-Tunnel Correlation

This and the following sections are discussed in detail in an earlier report by the authors (8). We will summarize the main points here.

1. Laminar K_{eff} values in the tunnel, plotted vs. R_τ, indicated that the $Re_m = 9.8 \times 10^6$ measurements of P_p were in error as they were also in cases 70.726 and 72.748. Correction was made according to NASA's directions (30) using case number 21.318 as a reference. The correction method is explained in point 5 below.

2. The laminar wind-tunnel correlation, based on the shifted data, was found to be

$$y^* = -0.0103\,(x^*)^2 + 0.6653\,x^* - 0.5946,$$
$$5.7 < x^* < 6.3,$$
$$0.30 \leq M_\infty \leq 0.95, \text{ and} \qquad (29)$$
$$9.8 \times 10^6 \leq Re_m \leq 16.4 \times 10^6.$$

3. The r.m.s. scatter of $\bar{C}_f$ about Eqn. (29) is only 0.98%. This very low scatter demonstrates the importance of including a variable K_{eff} in the correlation. Without it, $\bar{C}_{f,rms}$ was found to be 4.93%.

4. Eqn. (29) is not universal. Its empirical coefficients contain information peculiar to the 11 TWT. In fact, no Preston-tube correlation is universal unless it properly models the wind-tunnel environmental effects.

5. Procedure for correcting laminar wind-tunnel data:

The first objective is to align case 58.633 ($M_\infty = 0.7$, $Re_m = 9.8 \times 10^6$) with case 21.318 ($M_\infty = 0.7$, $Re_m = 13.1 \times 10^6$) which is considered the reference. Then shift all the cases whose $Re_m = 9.8 \times 10^6$ accordingly. The second objective is to align case 70.726 ($M_\infty = 0.7$, $Re_m = 13.1 \times 10^6$), with case 21.318, then shift case 72.748 ($M_\infty = 0.7$, $Re_m = 13.1 \times 10^6$) accordingly.

a. Evaluate $\bar{R}_\tau$ of case 58.633 as the average of all R_τ values in this case. Denote it by $\bar{R}_{\tau,58}$.

b. Extrapolate the data in case 21.318 up to $\bar{R}_{\tau,58}$. Use a French curve or do a least-squares curve fit of the data for case 21.318.

c. Evaluate K_{eff} at $\bar{R}_{\tau,58}$ as given by the extrapolated curve; denote it by $K_{eff,21}$. Also read K_{eff} at $\bar{R}_{\tau,58}$ as given by case 58.633 (the original value). Call this value $K_{eff,58}$.

d. Compute $\Delta K_{eff,58} = K_{eff,21} - K_{eff,58}$. This is the incremental adjustment of K_{eff} for the $Re_m = 9.8 \times 10^6$ cases.

e. Find $\Delta P_{o,58}$ = corresponding total pressure adjustment (from theoretical STAN-5 profiles). Add this increment, algebraically, to all P_p measured values in case 58.633.

f. Find ΔP_o's for other cases in the $Re_m = 9.8 \times 10^6$ group which correspond to the same value of $\Delta K_{eff,58}$ above and shift these cases

by the proper increment of total pressure.

g. The procedure for shifting cases 70.726 and 72.748 is similar to steps a-f above.

Laminar Flight Correlation

1. Original values of K_{eff} were plotted vs. R_τ, see Ref. (8). The plot strongly suggests that the flight data have random errors.

2. The authors tried several correction approaches. The approach we recommended in Ref. (8) is based on the assumption that the data of Flight #349.1400 are correct. The correction is done with the aid of the following equation which is a curve fit of the laminar, shifted wind-tunnel data.

$$K_{eff} = 2.865e^{-0.273R_\tau} + 0.655\ (1 - M_\infty^2)^{0.173}, \qquad 0.60 \leq M_\infty \leq 0.95. \tag{30}$$

Eqn. (30) was used to develop incremental adjustments to the flight values of K_{eff}. It is plotted in Fig. 11 and is superimposed on the laminar, shifted wind-tunnel data. The correction procedure is outlined in point 5 below.

It was noticed that the correction of flight data resulted in changes to individual $K_{eff} - R_\tau$ distributions, compare Figs. 12 and 13. Since $\frac{\partial K_{eff}}{\partial x}$ is a function of $\frac{\partial P_p}{\partial x}$, $\frac{\partial P_o}{\partial x}$ and $\frac{\partial P_o}{\partial Y}$, it is expected to change with movement across a profile. Fig. 14 clearly illustrates this idea for an actual case.

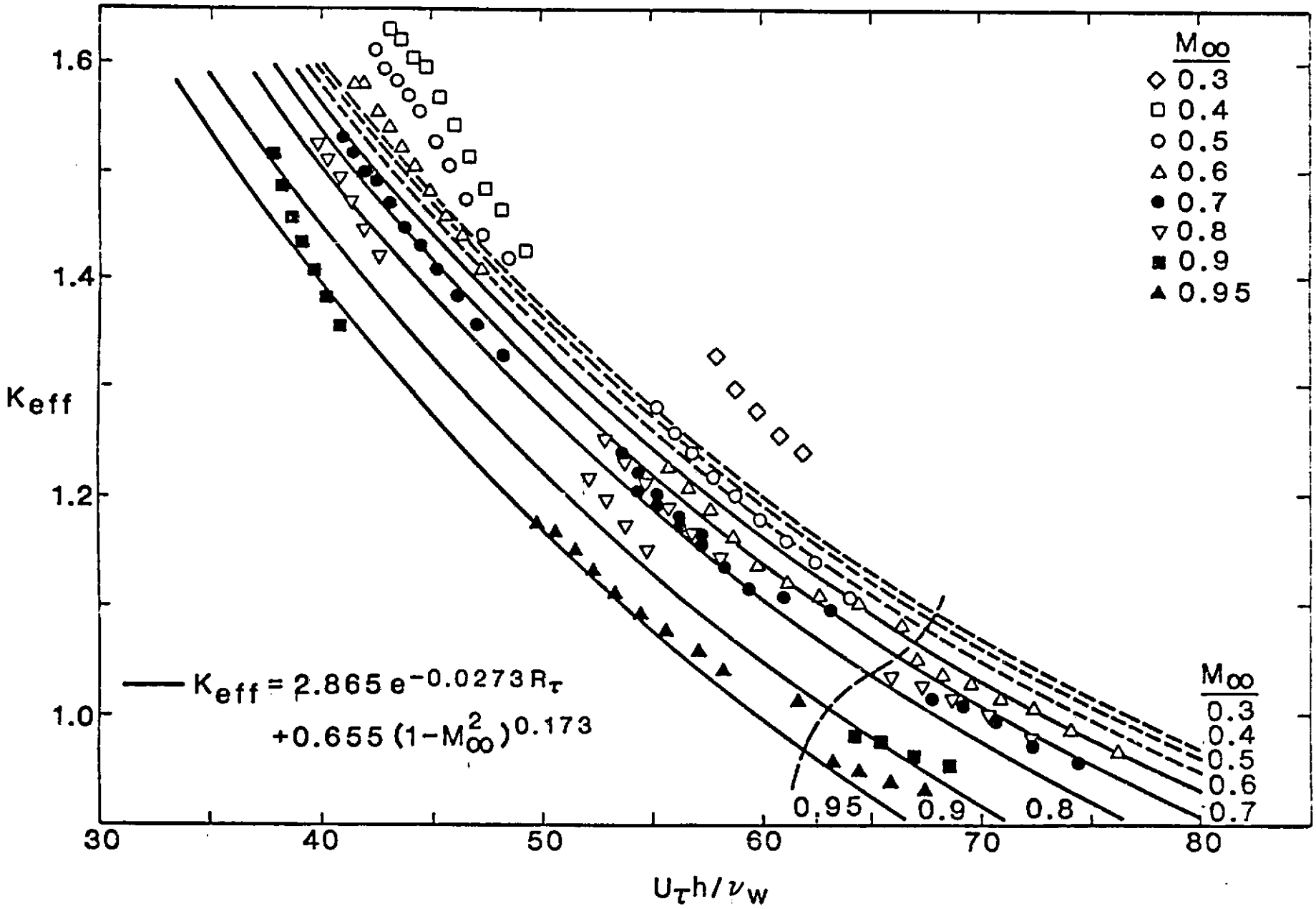

Figure 11. Distribution of Effective Probe Height as Determined from the Shifted Laminar Wind Tunnel Data.

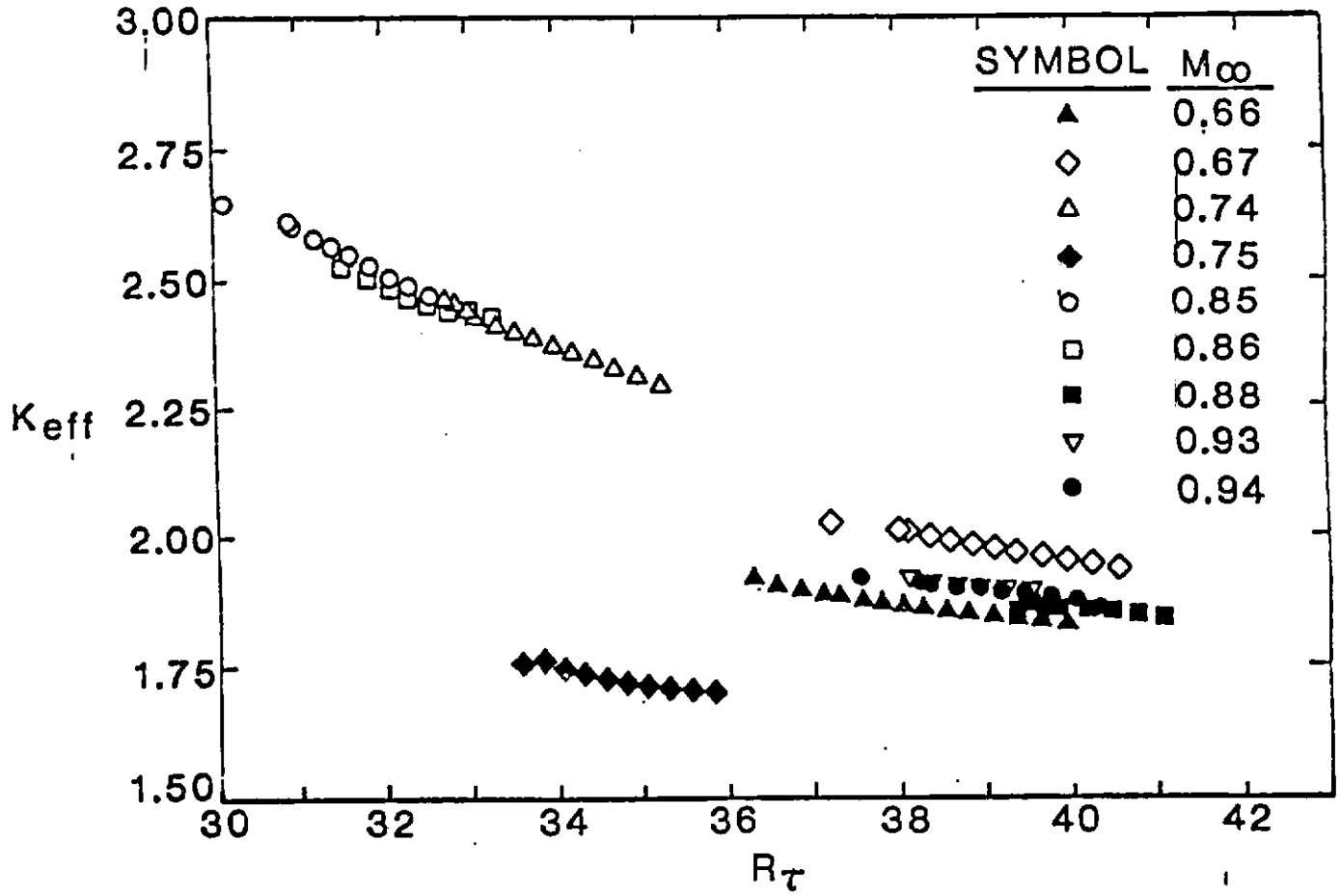

Figure 12. Distribution of Effective Probe Height as Determined from the Original Laminar Flight Data

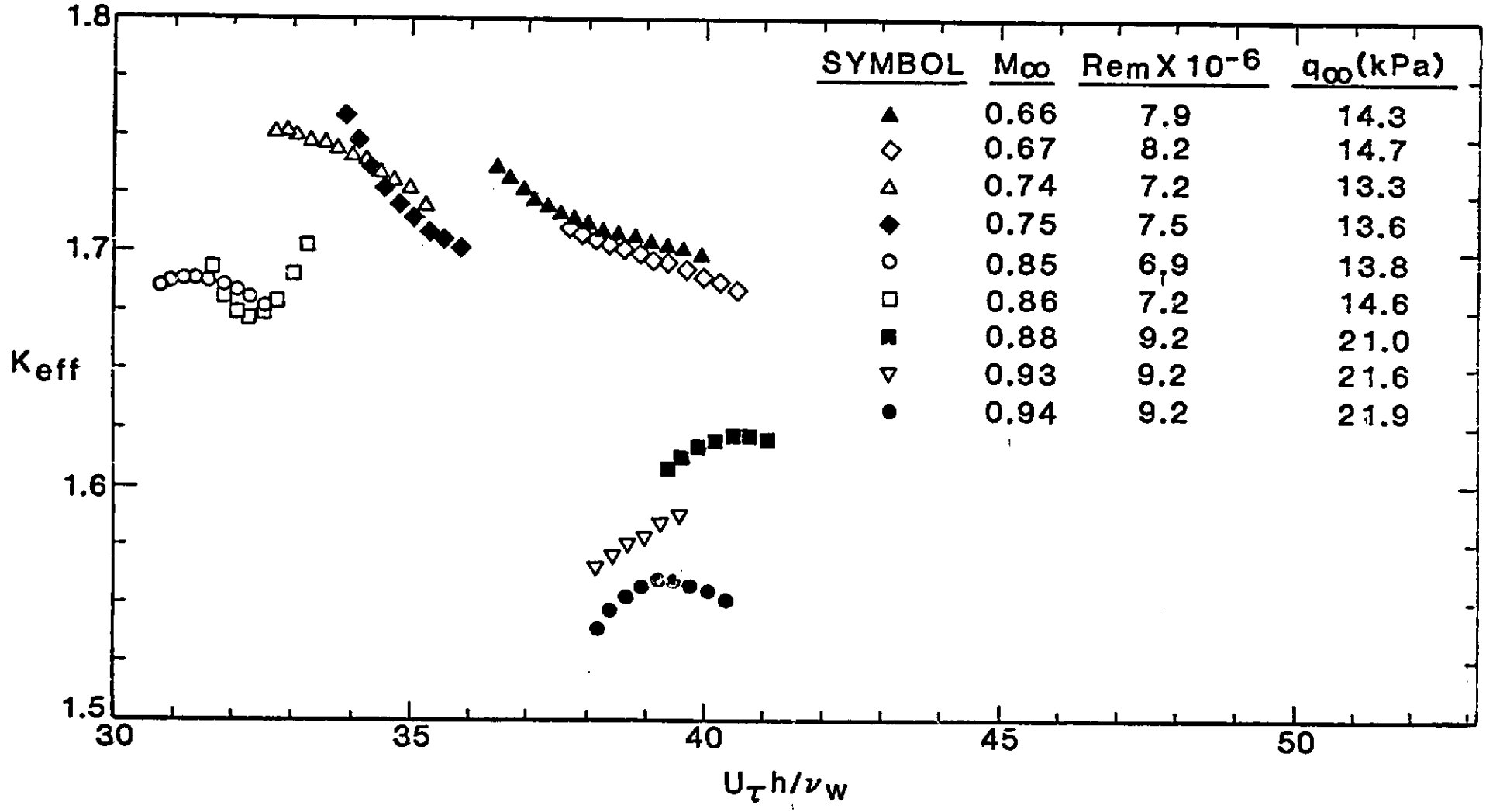

Figure 13. Distribution of Effective Probe Height as Determined from the Corrected Laminar Flight Data.

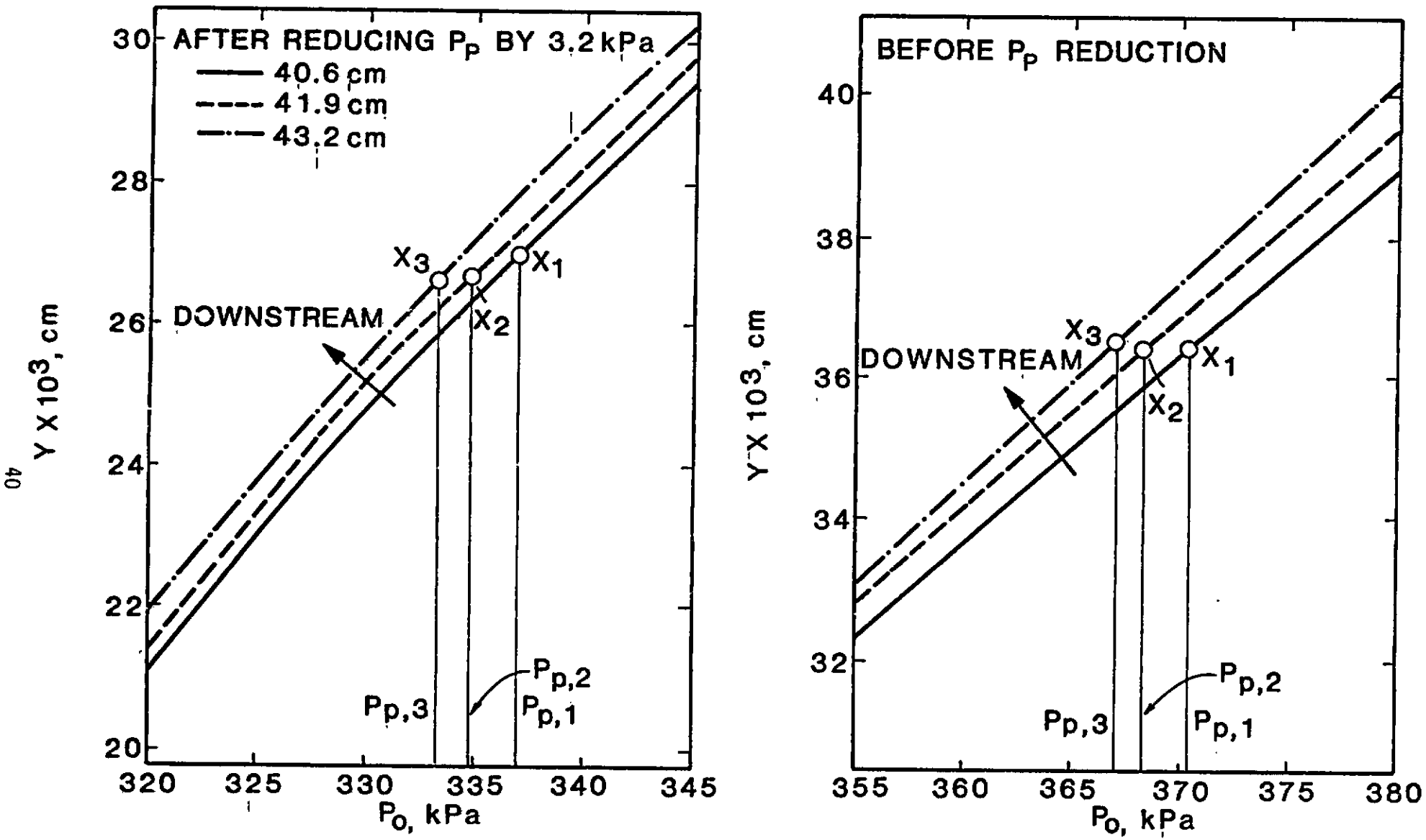

Figure 14. Effect of Changing Preston-Tube Pressure on the Effective Probe Height.

3. The laminar flight correlation based on the corrected data was found to be

$$y^* = 0.05981\ (x^*)^2 - 0.1777\ x^* + 1.928, \qquad (31)$$
$$5.6 < x^* < 6.7,$$
$$0.66 \leq M_\infty \leq 0.94, \text{ and}$$
$$6.9 \times 10^6 \leq Re_m \leq 9.2 \times 10^6.$$

The r.m.s. error in C_f is only 0.37%.

4. Eqn. (31), to the best of our knowledge, is the first correlation in the literature for Laminar Preston-tube measurements in flight.

5. Procedure for correcting the flight data:

a. Let $K_{eff,FD}\ (R_\tau, M_1)$ = the value of K_{eff} at R_τ for the flight case with $M_\infty = M_1$. Similarly define $K_{eff,WT}\ (R_\tau, M_1)$.
Let $\{M_1\}_{FD}$ = set of all R_τ values in the flight case with $M_\infty = M_1$.
Let $\{M_1, M_2\}_{FD}$ = set of all R_τ values common between the two flight cases whose M_∞'s are M_1 and M_2, i.e. $\{M_1, M_2\}_{FD} = \{M_1\}_{FD} \wedge \{M_2\}_{FD}$.
Let $\bar{R}_\tau(M_1, M_2)_{FD}$ = the average of all R_τ values in $\{M_1, M_2\}_{FD}$.
Let $\Delta K_{eff,FD}(M_1, M_2) = K_{eff,FD}(\bar{R}_\tau, M_1) - K_{eff,FD}(\bar{R}_\tau, M_2)$. Similarly define $\Delta K_{eff,WT}(M_1, M_2)$. Refer now to Fig. 13.

b. The reference case for all flight cases is flight #349.1400, i.e. $M_2 = 0.75$. To shift a flight case $\{M_1\}_{FD}$, first determine $\{M_1, 0.75\}_{FD}$.
If $\{M_1, 0.75\}_{FD} = \phi$, i.e., no R_τ values are shared by the two cases then we have one of two situations.

- $\{0.75\}_{FD} > \{M_1\}_{FD}$, in which case set $\bar{R}_\tau(M_1, 0.75)_{FD}$ to be equal to the largest R_τ in $\{M_1\}_{FD}$.
- $\{M_1\}_{FD} > \{0.75\}$, in which case set $\bar{R}_\tau(M_1, 0.75)_{FD}$ to be equal to the smallest R_τ in $\{M_1\}_{FD}$. An example of such a situation is $\{0.66\}_{FD}$, see Fig. 12.

Then, go to step d below.

c. This is the case where $\{M_1, 0.75\}_{FD}$ is defined ($\neq \phi$) such as $\{0.74\}$. So, calculate $\bar{R}_\tau\ (M_1, 0.75)_{FD}$.

d. Find $K_{eff,FD}(\bar{R}_\tau, M_1)$ and $K_{eff,FD}(\bar{R}_\tau, 0.75)$ hence $\Delta K_{eff,FD}\ (M_1, 0.75)$.

e. Find $K_{eff,WT}(\bar{R}_\tau, M_1)$ and $K_{eff,\ WT}(\bar{R}_\tau, 0.75)$ hence $\Delta K_{eff,WT}(M_1, 0.75)$ from curve-fit equation of K_{eff} vs. R_τ in the wind tunnel, such as Eqn. (30). Notice that $\bar{R}_\tau(M_1, 0.75)_{WT} = \bar{R}_\tau(M_1, 0..75)_{FD}$ Also, $\Delta K_{eff,WT}(M_1, 0.75)$ will be negative if $M_1 > 0.75$.

f. Calculate $\Delta K_{eff,shift}(M_1)_{FD}$ = incremental adjustment of K_{eff} values in the flight $M_1 = \Delta K_{eff,FD}(M_1, 0.75) - \Delta K_{eff,WT}(M_1, 0.75)$.

g. From the theoretical P_o profiles for the flight case M_1, obtain $\Delta P_{o,shift}(M_1)_{FD}$ which corresponds to $\Delta K_{eff,shift}(M_1)_{FD}$ at the location where $R_\tau = \bar{R}_\tau$. This is the incremental pressure adjustment for flight case M_1.

h. For all points in $\{M_1\}_{FD}$, obtain $P_{p,shift}(M_1)_{FD} = P_p(M_1)_{FD} - \Delta P_{o,shift}(M_1)_{FD}$, $P_p(M_1)_{FD}$ being the original, measured value of Preston-tube pressure.

Laminar Effective Reynolds Number

Based on Eqns. (29) and (31), the effective freestream unit Reynolds number was computed and plotted versus M_∞. The plot, Fig. 15 resembles the curve for noise data on the AEDC cone in the 11 TWT†, Fig. 16, and has a peak at $M_\infty = 0.70$ - as does the noise. Actually, $\Delta R_{eff} \equiv (Re_{m,eff} - Re_m)/Re_m$ correlated with noise by the following equation.

---

† These data include installation effects in addition to wall-generated noise.

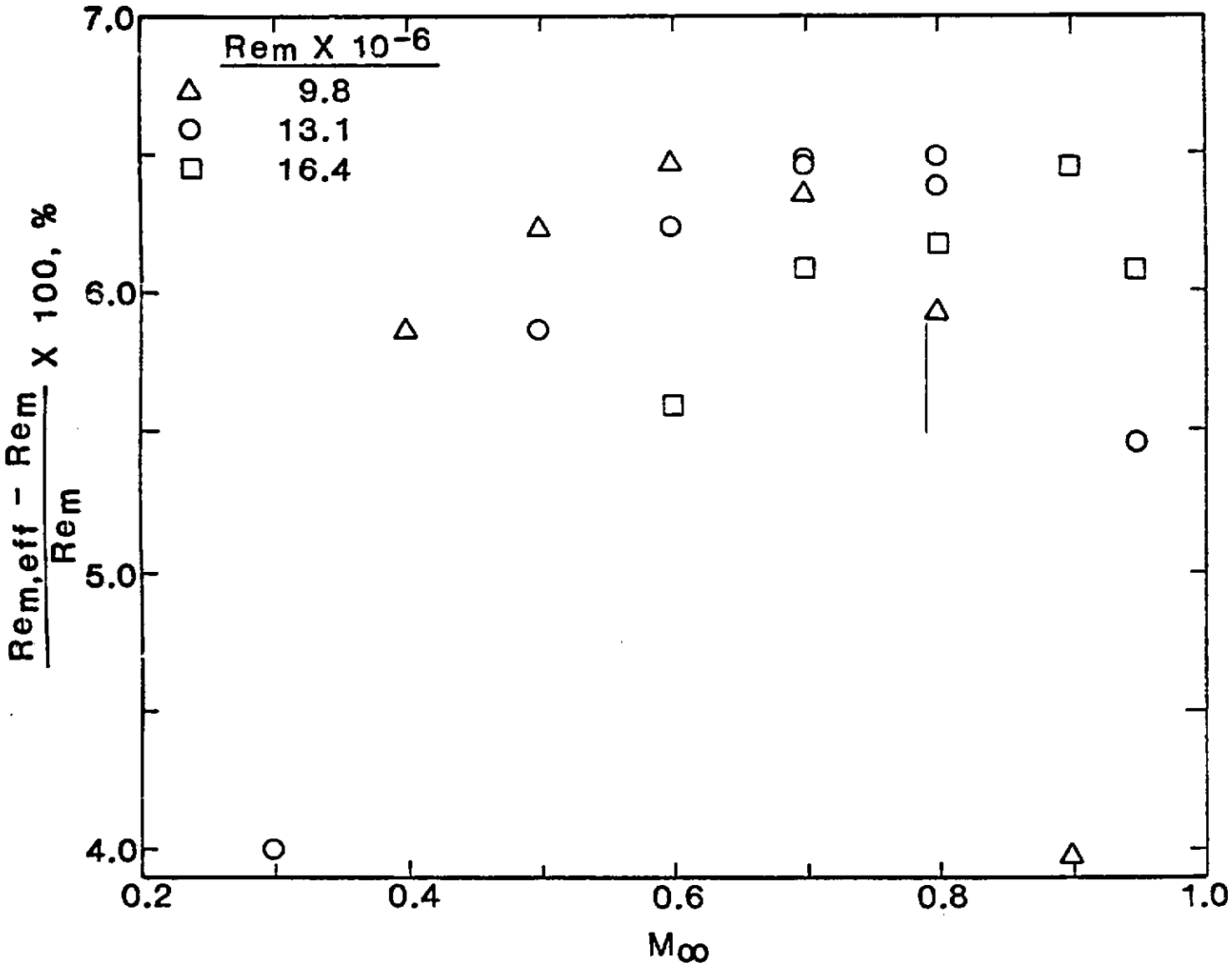

Figure 15. Distribution of Laminar Effect Reynolds Number Based on Corrected Data.

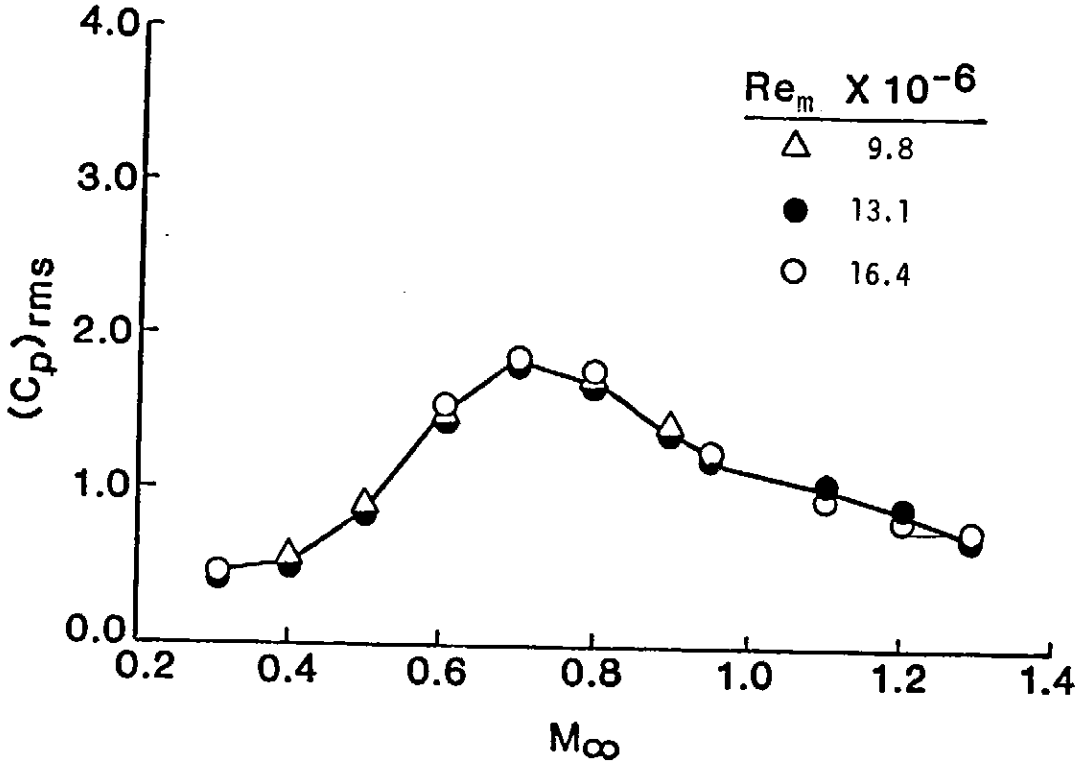

Figure 16. Noise Data on the AEDC Cone in the 11-Ft Transonic Wind Tunnel

$$\Delta R_{eff} \simeq 6.25 \, (C_{P,rms})^{0.07} \, \dagger \qquad (32)$$

This supports the thesis that environmental effects in a wind tunnel can be calibrated by a single number, i.e., $Re_{m,eff}$. So, in order to measure the same average, theoretical skin friction coefficient, or the same measurement of P_p, in flight as is measured in the tunnel, the flight value of freestream unit Reynolds number should be increased to $Re_{m,eff}$. This effective Reynolds number will not necessarily equate the measurable values of C_f. Indeed, the effects of noise on directly measured skin friction, if any, are unknown.

The Transition Region

Recall Dhawan and Narasimha's (21) intermittency function for transitional flow:

$$\gamma(x) = 1 - e^{-A\xi^2(x)} \, . \qquad (19)$$

In order to be able to use Eqn. (19), λ needs to be known for each case. Since measurements of $\gamma(x)$ are not available for this study, Eqn. (21) cannot be used. Another method was developed to calculate λ as will be shown now.

Calculation of λ

This method makes use of the available Preston-tube data. Since it is assumed that the distribution of C_f follows Preston-tube measurements (see Eqn. 4), one can assume that the location x_T where P_p peaks is the same location where C_f peaks. Within the transition zone, the C_f distribution is calculated using the γ-function in the following manner:

---

† The accuracy of this correlation is not very good since it does not include other environmental effects such as freestream turbulence intensity. $Re_{m,eff}$ calibrates all these effects and not only noise. It should be noted, however, that noise effects are dominant in the 11-Ft Transonic Wind Tunnel, (1).

$$C_f = (1 - \gamma)\, C_{f,\ell} + \gamma\, C_{f,T} \,, \qquad (33)$$

where $C_{f,\ell}(x)$ is the local laminar skin friction coefficient if it were to occur at the given location x, and $C_{f,T}(x)$ is the local turbulent skin friction coefficient if it were to occur at x. The origin of the turbulent boundary layer is determined from the fully-developed turbulent flow at or downstream from x_E, the end-of-transition location, as will be explained later. The value of x_E corresponds to $\xi = 4.0$ (or $\gamma = 0.9986$) as recommended by Dhawan and Narasimha (21).

Differentiating Eqn. (33) with respect to x and evaluating at x_T yields the following relation:

$$\left.\frac{dC_f}{dx}\right|_{@x_T} = 0 = \left[(C_{f,T} - C_{f,\ell})\frac{d\gamma}{dx} + \left(\frac{dC_{f,T}}{dx} - \frac{dC_{f,\ell}}{dx}\right)\gamma + \frac{dC_{f,\ell}}{dx}\right]_{x_T} . \qquad (34)^{\dagger}$$

A following formula for calculating $C_{f,T}$ is reported by White (31) to be reasonably accurate.

$$C_{f,T} = \frac{0.455}{S^2 Ln^2 \left[\frac{0.06}{S} Re_{x_v} \frac{\mu_e}{\mu_w} \left(\frac{T_e}{T_w}\right)^{.5}\right]}$$

---

† Eqn. (34) is also valid at x_t, location of minimum P_p. Solving for x_B which appears in the definition of γ, it was found that $x_B \approx x_t$. Therefore, the value of x_t is used from here on to designate the transition onset location.

Using Sommer and Short's model for S, a compressibility factor (see Ref. 31), to correct for variable properties and Tetervin's (32) correction for axisymmetric flow and making the approximation that $\frac{\sqrt{\rho_w}\sqrt{\rho'}}{\mu_w} \simeq \frac{1}{\nu'}$ the following equation can be derived.

$$C_{f,T} = \frac{\rho'}{\rho_e} \frac{0.455}{Ln^2 \left[\frac{U_e x_v}{37.8 \nu'} \right]} \tag{35}$$

Here x_v = distance along cone surface measured from the virtual origin of the turbulent boundary layer. It can be written in the form

$$x_v = x - \Delta x, \tag{36}$$

where Δx is the location of the virtual origin (see Fig. 17). It is now clear that Eqn. (34) can be solved for λ if Δx is known. The following section explains how this is done.

Calculation of Δx

Eqn. (35) can be rewritten in the form

$$x_v = x - \Delta x = \frac{37.8\nu'}{U_e} \exp \left[\frac{0.455\ \rho'}{C_{f,T}\ \rho_e} \right]^{0.5}. \tag{37}$$

So, all that is needed to calculate Δx is a reference $C_{f,T}$ in the fully-developed turbulent flow at a location $x_{ref} \geq x_E$.

Crawford and Kays (28), who developed the STAN-5 program, state that their program's calculation of turbulent C_f agreed with extensive measurements done at Stanford University. They used the following equation to effect gradual transition.

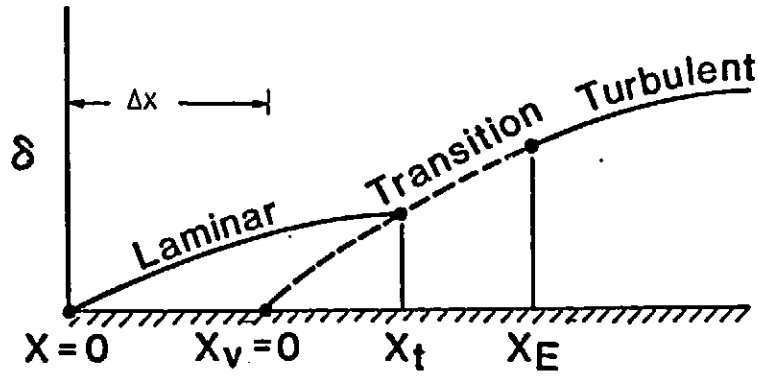

Figure 17. The Virtual Origin of a Turbulent Boundary Layer

$$A^+ = A_\ell^+ + (300 - A_\ell^+)\left[1 - \sin\left(\frac{\pi}{2}\,\frac{Re_\theta(x) - Re_\theta(x_B)}{Re_\theta(x_B)}\right)\right]^2 \qquad (38)$$

Here $A^+(x)$ is an effective sublayer thickness used in the van Driest damping model

$$D = 1 - e^{-Y^+/A^+} \; . \qquad (39)$$

Fig. 18 shows a plot of Eqn. (38) for a typical wind tunnel case. The damping coefficient is used in the Prandtl mixing length model for turbulent boundary layer calculations near the wall as follows.†

$$\ell = \kappa\, Y\, D, \quad \kappa = 0.41 \qquad (40)$$

And

$$A_\ell^+ = \frac{\rho_w}{\mu_w\, U_\tau^3}\,\frac{dP_w}{dx} \qquad (41)$$

Now, in Eqn. (38), it is assumed that

$$Re_\theta(x_E) = 2\, Re_\theta(x_B) \; .$$

This was not found to be true at values of $x_E = x_B + 4\lambda$ (recommended by Dhawan and Narasimha (21)). In addition, this transition model does not

---

† The mixing length model is also the one used in this study to calculate the fully-developed turbulent boundary layer.

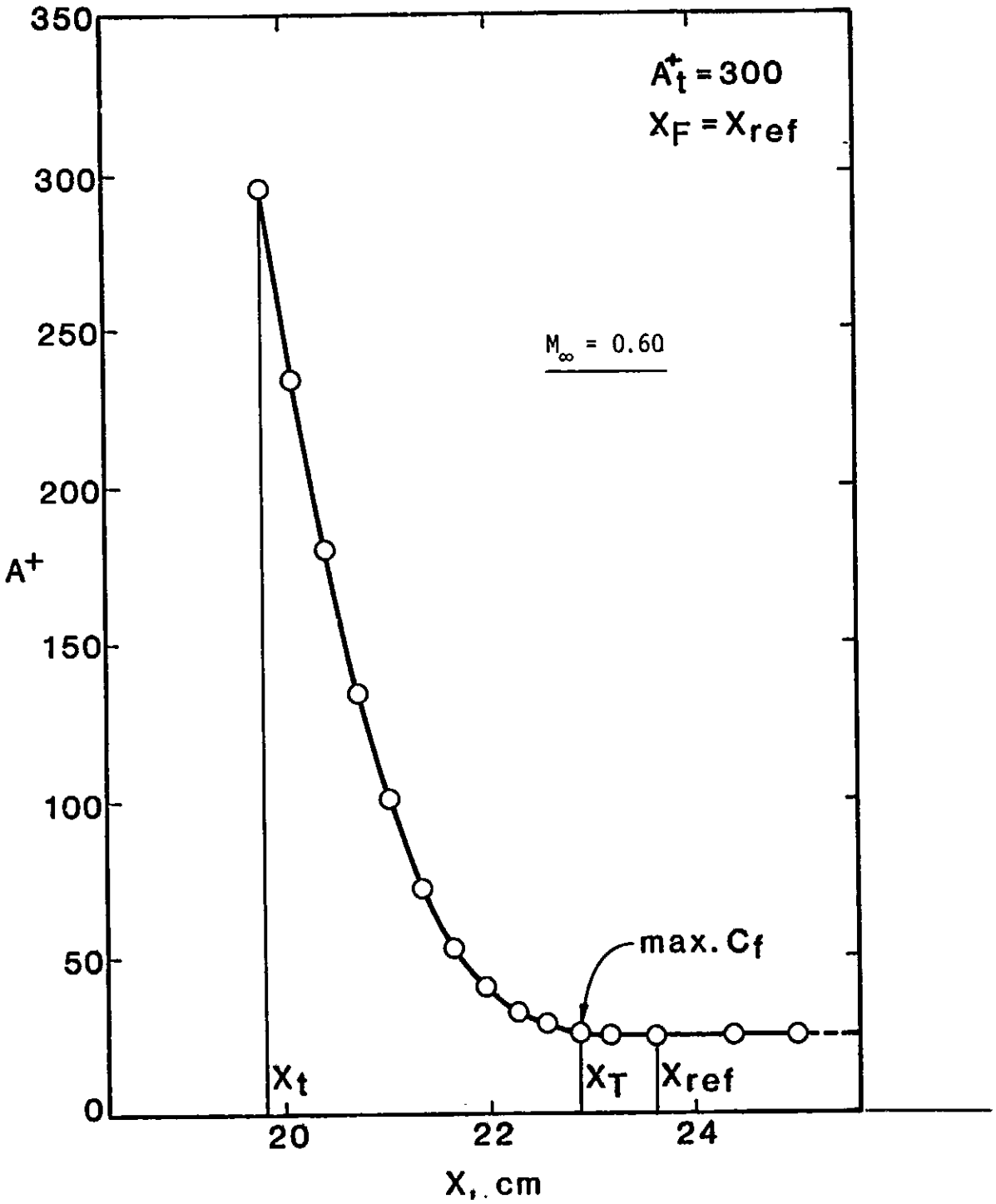

Figure 18. Distribution of Effective Sublayer Thickness for a Typical Case.

produce a peak in C_f at x_T. Instead, we used the following slightly different equation:

$$A^+ = A^+_\ell + [500 - A^+_\ell][1 - \sin(\frac{\pi}{2}\frac{Re_x - Re_B}{Re_F - Re_B})]^2 , \qquad (42)$$

where Re_F is the local length Reynolds number at a location x_F which is changed so that a peak in C_f occurs at x_T. This trial-and-error procedure is illustrated in Fig. 19. It is important here to mention that Eqn. (42) is not used as a transition model. Its sole role is to effect gradual transition so that the turbulent flow downstream is accurately computed. Indeed, when either of Eqns. (38) or (42) was used to simulate transition, the computed skin friction was found to be greatly underestimated as compared to the Dhawan-Narasimha model.

To sum up, Eqn. (42) is used to prepare to compute turbulent flow, and hence obtain a good estimate of a reference value for $C_{f,T}$ at x_E or downstream. The location $x_{ref} \geq x_E$ is estimated from the Preston-tube data traces as the location downstream from x_E where the P_p measurements exhibit a slope characteristic of fully-developed turbulent flow (see Fig. 20). However, this estimate of x_{ref} need not be precise, as long as it is sufficiently downstream from x_E.

Using $C_{f,L,ref}$ at x_{ref} and substituting in Eqn. (37), Δx may be calculated. Hence, λ can be calculated from Eqn. (34). Thus, the γ-function is now fully defined, and the C_f distribution can be computed using Eqn. (33).

In the above argument, it is assumed that White's formula, Eqn. (35), accurately calculates $C_{f,T}$ and/or x_v. The authors have found, by trial and error, that $C_{f,T}$ at x_{ref} computed by STAN-5 and using Δx obtained from Eqn. (35) was always different from $C_{f,T,ref}$. Best results were obtained when the

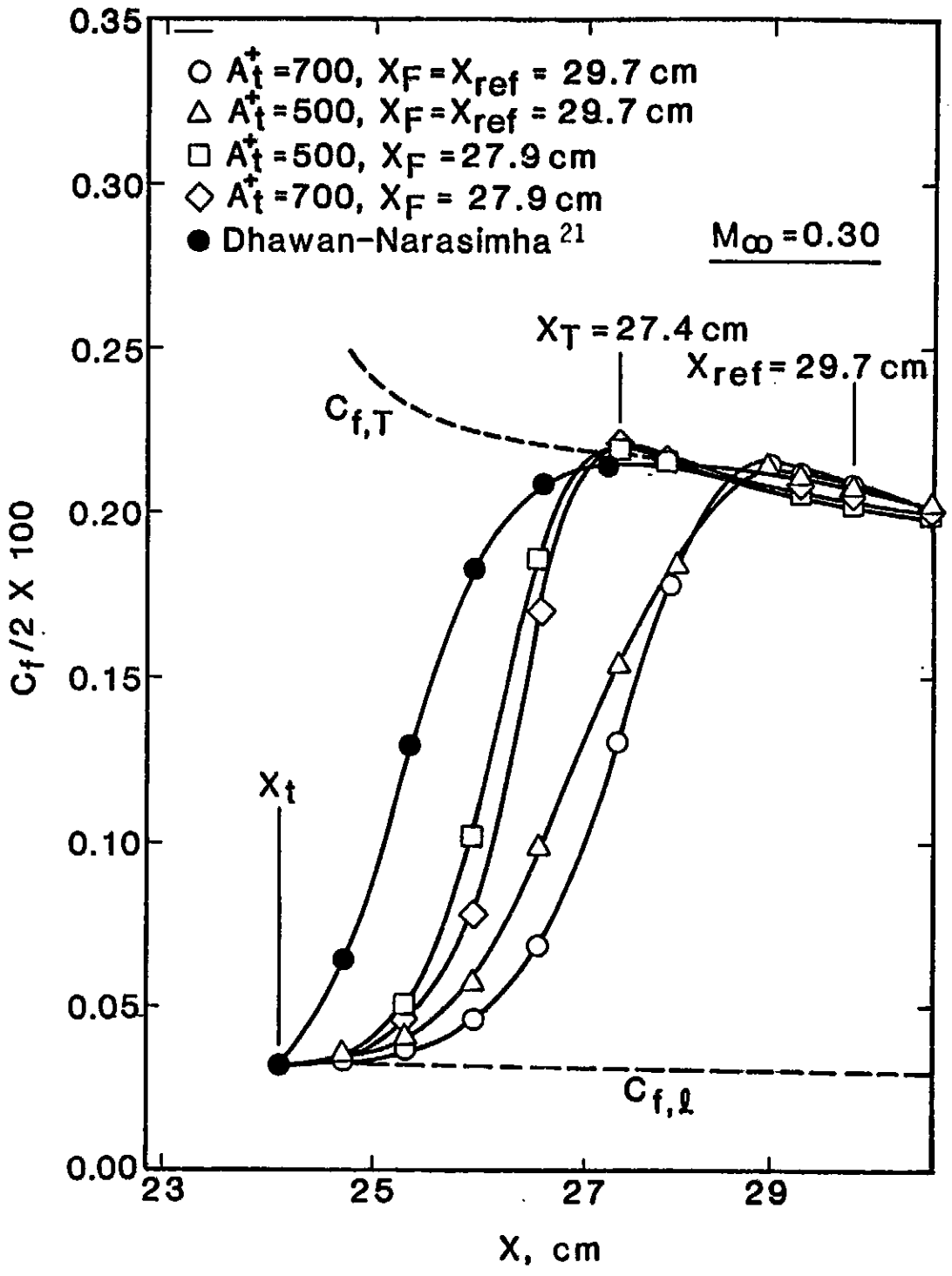

Figure 19. Effect of Sublayer Thickness Distribution on Transitional Skin Friction Coefficient.

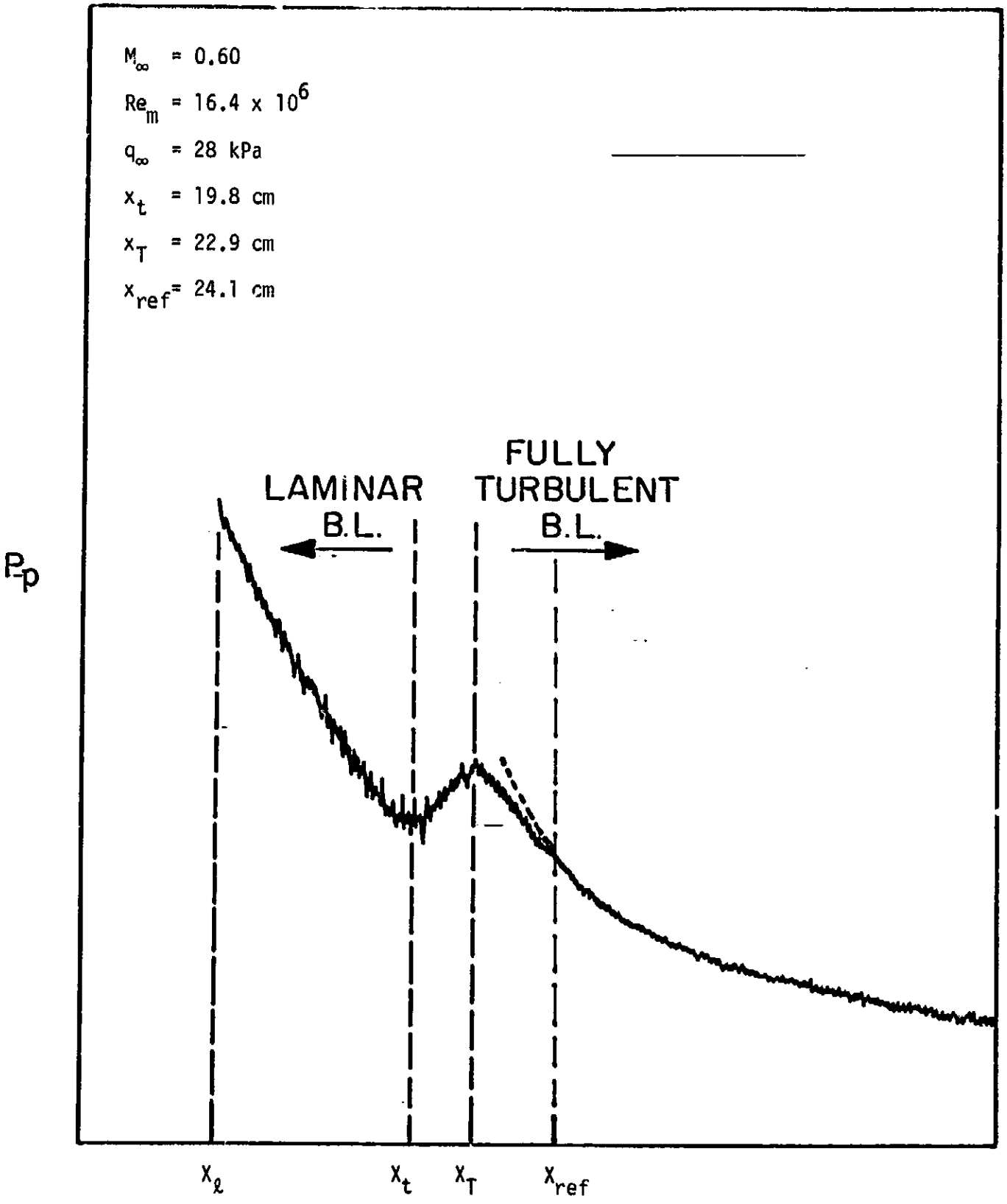

Figure 20. Pattern of Typical Preston-Tube Data Measured in the 11-Ft Transonic Wind Tunnel

virtual origin coincided with the transition point, i.e., $x_v(0) = x_t = \Delta x$. This finding was also reported by Dhawan and Narasimha. (21) Based on this finding an improved procedure to calculate λ and hence γ is described next.

The following variation of White's equation is used in place of Eqn. (35).

$$C_{f,T}(x) = C \frac{\rho'/\rho_e}{Ln^2 \left[\frac{u_e(x - x_t)}{\nu'}\right]}, \qquad (43)$$

where C is a constant that has a different value for each case and can be directly evaluated from Eqn. (43) at x_{ref}.

Eqn. (43), then, together with its derivative w.r.t. x, the laminar STAN-5 calculations of $C_{f,\ell}$ and its derivative w.r.t. x are substituted in Eqn. (34) to solve for λ and hence γ.

The Transition Correlations

In order to completely define the correlation parameters x* and y*, theoretical velocity and total pressure profiles in transition need to be computed to obtain $U_p(x)$ and $K_{eff}(x)$. These profiles may be calculated using the γ-function in a manner similar to skin friction, Eqn. (33).

$$U(Y) = (1 - \gamma)\, U_\ell(Y) + \gamma\, U_T(Y), \qquad (44)$$

$$T(Y) = (1 - \gamma)\, T_\ell(Y) + \gamma T_T(Y). \qquad (45)$$

From these two profiles, calculate $P_o(Y)$ as follows:

$$M(Y) = U(Y)/(555\sqrt{T(Y)})$$

$$P_o(Y) = P_w[1 + 0.2\,M^2(Y)]^{3.5} \qquad (46)$$

Initial profiles for turbulent flow computation can be obtained by rescaling available fully-developed turbulent profiles (at x_{ref}) using edge velocity and boundary-layer thickness at the initial location which can be estimated using Musker's equation, Musker (33), as follows:

$$\delta = e^{0.41\,U_e^+ - 3.0504}\,\nu'\,U_e^+/U_e \quad \text{at } x_{initial}, \qquad (47)$$

where $U_e^+ = \left(\frac{C_{f,T}}{2}\,\frac{\rho_e}{\rho_w}\right)^{0.5}$ at $x_{initial}$. $C_{f,T}$ at $x_{initial}$ can be calculated using Eqn. (35) with $x_v = x_{initial} - \Delta x$ and all properties evaluated at $x_{initial}$ which is downstream from x_t.

Values of U_p and K_{eff} can then be computed by interpolation of measured Preston-tube pressures in velocity and total pressure profiles given by Eqns. (44 and 46).

Based on the above analysis the transition correlations for the original data are:

Wind Tunnel:

$$y^* = 0.06935\,(x^*)^2 + 0.02795\,x^* + 0.9678,$$
$$5.2 < x^* < 6.3\ ,\ 9.8 \times 10^6 \le Re_m \le 16.4 \times 10^6,\ 0.30 \le M_\infty \le 0.95,$$
$$C_{f,rms} = 2.19\%, \text{ and} \qquad (48)$$

Flight:

$$y^* = 0.02094(x^*)^2 + 0.5988x^* - 0.7112,$$
$$5.5 < x^* < 7.1\ ,\ 6.9 \times 10^6 \leq 9.2 \times 10^6_\infty,\ 0.66 \leq M_\infty \leq 0.94, \qquad (49)$$
$$C_{f,rms} = 3.64\%.$$

A plot of Eqn. (48) with the superimposed wind-tunnel data appears in Fig. 21. Fig. 22 is a plot of C_f scatter about Eqn. (48). Figures 23 and 24 illustrate the same for the flight data.

Not all the available data in transition are included in the above correlations; only the points at which x* and y* are proportional are included (These amount to slightly more than 60% of the total number of points in the transition region.) This requirement is suggested by the basic Eqn. (4).

Figures 25 and 26 are plots of transitional values of K_{eff} vs. R_τ in the wind tunnel and flight, respectively. Notice that the data, again, indicate large errors in the flight tests. Before discussing how these errors are corrected, we first present the results from the analysis of turbulent data.

The effective Reynolds number distribution based on Eqns. (48) and (49) is shown in Fig. 27. It does not correlate with noise. This situation may change after correcting the experimental data.

The Turbulent Region

The procedure, which is described two sections earlier, for estimation of a reference $C_{f,T}$ provides an accurate and complete method for theoretical computations of C_f, velocity and enthalpy profiles in the turbulent flow region. Therefore, all the information needed to define x* and y* for this region is available.

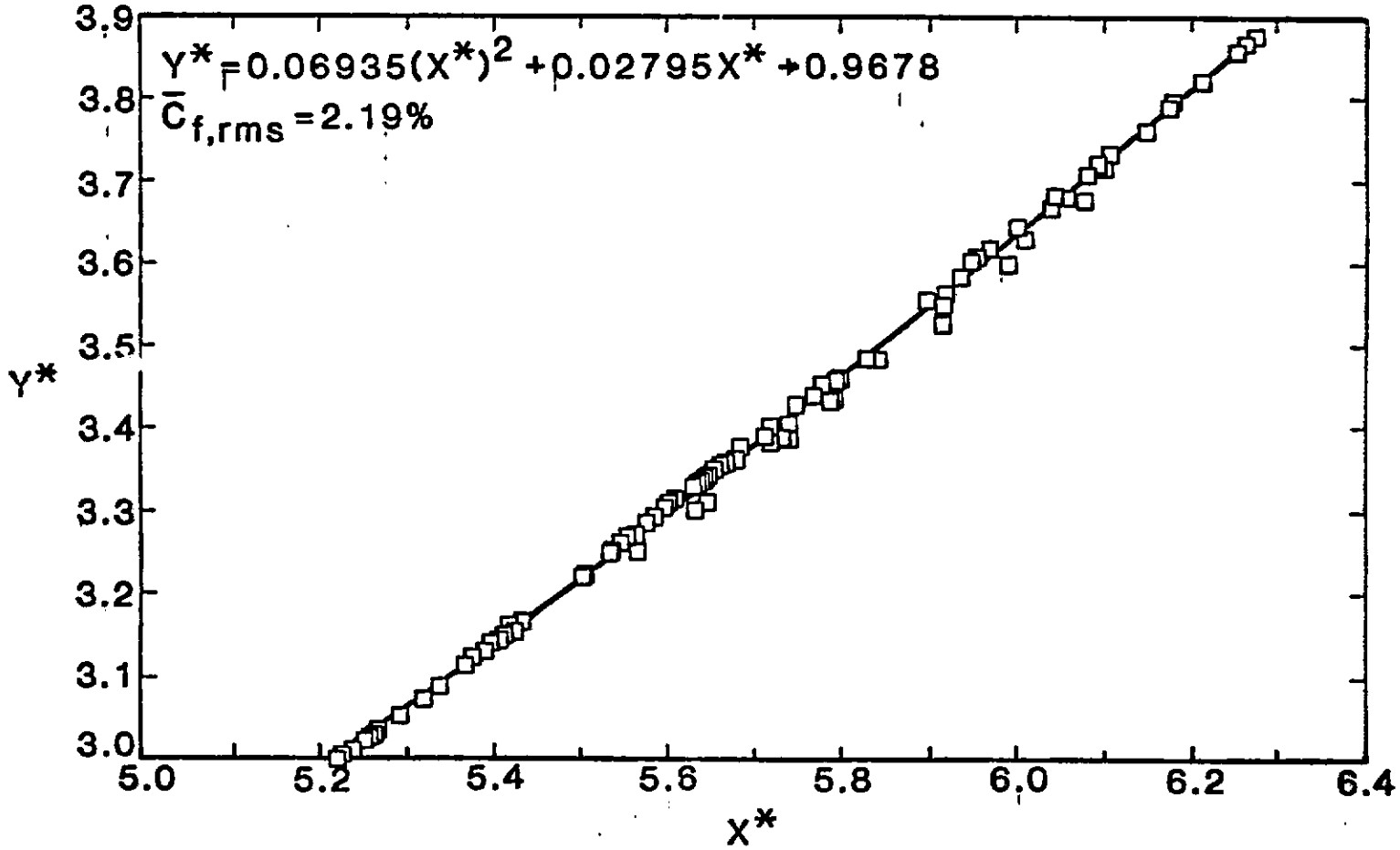

Figure 21. Transitional Correlation for Original Wind Tunnel Data.

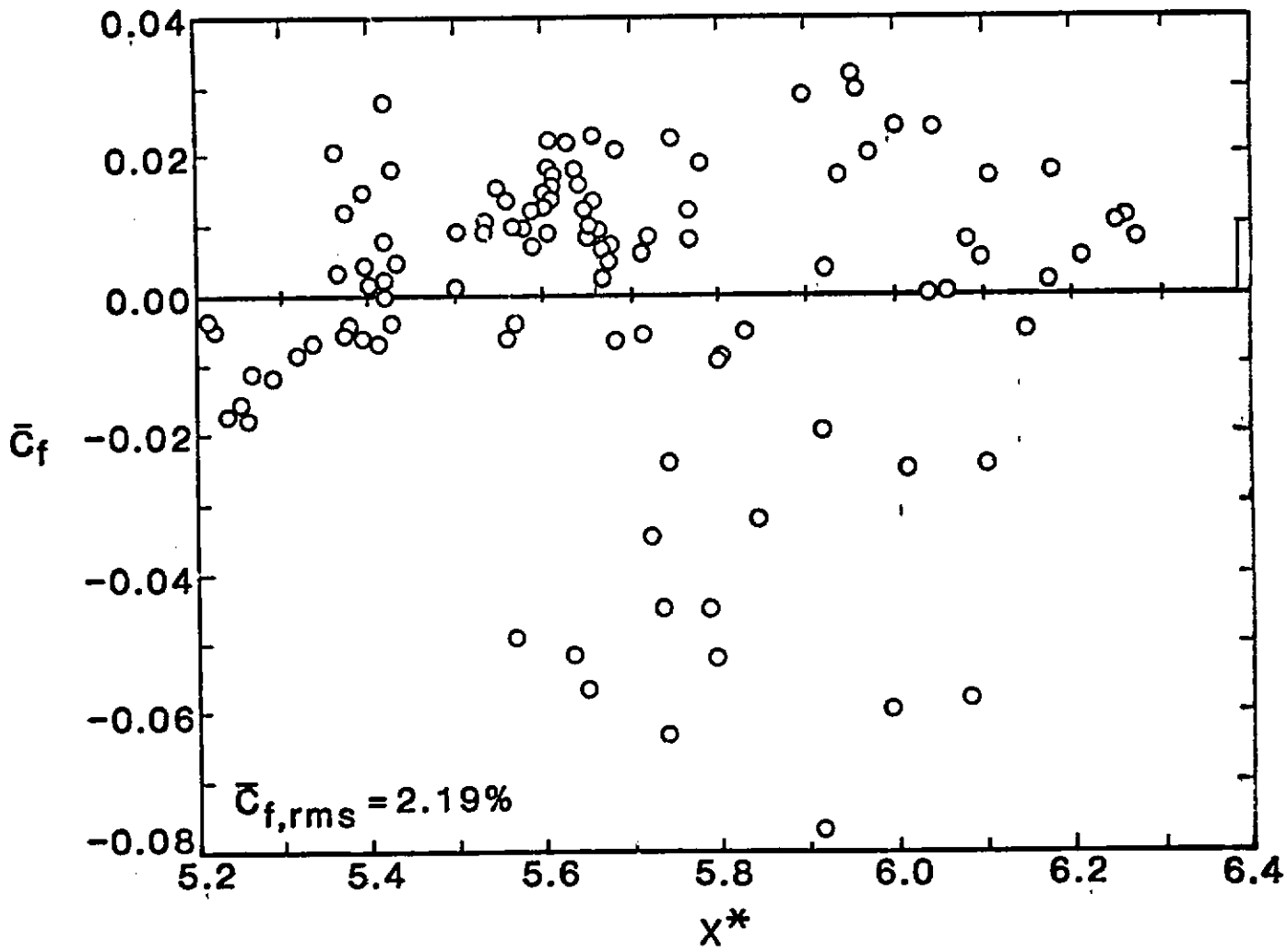

Figure 22. Scatter of Transitional Skin Friction Coefficient About Correlation for Original Wind Tunnel Data.

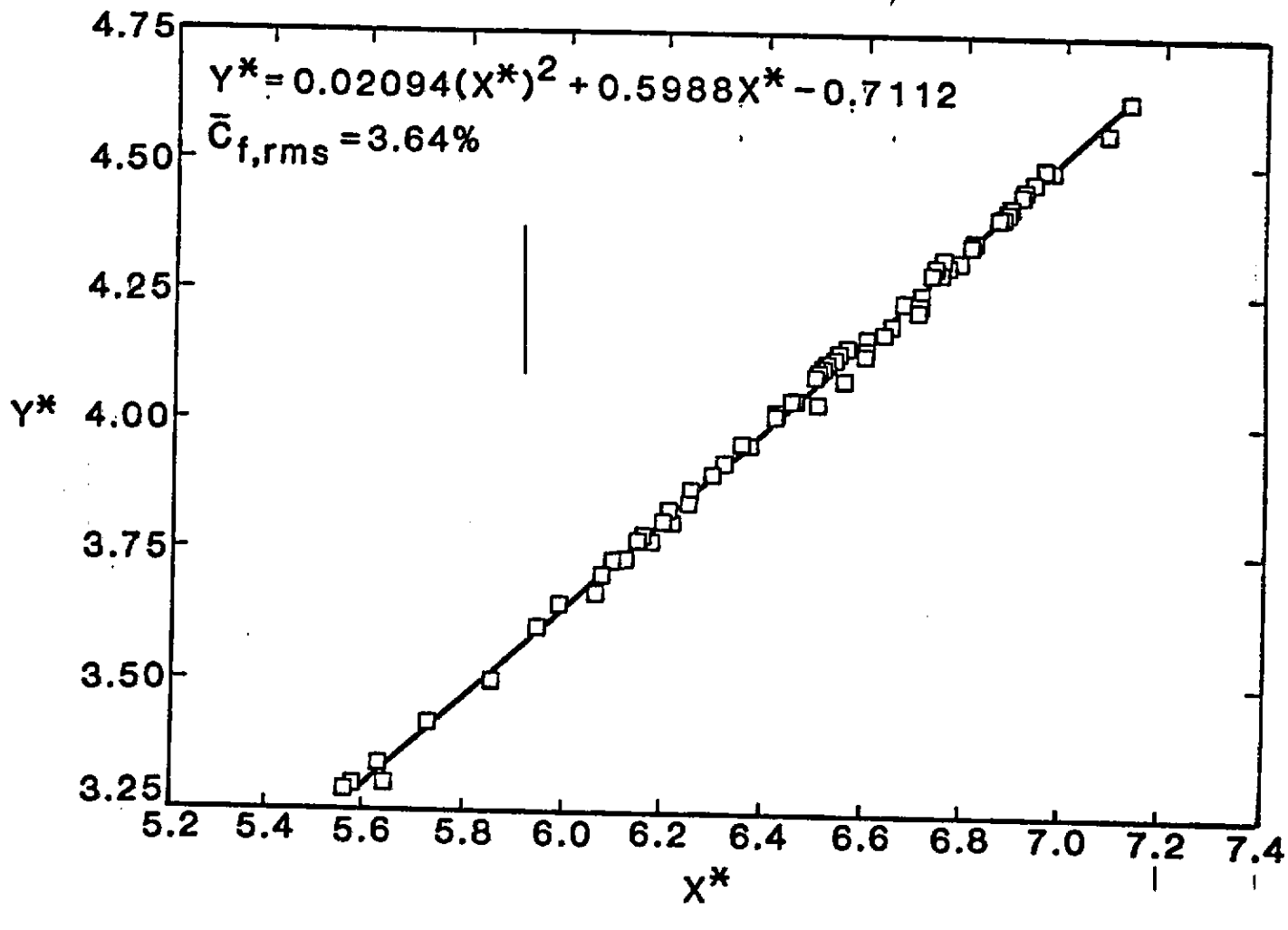

Figure 23. Transitional Correlation for Original Flight Data.

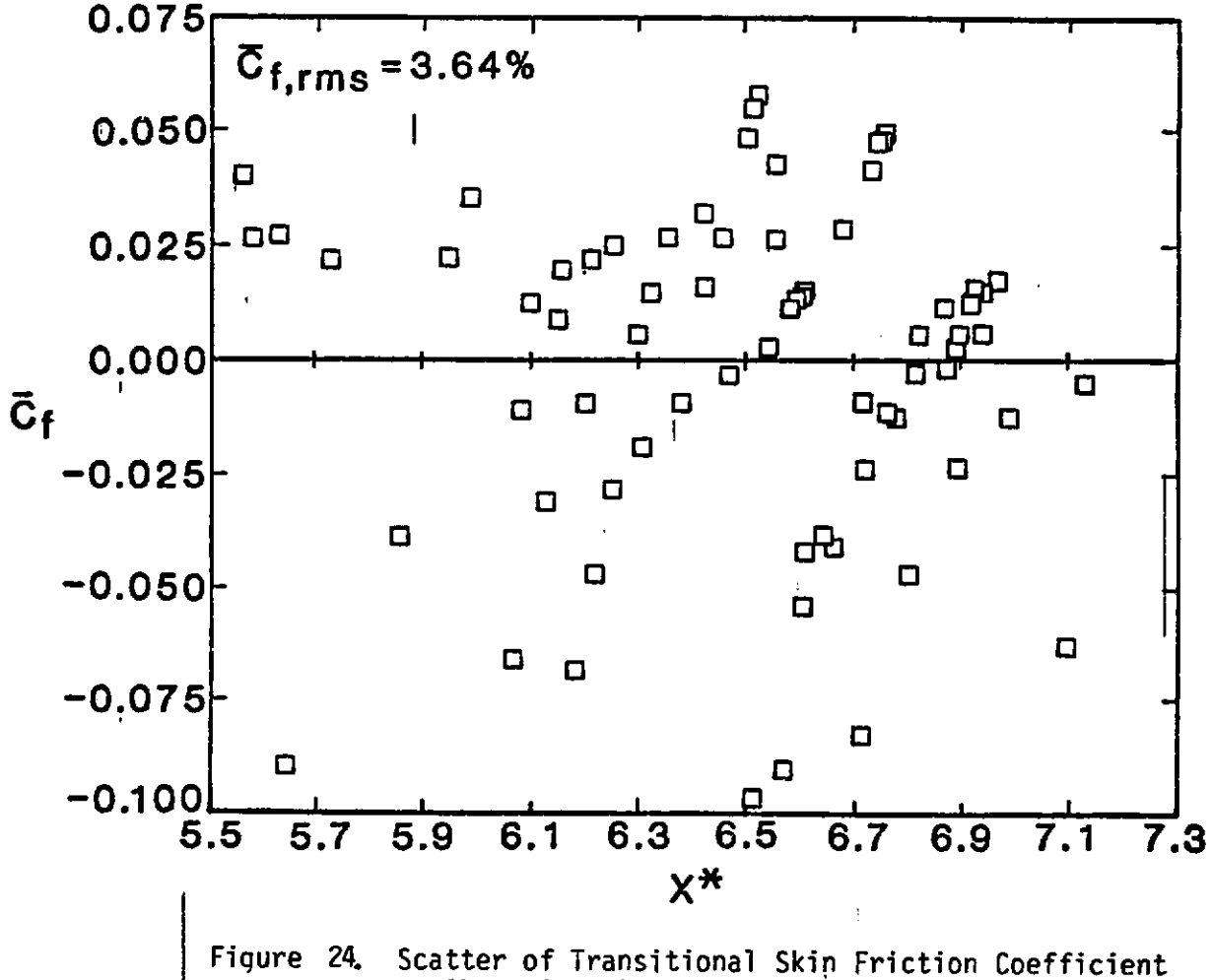

Figure 24. Scatter of Transitional Skin Friction Coefficient About Correlation for Original Flight Data.

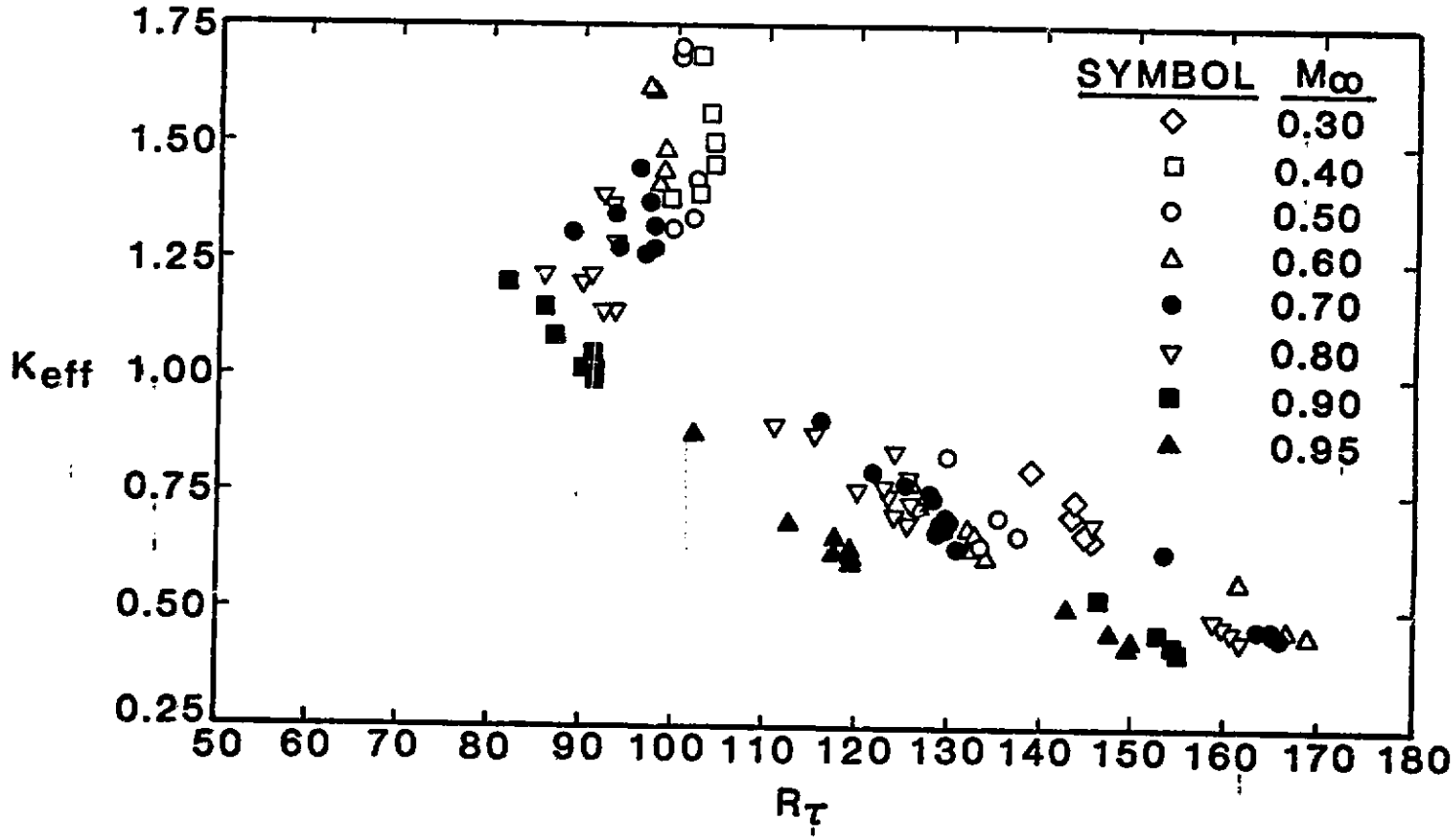

Figure 25. Distribution of Effective Probe Height as Determined from the Original Transitional Wind Tunnel Data.

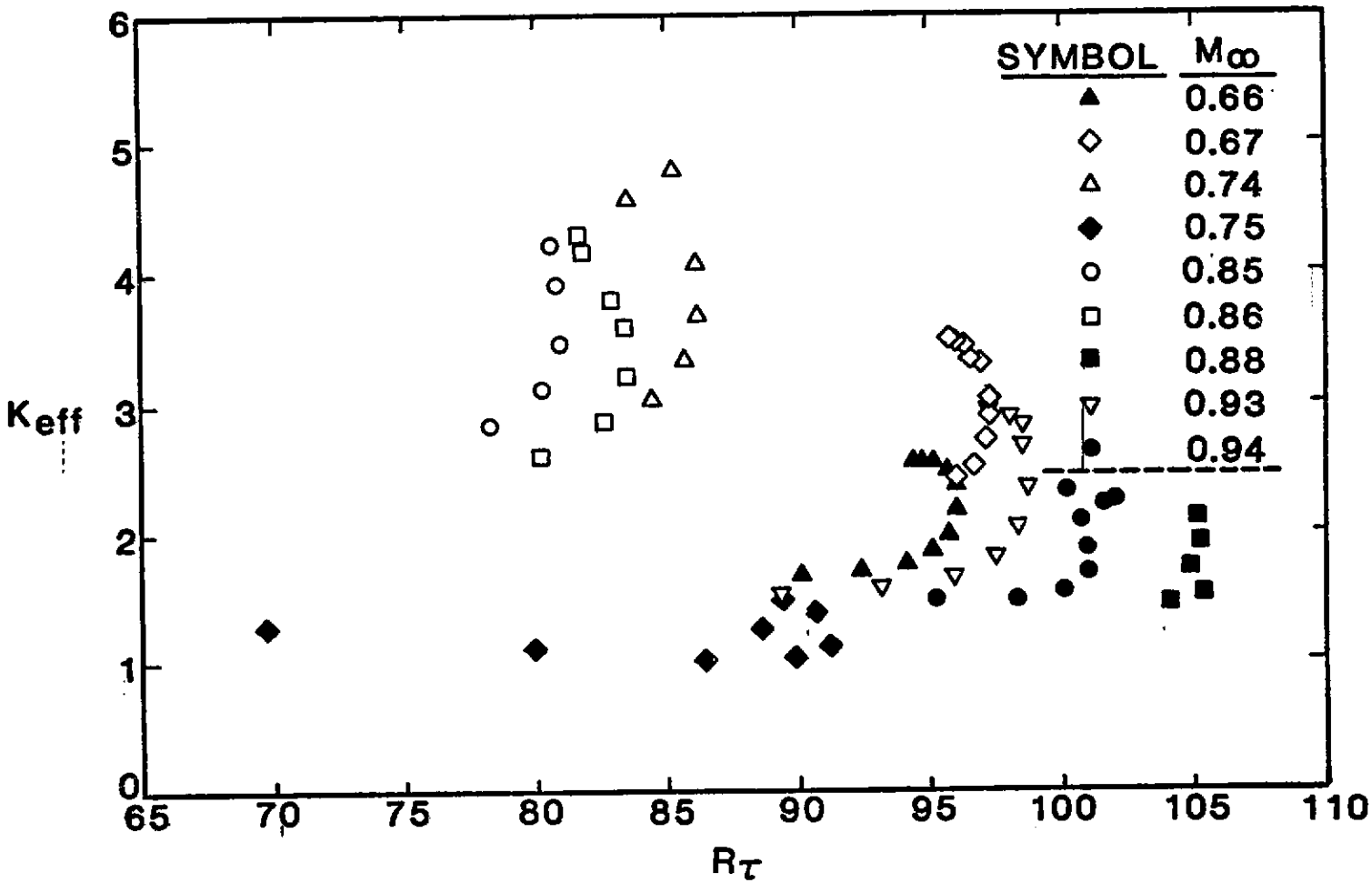

Figure 26. Distribution of Effective Probe Height as Determined from the Original Transitional Flight Data.

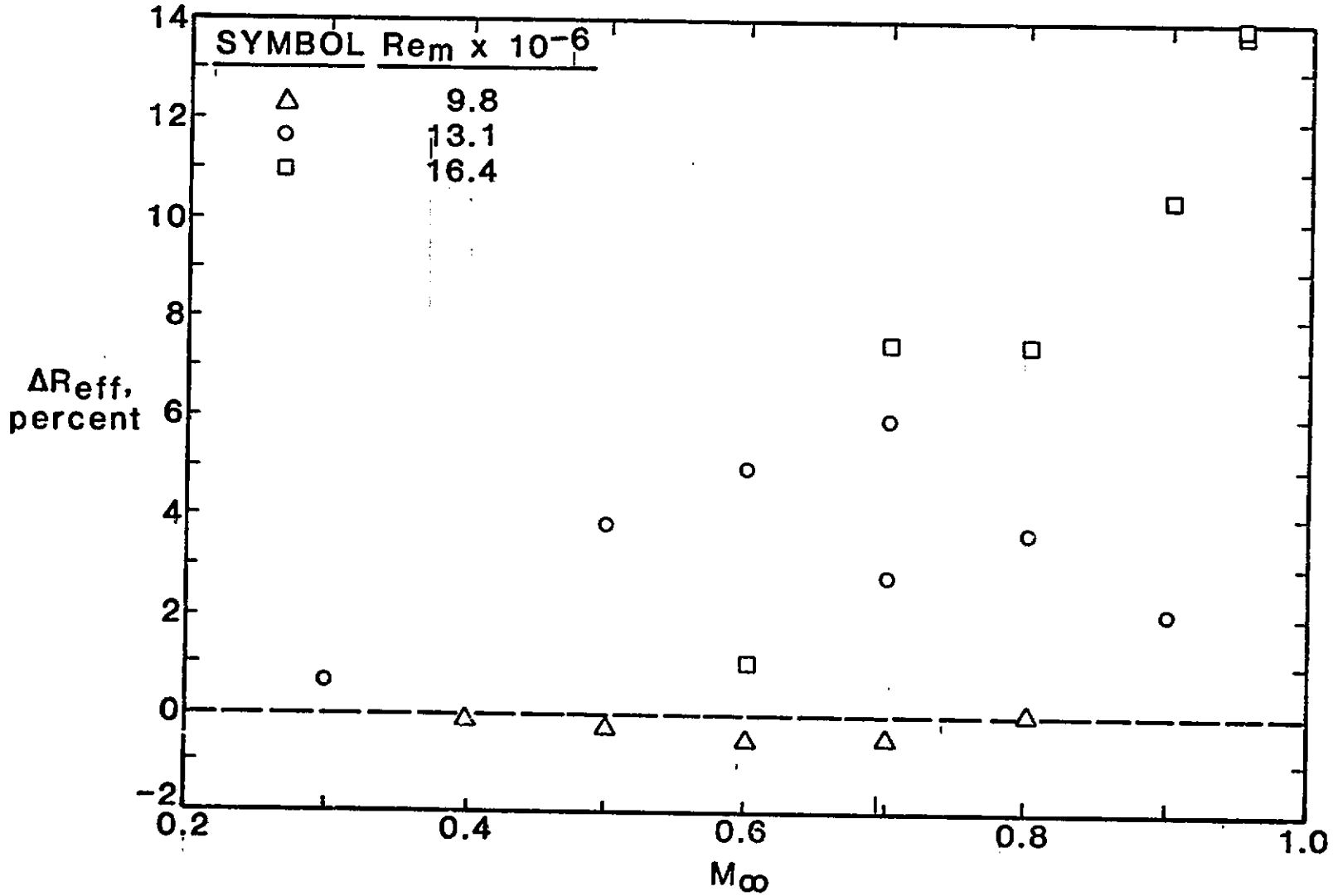

Figure 27. Distribution of Transitional Effective Reynolds Number Based on Original Data.

The wind tunnel data are corrected in a manner similar to the laminar data, viz., by referencing all cases to case 21.318 (M_∞ = 0.7, Re_m = 13.1 x 10^6, q_∞ = 26.3 kPa). Unlike the laminar data, the Re_m = 9.8 x 10^6 cases already form continuous curves of K_{eff} versus R_τ, Fig. 28. So, the only cases which are shifted are cases 70.726 (M_∞ = 0.7, Re_m = 13.1 x 10^6, q_∞ = 25.8 kPa) and 72.748 (M_∞ = 0.8, Re_m = 13.1 x 10^6, q_∞ = 29.0 kPa).

Similarly, the flight data are corrected in the same manner as the laminar data, see outline at the beginning of this chapter.

The turbulent correlations without corrections are found to be:

Wind Tunnel:

$$y^* = 0.02337\,(x^*)^2 + 0.5715x^* - 0.6202,$$

$$5.1 < x^* < 6.9,\ 9.8 \times 10^6 \leq Re_m \leq 16.4 \times 10^6,\ 0.30 \leq M_\infty \leq 0.95, \qquad (50)$$

$$\bar{C}_{f,rms} = 1.20\% \text{ , and}$$

Flight:

$$y^* = 0.007512(x^*)^2 + 0.7749x^* - 1.272,$$

$$6.0 < x^* < 7.7,\ 6.9 \times 10^6 \leq Re_m \leq 9.2 \times 10^6,\ 0.66 \leq M_\infty \leq 0.94, \qquad (51)$$

$$\bar{C}_{f,rms} = 1.10\% \text{ .}$$

Eqns. (50, 51) are plotted with the data in Figs. 29 and 30. The scatter of C_f is shown in Figs. 31 and 32. Figures 28 and 33 show the distribution of K_{eff} vs. R_τ. Notice that the relative positions of different flights in Fig. 33 is the same as shown in Fig. 21 of Ref. (8) which is reproduced in Fig. 12. This suggests that the same correction procedure can be successfully applied. It was indeed as will be shown shortly.

The effective Reynolds number distribution based on Eqns. (50) and (51) is shown in Fig. 34. Again, it does not look like the noise curve, Fig. 15,

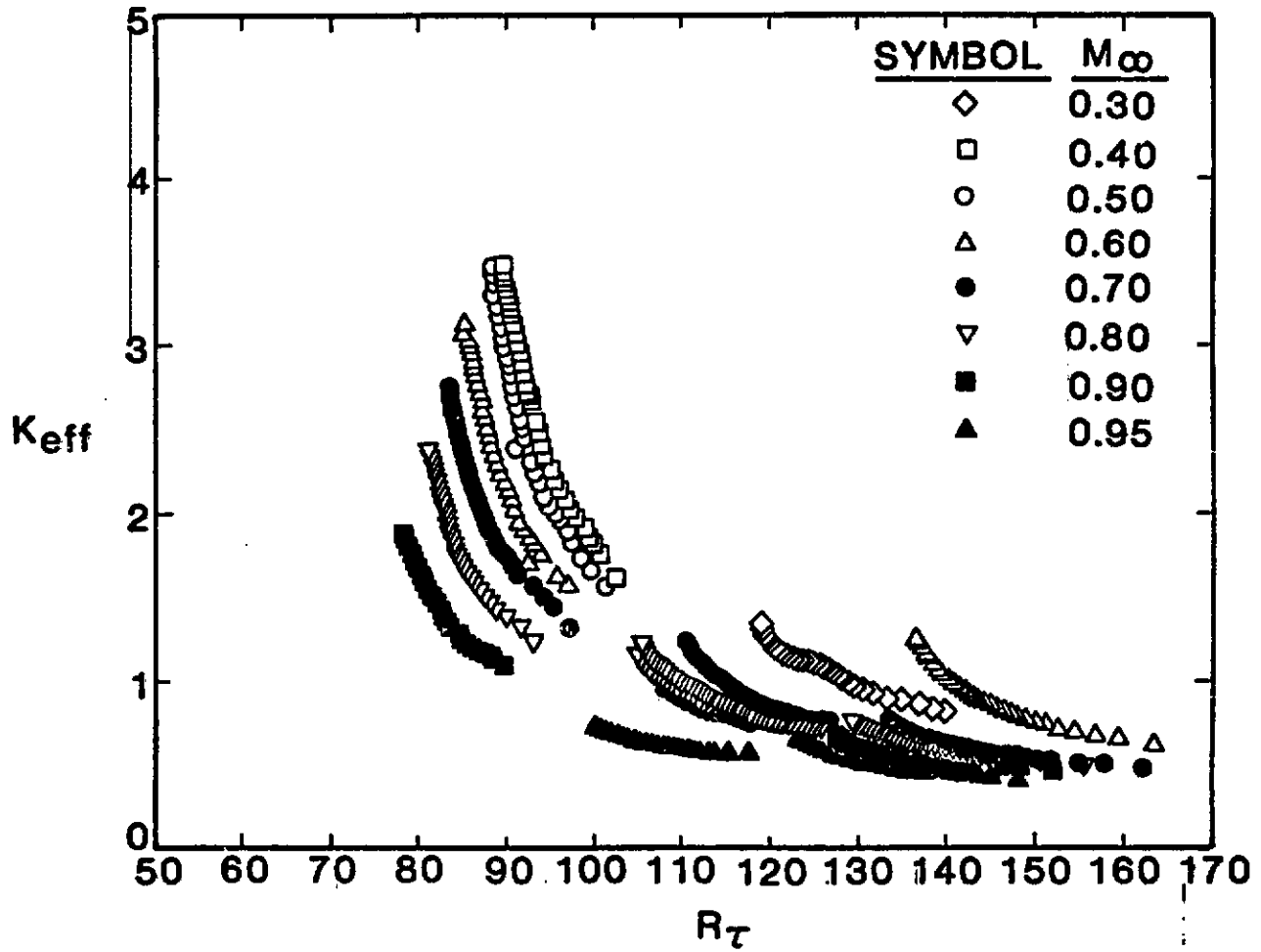

Figure 28. Distribution of Effective Probe Height as Determined from the Original Turbulent Wind Tunnel Data.

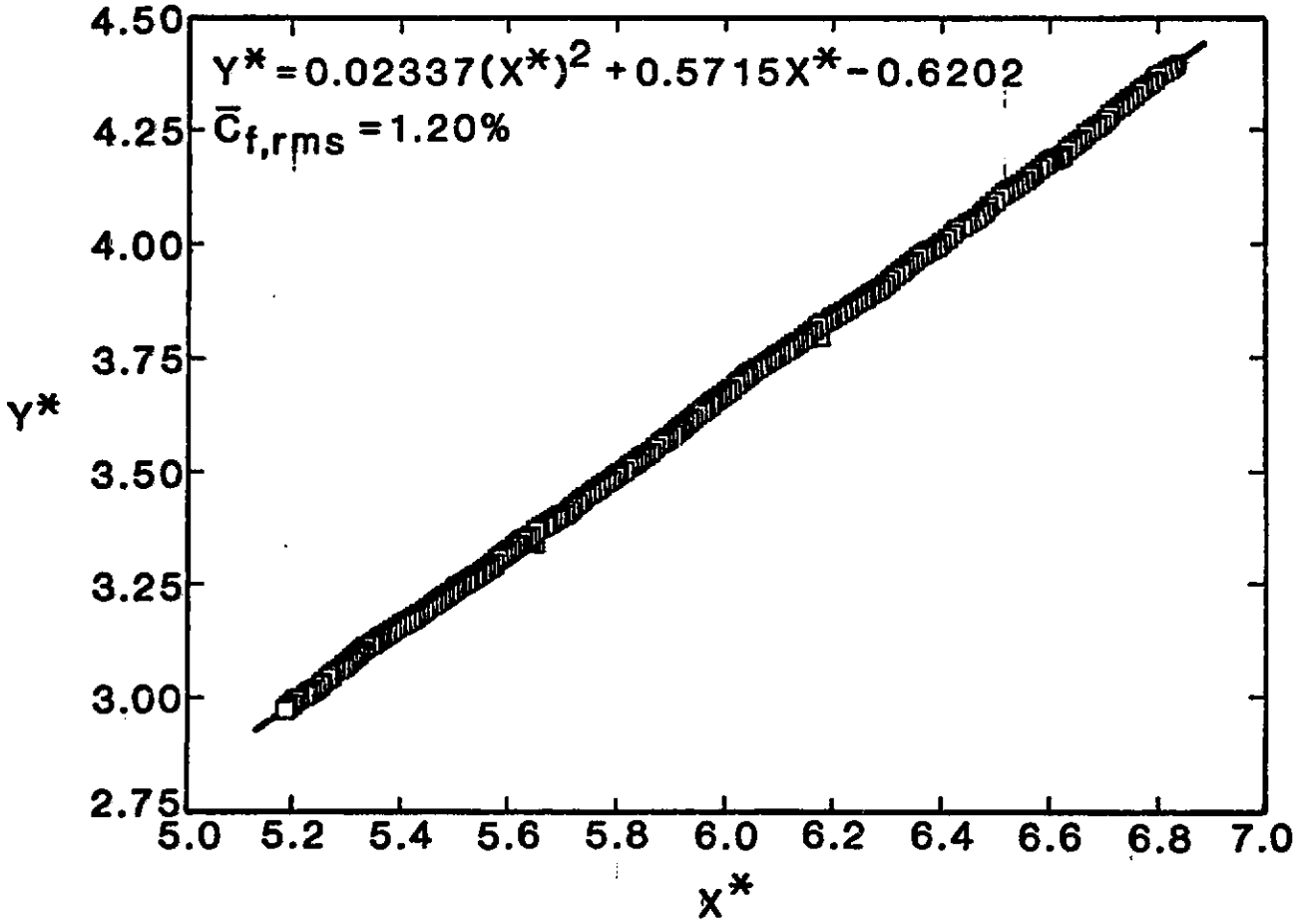

Figure 29. Turbulent Correlation for Original Wind Tunnel Data.

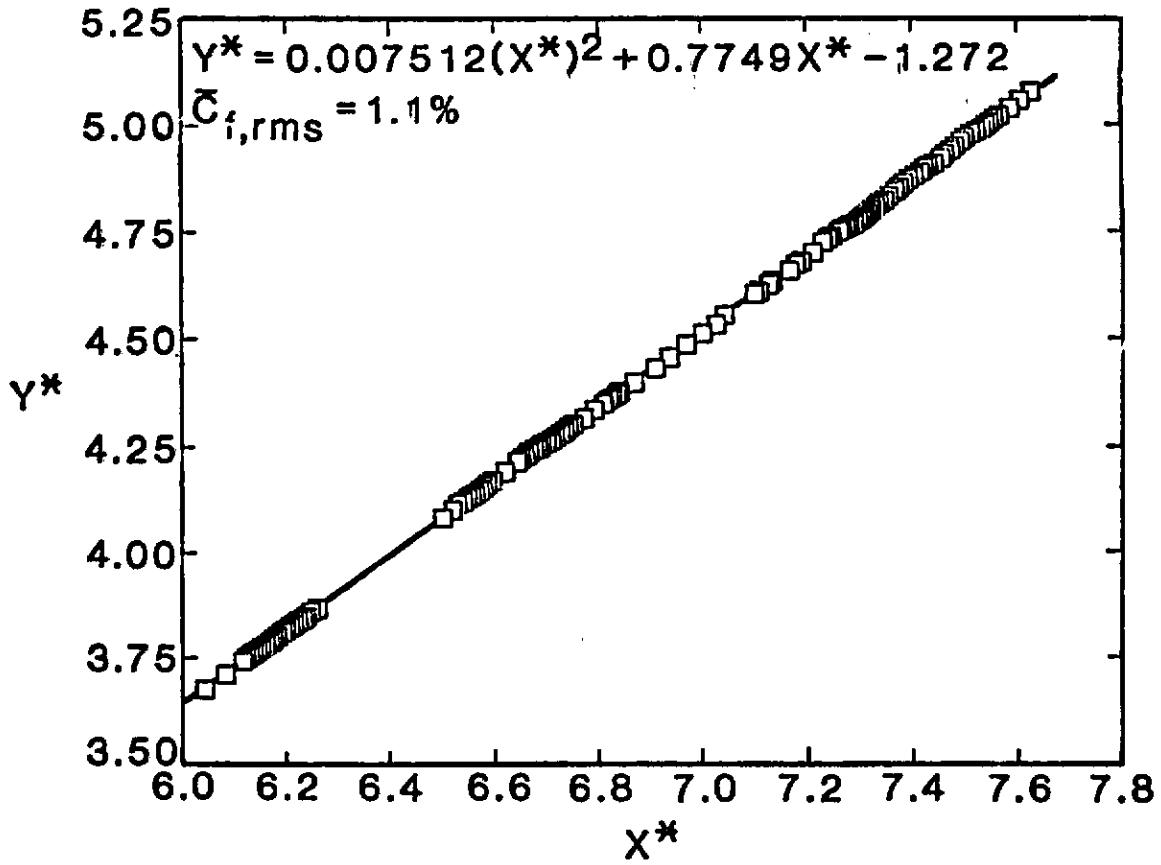

Figure 30. Turbulent Correlation for Original Flight Data.

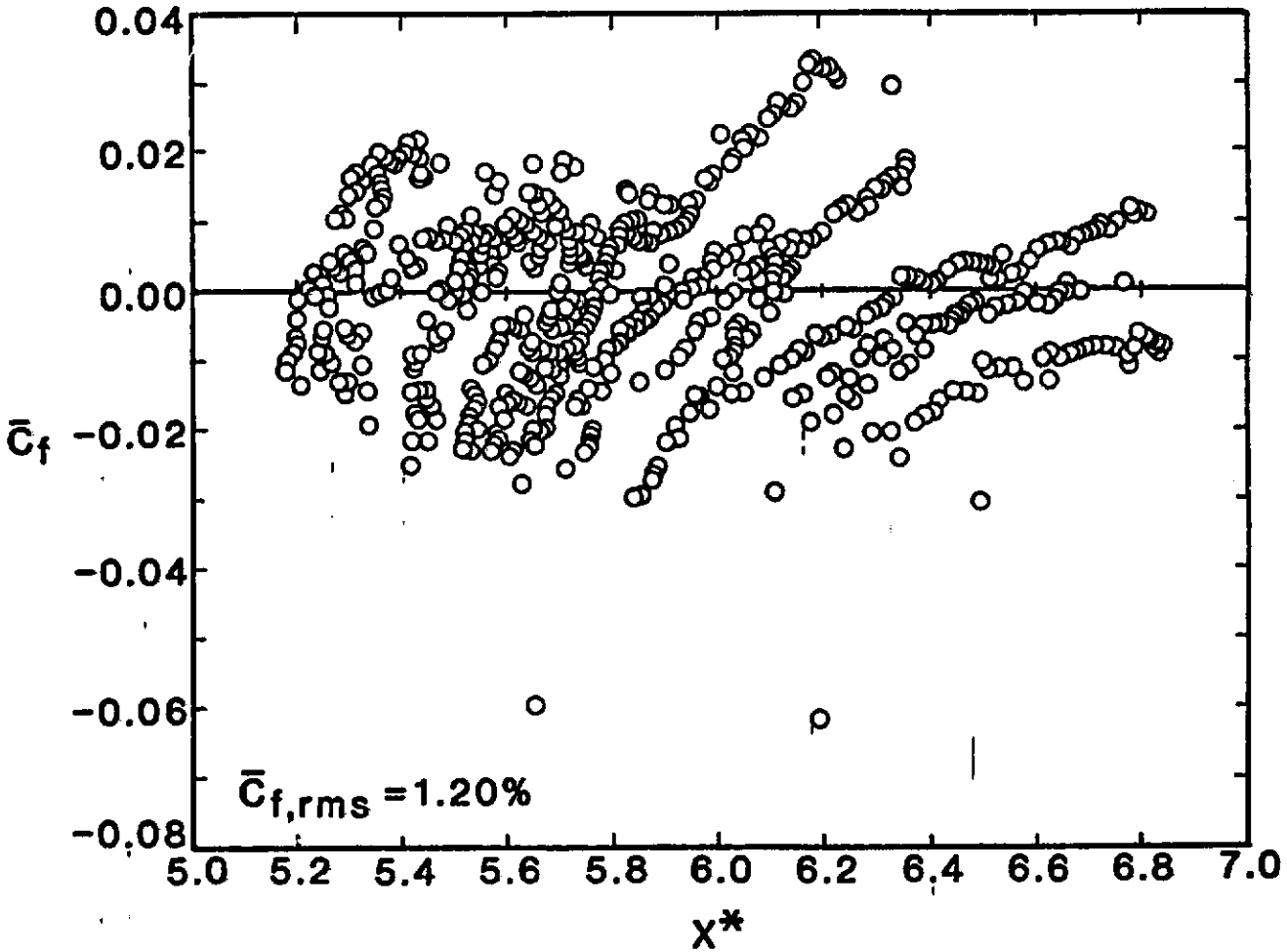

Figure 31. Scatter of Turbulent Skin Friction Coefficient About Correlation for Original Wind Tunnel Data.

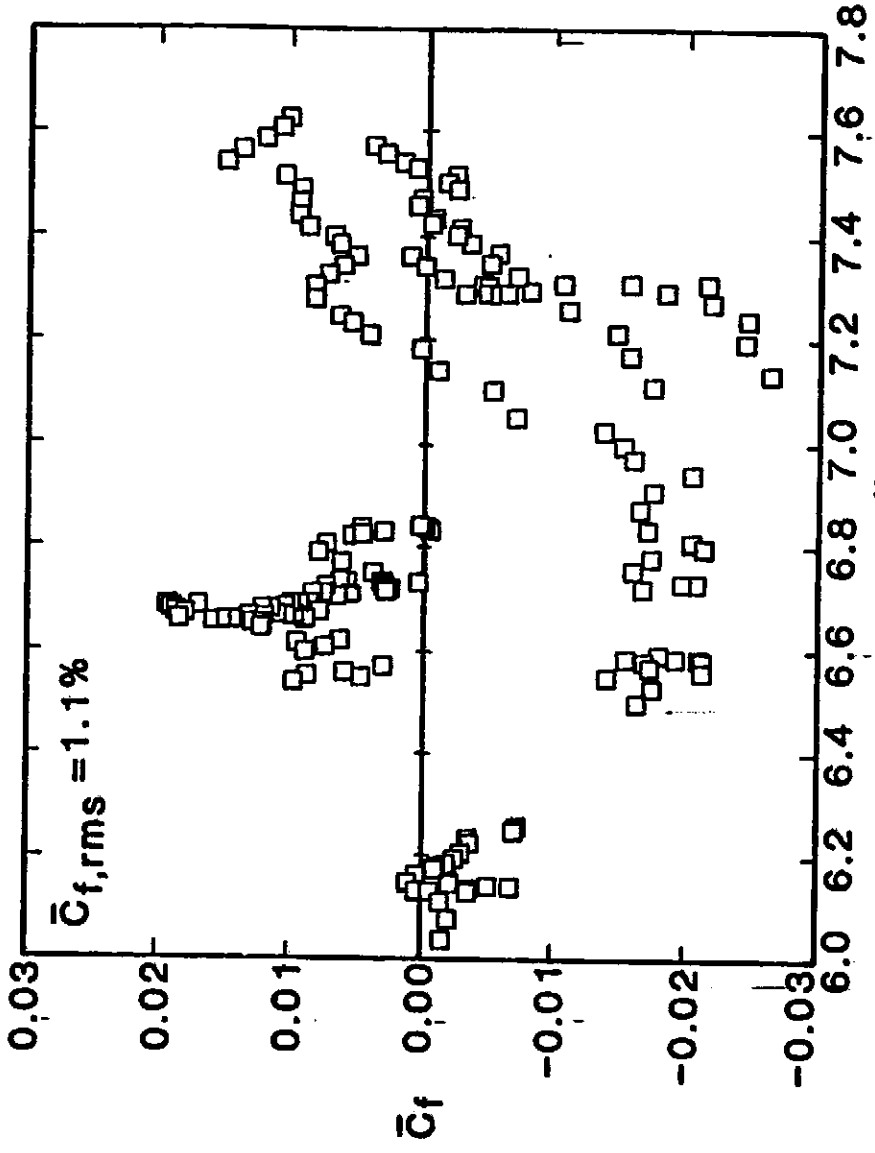

Figure 32. Scatter of Turbulent Skin Friction Coefficient About Correlation for Original Flight Data.

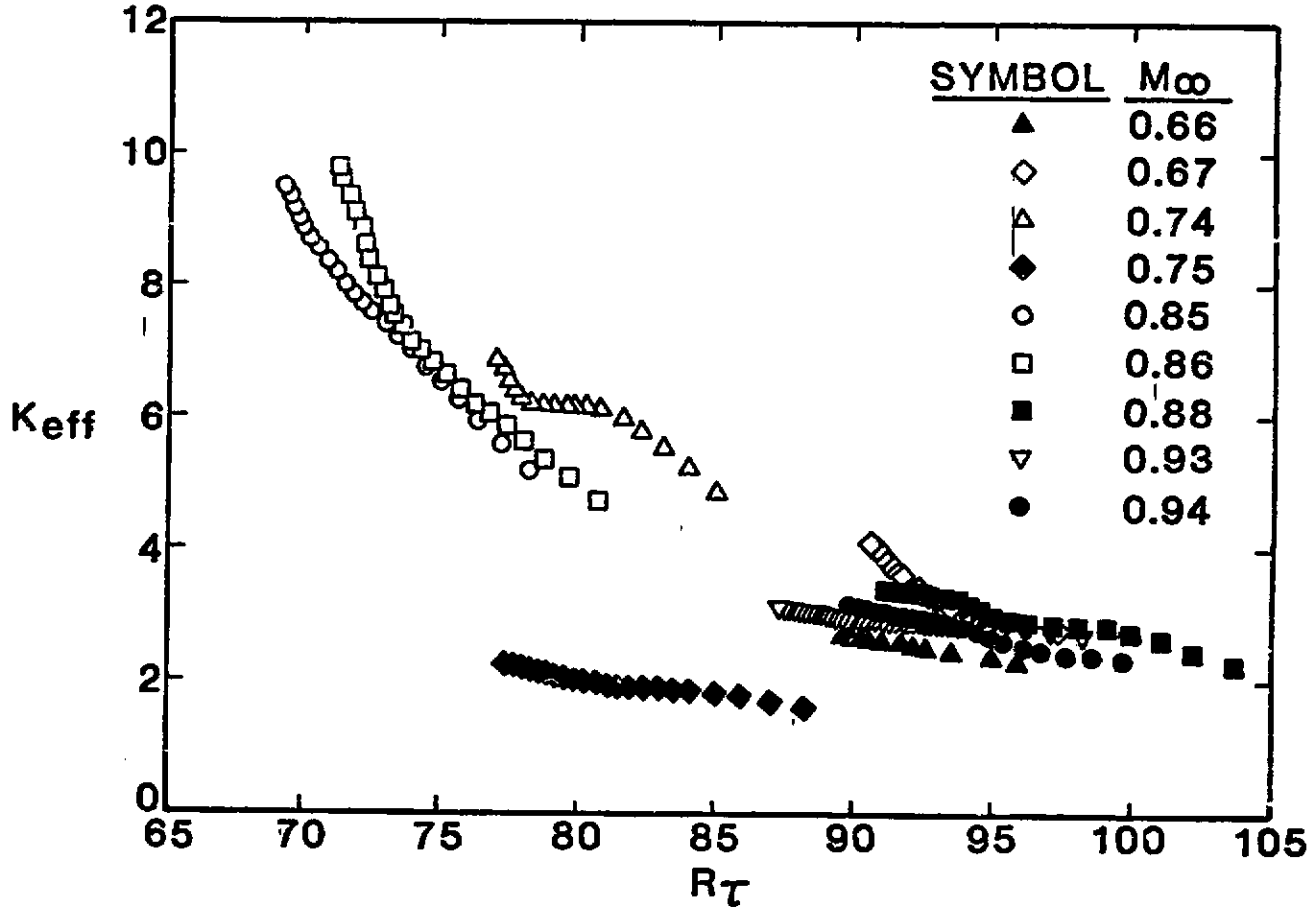

Figure 33. Distribution of Effective Probe Height as Determined from the Original Turbulent Flight Data.

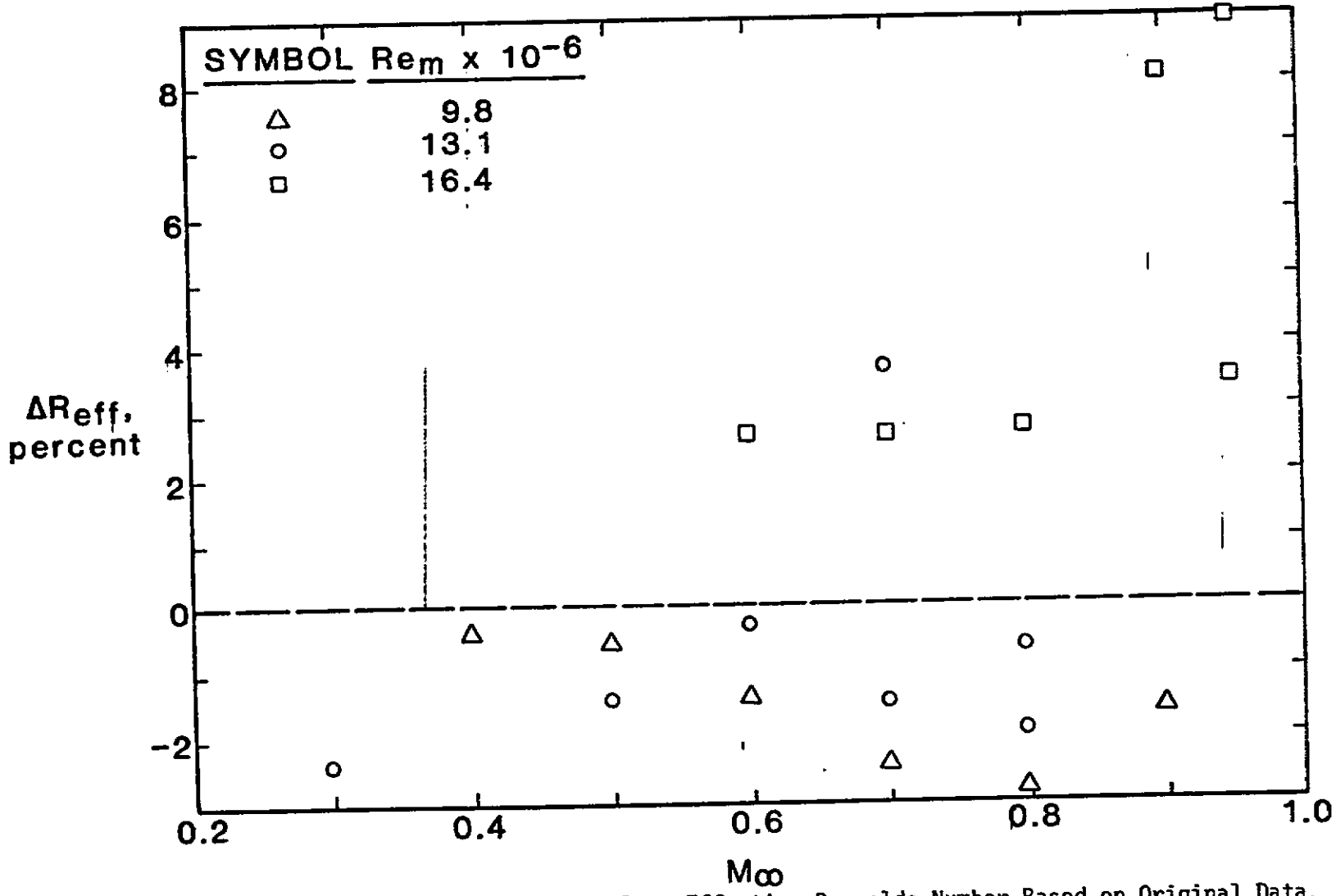

Figure 34. Distribution of Turbulent Effective Reynolds Number Based on Original Data.

which may be caused by the errors in the experimental data. The correction procedure used to correct the laminar data should result in a ΔR_{eff} distribution which is closer to the noise distribution, as can be observed in Fig. 36 of Ref. (8) reproduced in Fig. 15.

Results After Data Corrections

The Turbulent Region:

The turbulent wind tunnel data after shifting a subset of it as explained before are shown in Fig. 35. The correlation is given by

$$\begin{aligned} y^* &= 0.02282(x^*)^2 + 0.5782x^* - 0.6409, \\ 5.1 &< x^* < 6.9, \\ 9.8 \times 10^6 &\leq Re_m \leq 16.4 \times 10^6, \\ 0.30 &\leq M_\infty \leq 0.95 \text{ and} \\ \bar{C}_{f,rms} &= 1.20\% \ . \end{aligned} \tag{52}$$

Notice that there is no significant change to the correlation coefficients and accuracy since the shifting was minor. Eqn. (52) is shown in Fig. 36 with the data and the scatter of these data about Eqn. (52) is shown in Fig. 37.

The corrected flight data appear in Fig. 38. Notice, again, that the distributions of K_{eff} versus R_τ for individual cases has been altered by the correction procedure. The flight correlation is given by

$$\begin{aligned} y^* &= 0.005586(x^*)^2 + 0.7723\ x^* - 1.1867, \\ 5.45 &< x^* < 6.30, \\ 6.9 \times 10^6 &\leq Re_m \leq 9.2 \times 10^6 \\ 0.66 &\leq M_\infty \leq 0.94 \text{ and} \\ \bar{C}_{f,rms} &= 0.65\% \ . \end{aligned} \tag{53}$$

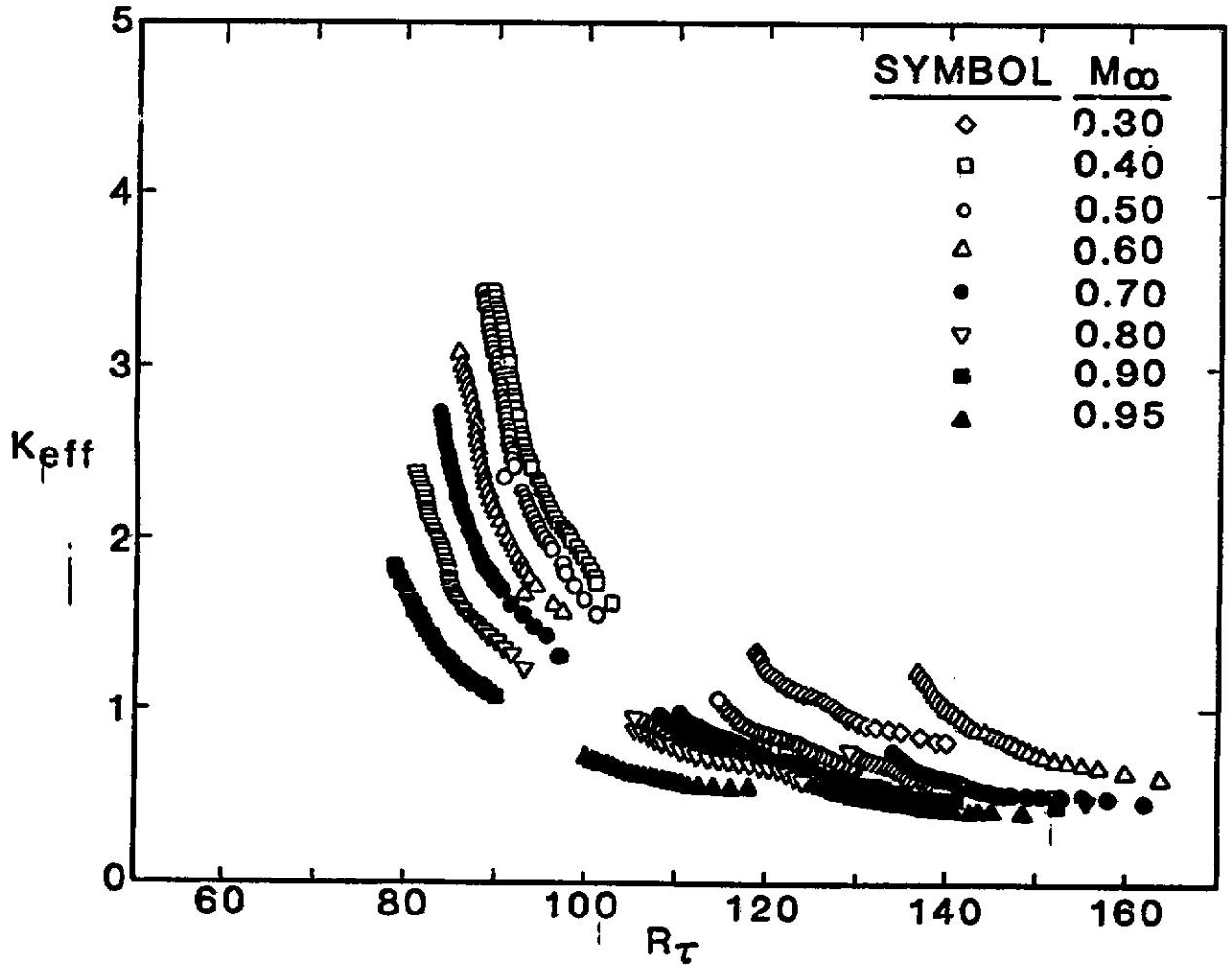

Figure 35. Distribution of Effective Probe Height as Determined from the Shifted Turbulent Wind Tunnel Data.

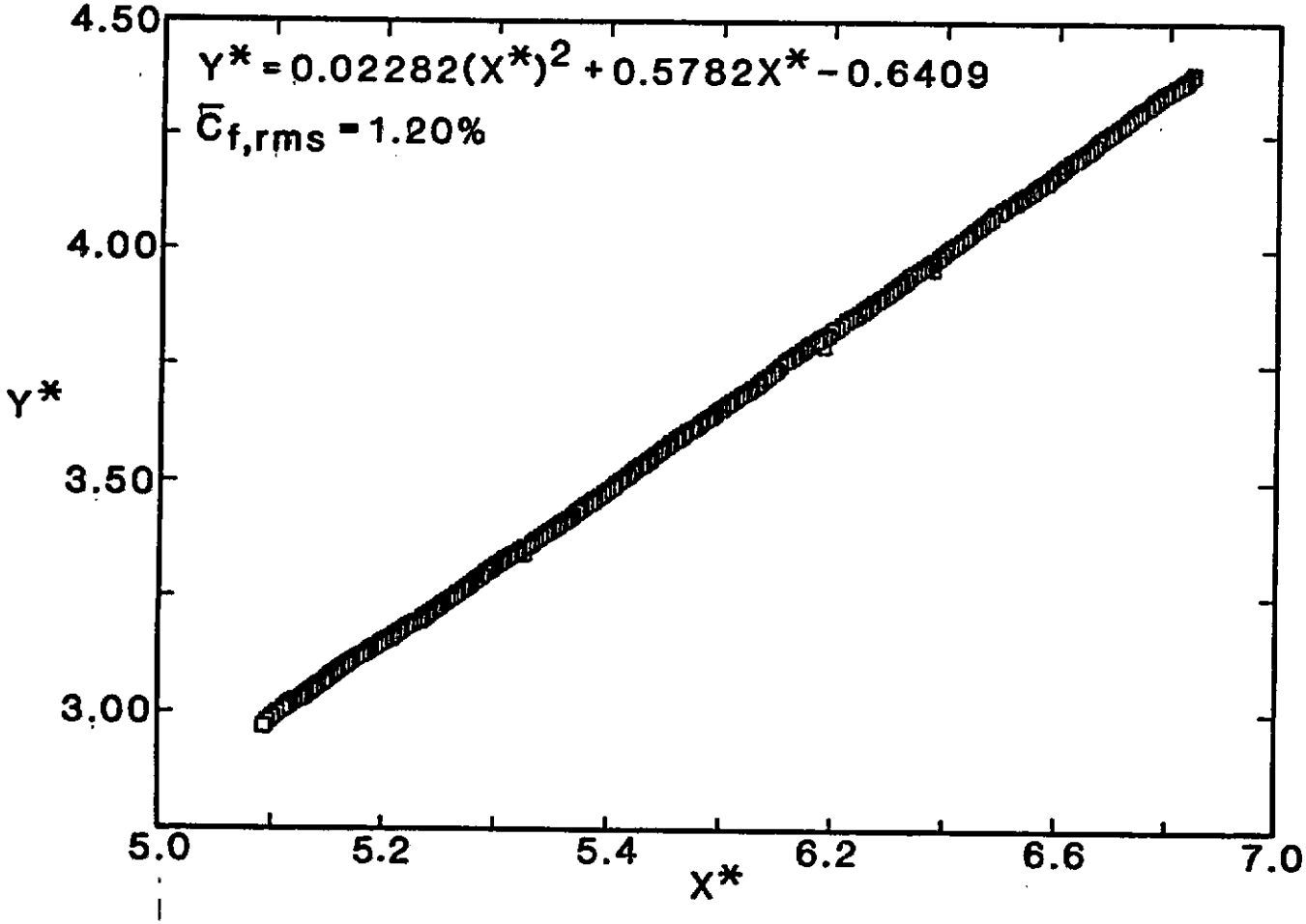

Figure 36. Turbulent Correlation for Shifted Wind Tunnel Data.

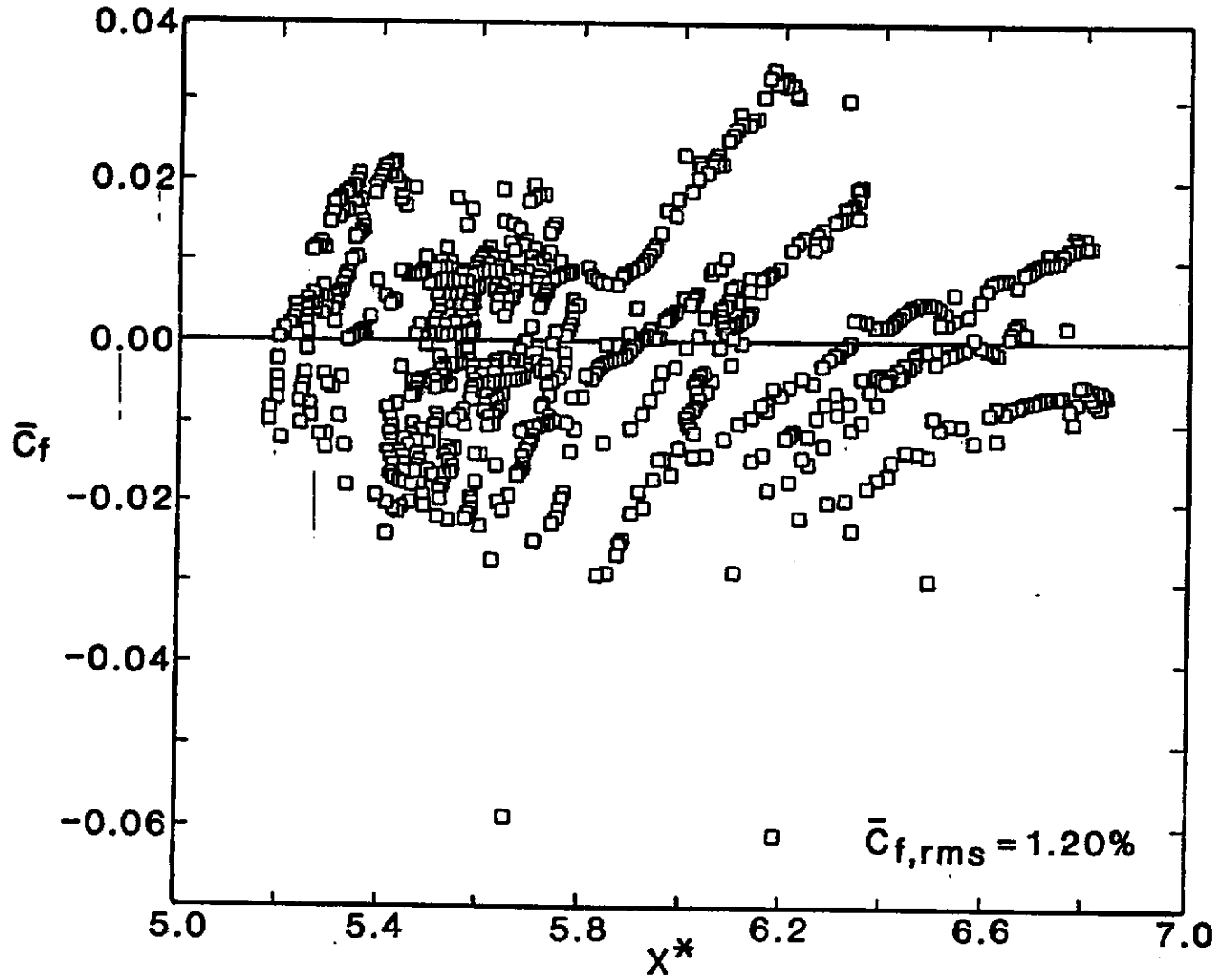

Figure 37. Scatter of Turbulent Skin Friction About Correlation for Shifted Wind Tunnel Data.

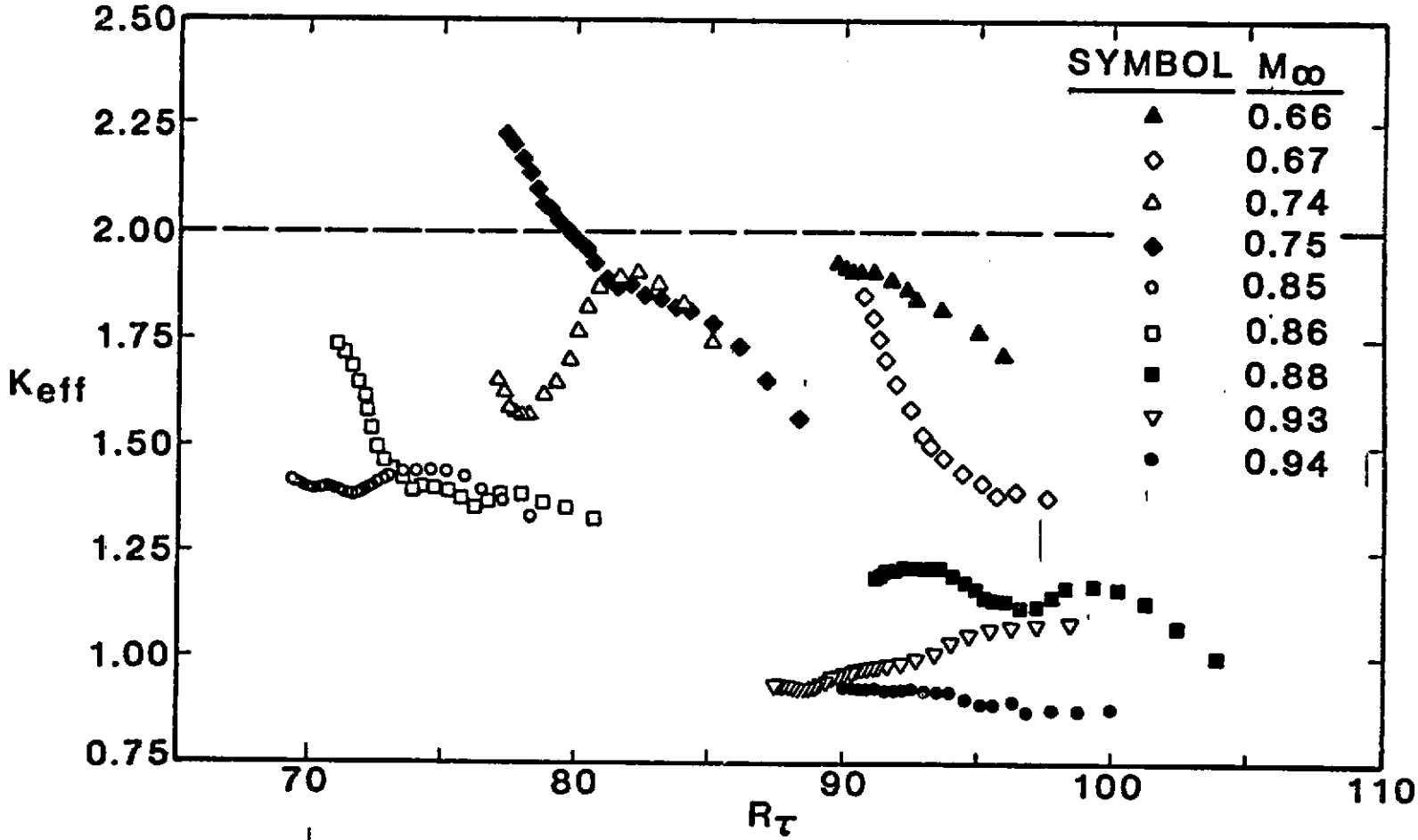

Figure 38. Distribution of Effective Probe Height as Determined from the Corrected Turbulent Flight Data.

This equation and the corrected data are shown in Fig. 39 and the data scatter are shown in Fig. 40.

Based on Eqns. (52) and (53), the ΔR_{eff} distribution is shown in Fig. 41. The distribution does not bear any resemblance to noise characteristics, Fig. 16. This means that despite the data correction, the information contained in them and their correlations are not sufficient to extract the expected $Re_{m,eff}$ information. The reason for this is the added complexity that is not present in the laminar analysis, namely the vorticity fluctuations in the boundary layer. As other investigators have found, these fluctuations are large enough to dominate pressure fluctuations caused by background noise and thus eliminate their effect on Preston-tube measurements. For example, Whitfield and Dougherty (24) reported the effects of background noise on transitional and turbulent boundary layers on the AEDC cone in four transonic wind tunnels. They noted that each of these tunnels had an acoustic resonance near $M_\infty = 0.8$, but that "the frequency components coming into resonance in these slotted-wall tunnels were so low (< approximately 200 Hz) that the cone boundary layer was insensitive to them and their influence on transition was nil." Weeks and Hodges (34) also concluded that even at noise levels up to $C_{p,rms} = 8\%$ "it was not possible to identify any effect of the noise itself on the boundary layer, and it is concluded that the acoustic disturbances generally found in the working sections of transonic wind tunnels are unlikely to exert measurable influence on the development of turbulent boundary layers on wind-tunnel models - at least for mild pressure gradients." Furthermore, Raghunathan, et al. (35) showed that turbulent skin friction coefficient was hardly affected by noise levels up to $C_{p,rms} = 2\%$. Based on these findings, the value of ΔR_{eff} for turbulent data is expected to be zero for flight and wind tunnel cases with identical freestream flow conditions. Wind tunnel case

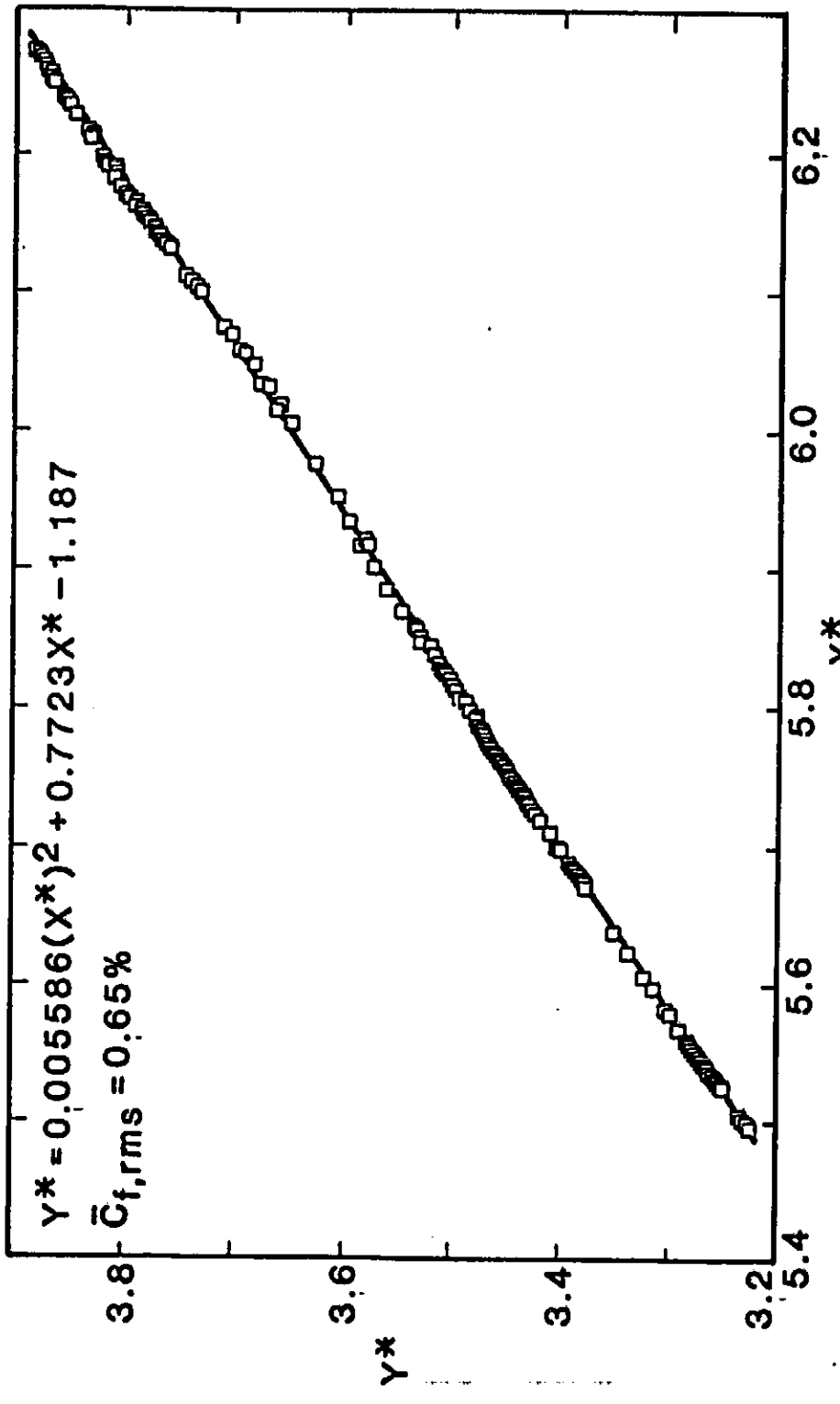

Figure 39. Turbulent Correlation for Corrected Flight Data

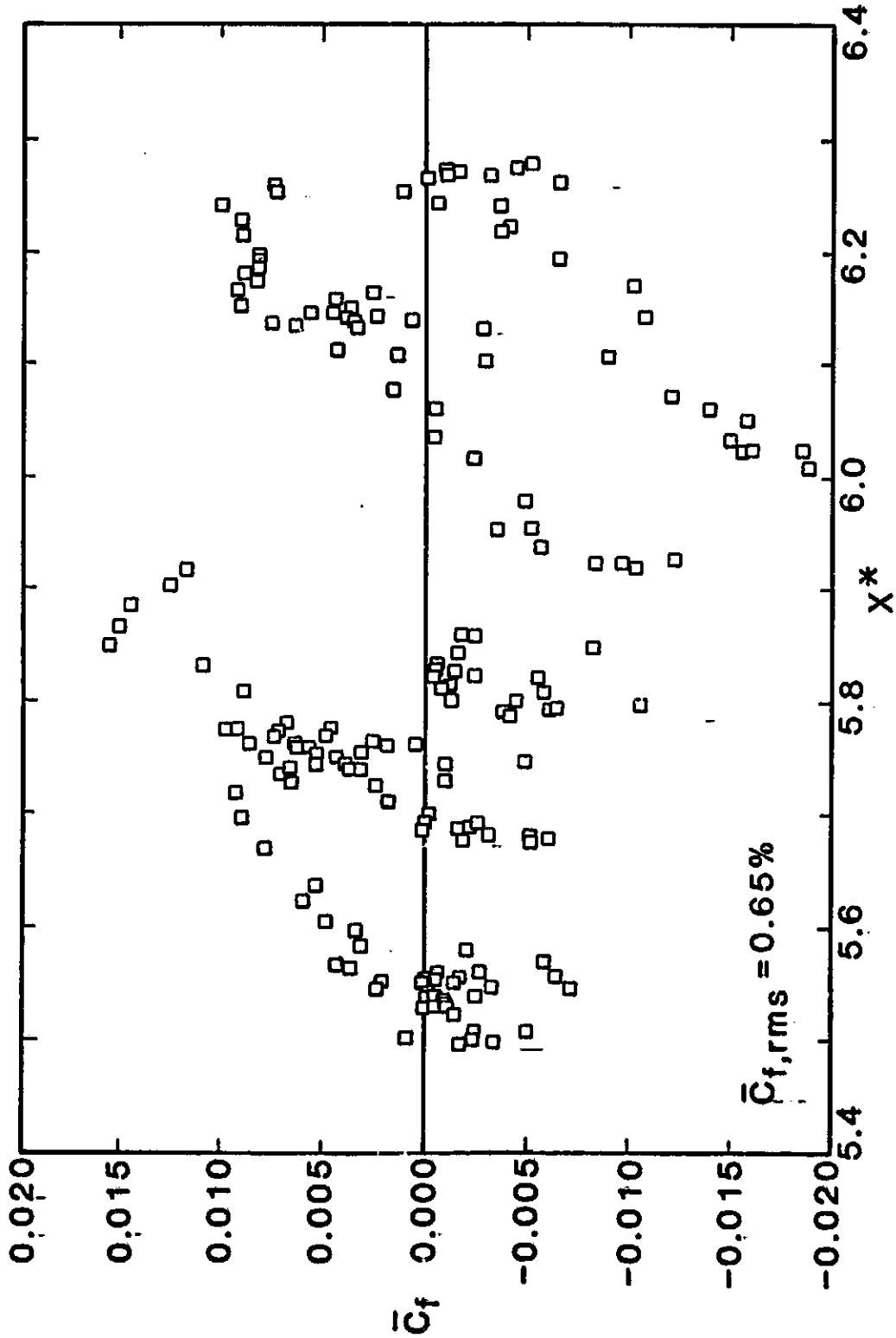

Figure 40. Scatter of Turbulent Skin Friction Coefficient About Correlation for Corrected Flight Data.

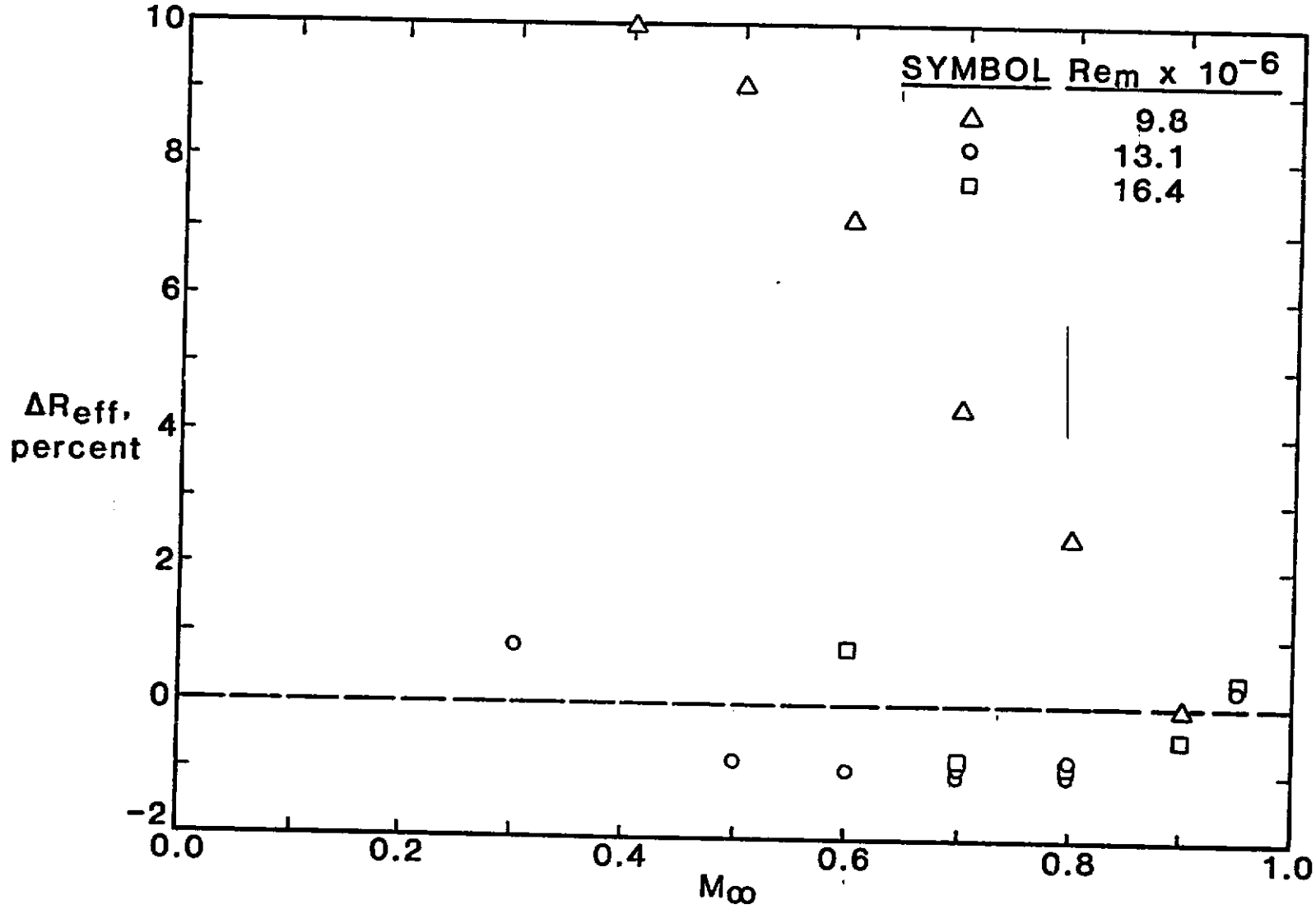

Figure 41. Distribution of Turbulent Effective Reynolds Number Based on Corrected Data.

#56.631 and flight case #333.1354 have similar flow conditions, and ΔR_{eff} for these conditions is indeed near zero, see Fig. 41 at $M_\infty = 0.90$.

As noted before, Becker and Brown (26) showed that pressure fluctuations decrease the measured Preston-tube pressure. Pressure fluctuations may be caused by background noise and/or by internal boundary layer turbulence. Since vorticity fluctuations in a laminar boundary layer are negligible, background noise and freestream turbulence dominate in this region, and the data analysis described in this report permits the calibration of these environmental effects. In transitional and turbulent boundary layers, on the other hand, internal fluctuations are dominant and background noise has no effect on the measurement of P_p and, therefore, cannot be calibrated. The $Re_m = 9.8 \times 10^6$ data show the greatest deviation of ΔR_{eff} from zero, Fig. 41. The reason is that this group of data has the greatest experimental uncertainty in P_p measurements, and it is the reference for correcting the flight data (i.e., $\bar{R}_\tau$ values at which correction is made correspond to a wind tunnel Reynolds number of 9.8×10^6. Thus, the corrections for the low Reynolds number, turbulent flight data appear to have been inadequate.

The Transitional Region:

In order to insure the continuity of the K_{eff} distribution during transition, the $\Delta P_{o,shift}$ increments used in the correction of flight data must vary gradually from the $\Delta P_{o,shift}$ values used in the laminar correction and those used in the turbulent correction. We used a linear variation in the following form:

$$\Delta P_{o,shift} = \Delta P_{o,shift,\ell} + \frac{x - x_t}{x_E - x_t} (\Delta P_{o,shift,T} - \Delta P_{o,shift,\ell}).$$

Fig. 42 shows the continuous $K_{eff} - R_\tau$ distribution for case 19.289 in the three regions of the boundary layer. The results after shifting the wind tunnel data and correcting the flight data are as follows.

Wind Tunnel:

$$y^* = 0.7814(x^*)^2 - 0.07967x^* + 1.2936,$$
$$5.25 < x^* < 6.30,$$
$$9.8 \times 10^6 \leq Re_m \leq 16.4 \times 10^6,$$
$$0.30 \leq M_\infty \leq 0.95, \qquad (54)$$

$\bar{C}_{f,rms} = 2.49\%$ and

Flight:

$$y^* = 0.09131(x^*)^2 - 0.2596x^* + 1.9066,$$
$$< x^* <$$
$$6.9 \times 10^6 \leq Re_m \leq 9.2 \times 10^6,$$
$$0.66 \leq M_\infty \leq 0.94 \text{ and} \qquad (55)$$

$\bar{C}_{f,rms} = 2.31\%$

Eqn. (54) with the wind tunnel data and their scatter are shown in Figs. 43, 44. Fig. 45 shows the $K_{eff} - R_\tau$ distribution. Figs. 46 through 48 show the same for the flight data.

Based on Eqn. (54) and (55), the ΔR_{eff} distribution is shown in Fig. 49. As expected the distribution cannot be correlated with noise effects for the same reason discussed in the turbulent analysis last section. Furthermore, the authors (8) have shown that the extent of transition, x_E -

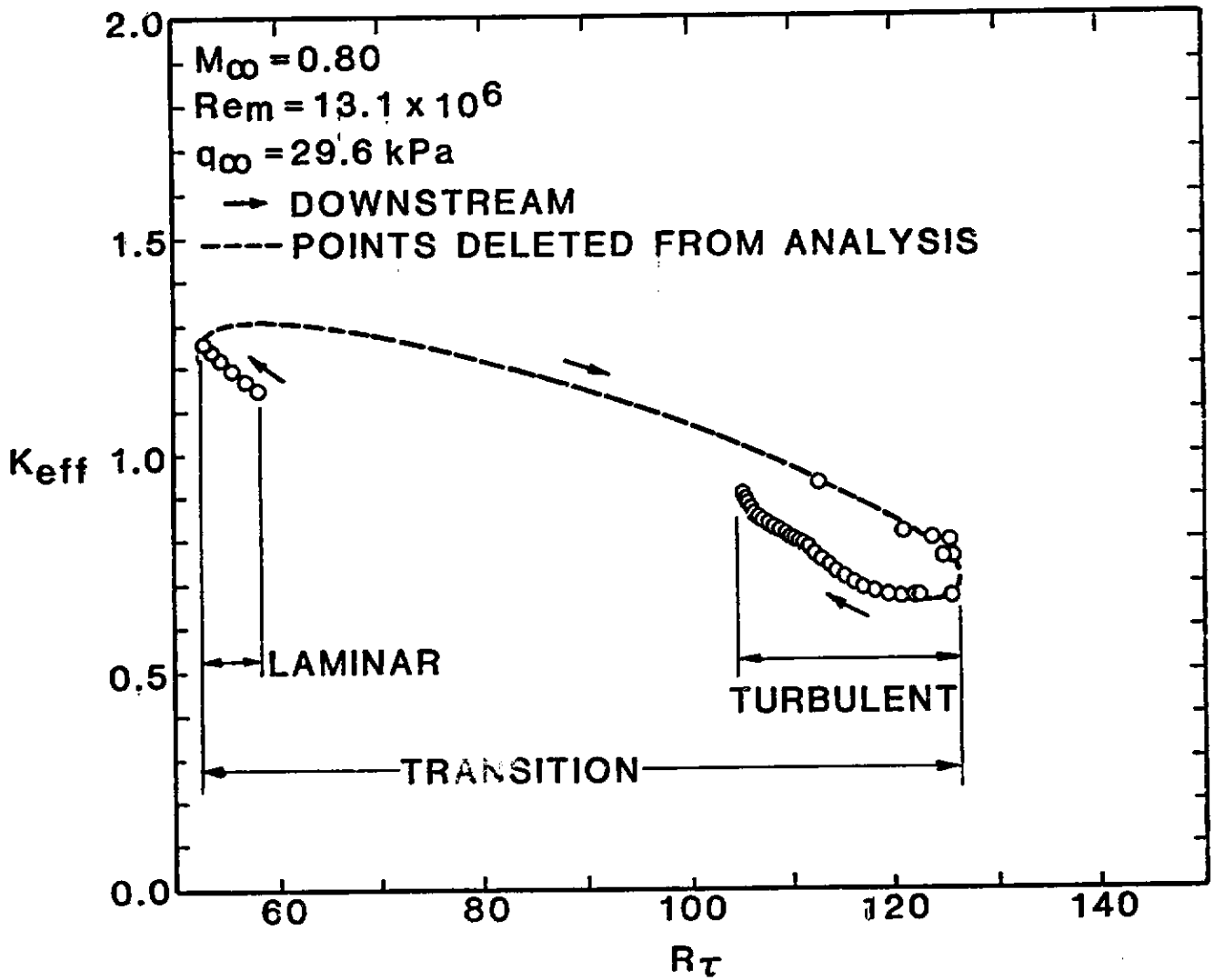

Figure 42. Distribution of Effective Probe Height for a Typical Case in the Three Boundary Layer Regions.

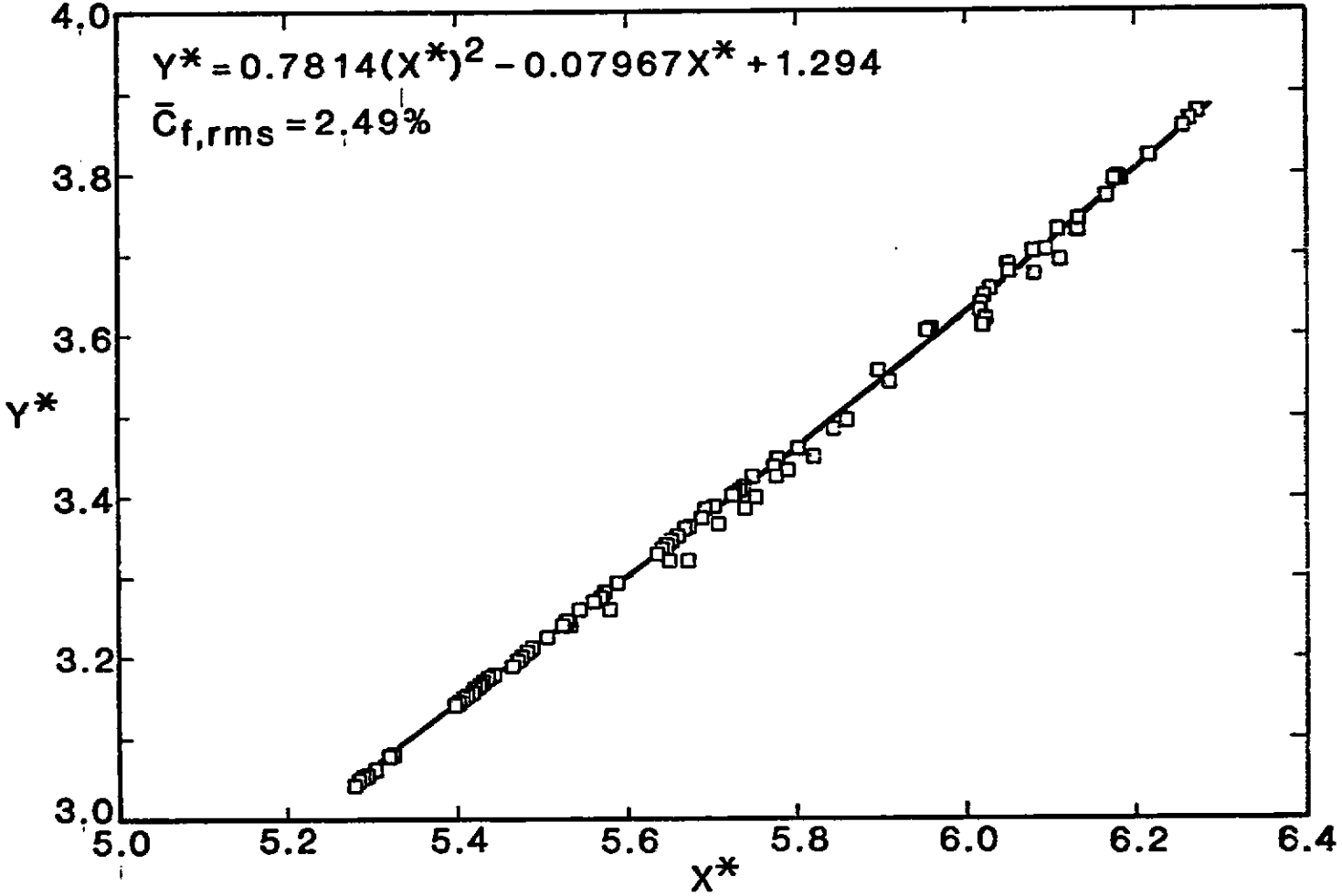

Figure 43. Transitional Correlation for Shifted Wind Tunnel Data.

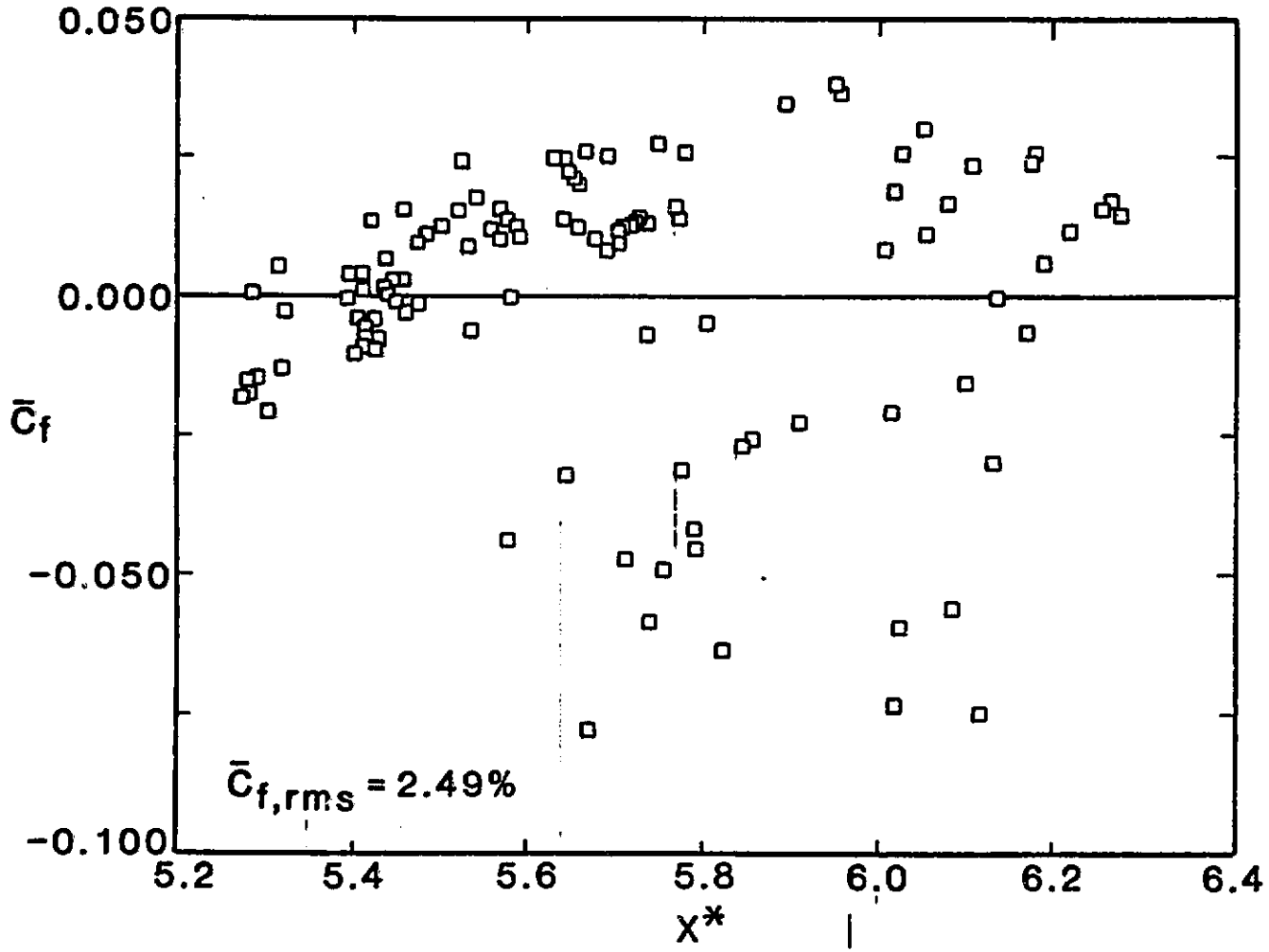

Figure 44. Scatter of Transitional Skin Friction Coefficient About Correlation for Shifted Wind Tunnel Data.

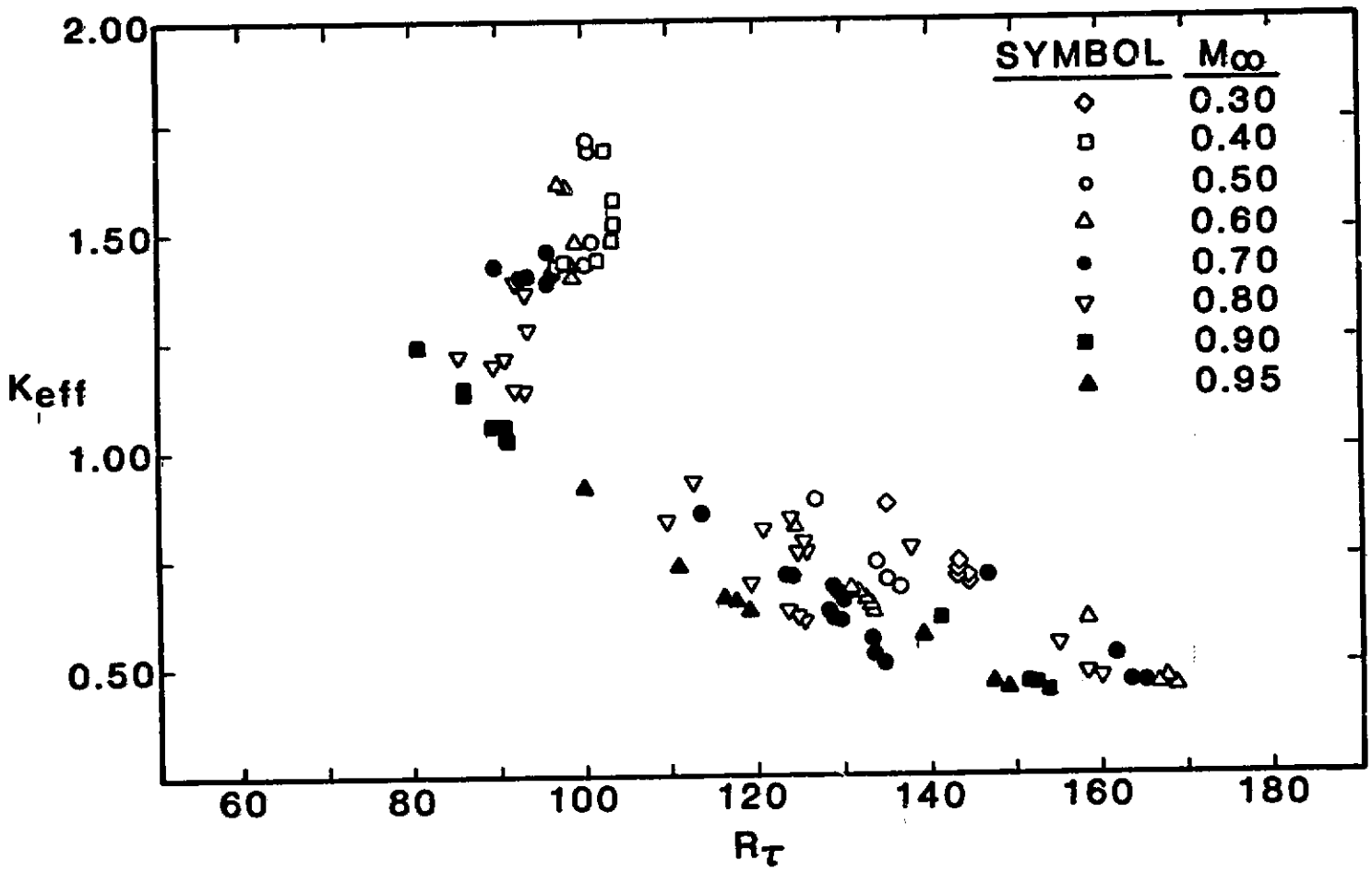

Figure 45. Distribution of Effective Probe Height as Determined from the Shifted Transitional Wind Tunnel Data.

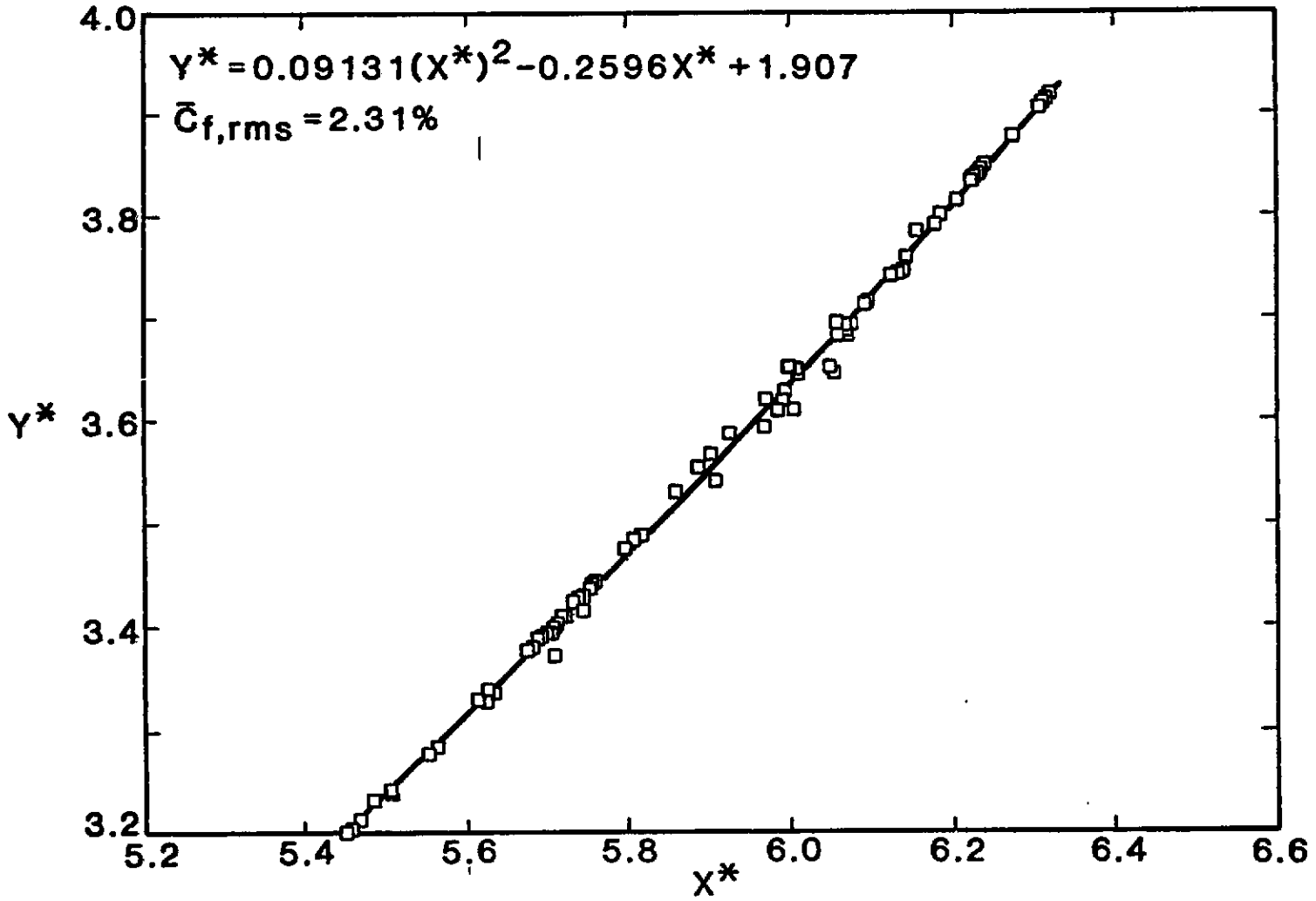

Figure 46. Transitional Correlation for Corrected Flight Data.

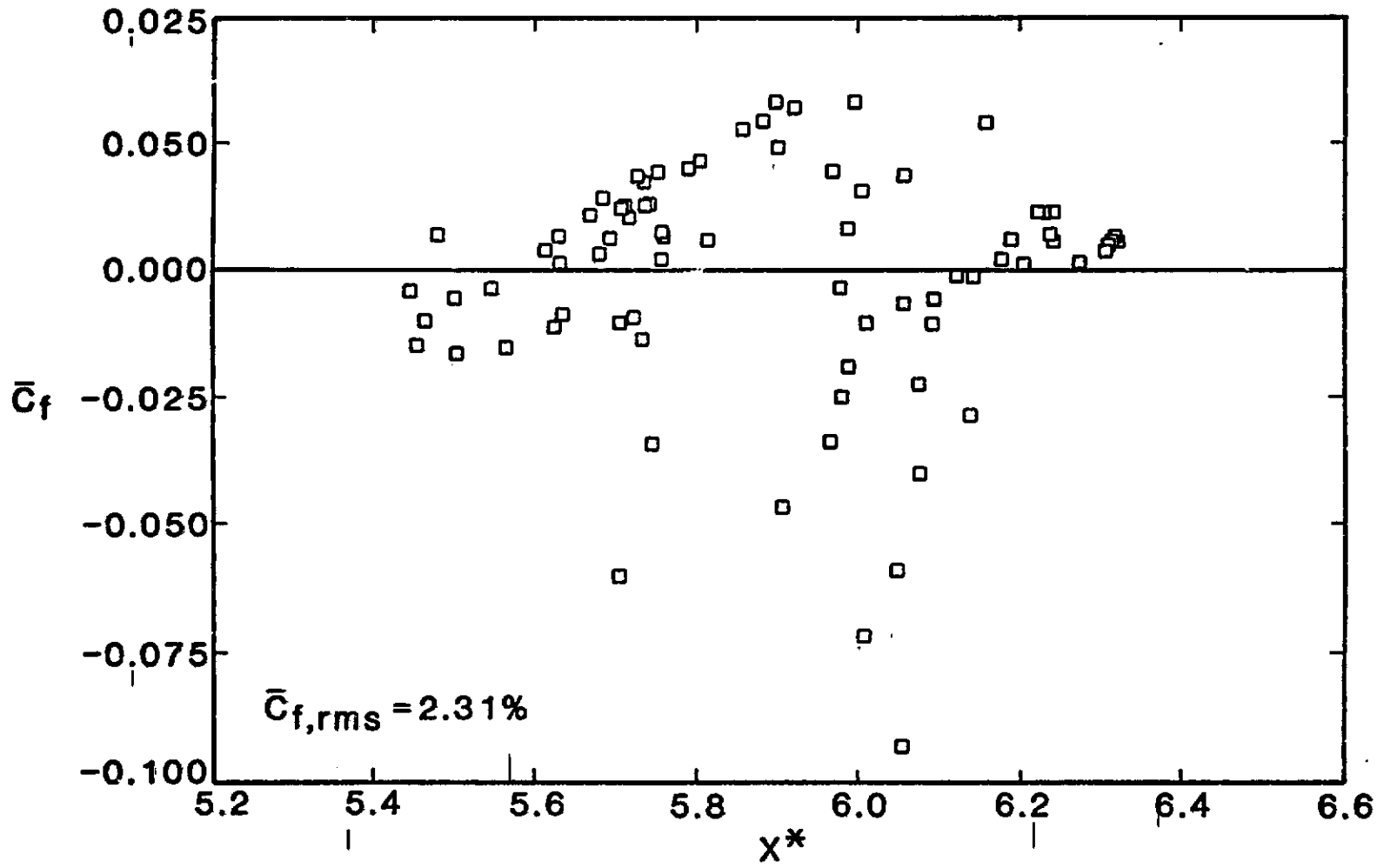

Figure 47. Scatter of Transitional Skin Friction Coefficient About Correlation for Corrected Flight Data.

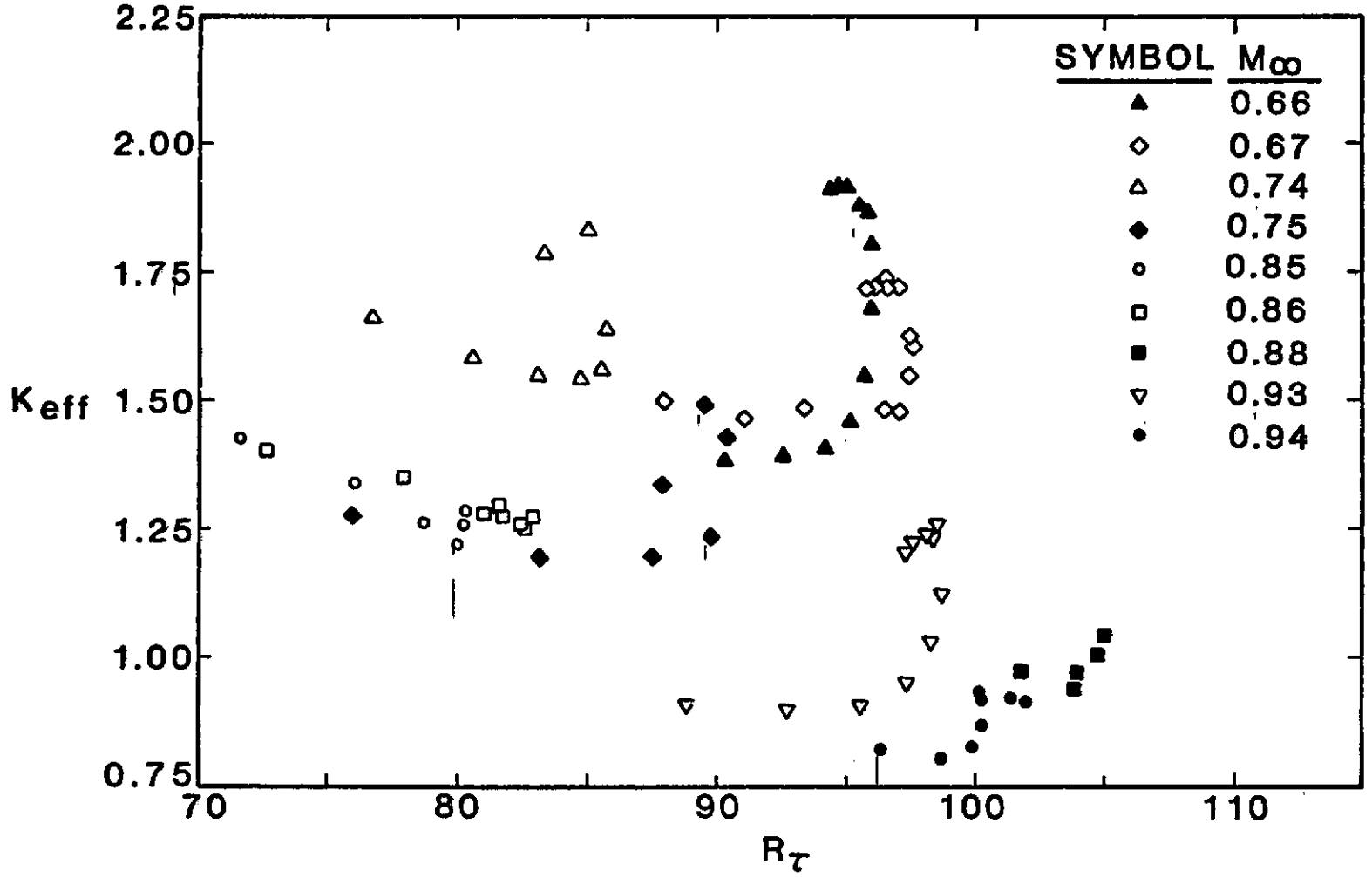

Figure 48. Distribution of Effective Probe Height as Determined from the Corrected Transitional Flight Data

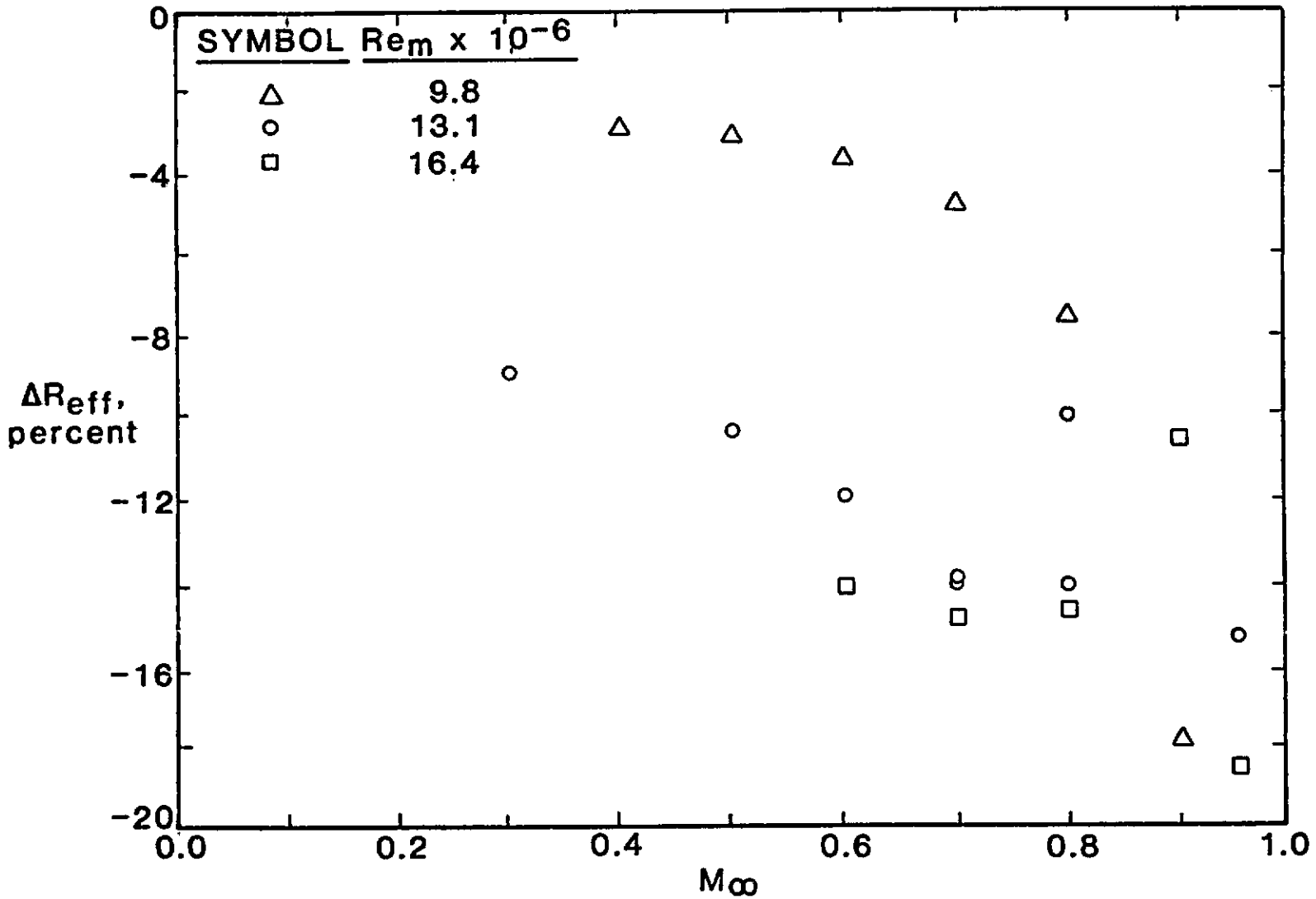

Figure 49. Distribution of Transitional Effective Reynolds Number Based on Corrected Data.

x_t, is larger in flight than in wind tunnel tests with the same flow conditions. This means that the transition process requires a larger distance in flight than in a wind tunnel, and the rms values of P_p indicate the laminar break-down in flight is more violent and, hence, creates larger vorticity. Indeed the rms fluctuating Preston-tube pressure coefficient in flight #333.1354 is nearly twice that in wind tunnel case #56.631. (These are the two cases with similar freestream conditions).

We conclude, therefore, that the calibration of wind tunnel environmental effects on Preston-tube measurements or theoretical skin friction by an effective freestream unit Reynolds number can only be achieved by analyzing the laminar data as described in this report.

CHAPTER V

SUMMARY AND CONCLUSIONS

A new procedure has been developed which uses Preston-tube data from wind tunnel and flight tests of the AEDC Transition Cone to compute an effective unit Reynolds number for transonic wind tunnels. The resulting effective Reynolds numbers are based on the requirement that the average Preston-tube pressure for a given type of boundary layer be equal in the wind tunnel and flight for a given M_∞ and q_∞ but differing Re_m. The procedure has been applied to laminar, transitional, and fully-developed turbulent boundary layers by using wind tunnel data obtained in the 11-TWT. The results for laminar boundary layers indicate that noise in the 11-TWT causes Preston-tube pressures to be low compared to the values that exist in flight for the same M_∞, Re_m, and q_∞. This results in the effective unit Reynolds number being higher than the reference or operating value by approximately 6.5%. Thus, in order to increase the laminar Preston-tube pressures, obtained in the 11-TWT, to match the corresponding flight data, it is necessary to increase the tunnel unit Reynolds number by 6.5%.

This unit Reynolds number trend is opposite to what is found in the technical literature on the effects of noise on boundary layer transition. In that context, transonic wind tunnel noise is known to promote early transition and is frequently viewed as being analogous to an increase in unit Reynolds number. With this perspective of matching the location of transition, transonic tunnels are though to have "effective" Reynolds numbers that are somewhat higher than the operating value selected by the tunnel operators. However, if for example a transonic tunnel is operated at a lower unit Reynolds to achieve matching of flight values of transition location on the

AEDC cone, one would not expect a match in drag values. In fact, the lower tunnel Reynolds number would result in lower skin friction within both the laminar† and turbulent portions of the boundary layer.

Unfortunately, actual measurements of skin friction were not performed in either the wind tunnel or flight tests. Thus, the authors are unable to reach any definitive conclusions as to the effects of tunnel noise on the actual laminar skin friction per se.

The basic achievements of this study are summarized below.

1. The law-of-the-wall is a valid way to correlate Preston-tube data in the form of Eqn. (4) or Eqn. (23).
2. The effective height of a Preston tube is not fixed.. It varies with $U_\tau h/\nu_w$, M_∞, aspect ratio and the position of the probe with respect to the wall, Chapter II, p. 13.
3. Including a variable K_{eff} in the correlation substantially improves its accuracy, Chapter IV, p. 34.
4. Plotting K_{eff} vs. R_τ permits the detection of errors in the experimental data, Chapter IV, p. 34.
5. The wind-tunnel data can be used to correct errors in P_p measurements in the flight tests. A systematic correction procedure was developed and successfully applied to the flight data, Chapter IV, p. 41.
6. Preston-tube correlations for laminar, transitional and turbulent data were obtained both for the wind-tunnel and free-flight tests. The flight correlations, Eqns. (31), (53) and (55), are the first of their kind in

---

† This assumes that noise does not change the steady-state laminar skin friction in any significant amount.

the literature.

7. A semi-empirical method has been developed to define and calculate an effective Reynolds number which calibrates environmental effects on Preston-tube measurements in wind tunnels, Chapter III, p. 31.

8. A computational model for the transition zone can be devised using laminar and fully-developed turbulent calculations (or measurements) of C_f and transitional Preston-tube pressure measurements without the need for hot-wire measurements of the intermittency factor, γ, Chapter IV, p. 44.

9. The virtual origin of the turbulent boundary layer on the AEDC cone coincides with the onset of transition which is found to occur at the location of minimum P_p, viz., x_t, Chapter IV, p. 46.

10. Experimental Preston-tube pressure measurements appear to have smaller errors in the turbulent portion of the boundary layer than in the other two portions, compare Figs. 25 and 28.

11. The effective freestream unit Reynolds number distribution obtained from the analysis of laminar data is apparently correlated with noise data on the AEDC cone, Eqn. (32). Therefore, calibration of environmental effects in a wind tunnel can be done by calculating ΔR_{eff} using laminar measurements of Preston-tube pressure. Best results are obtained when the freestream flow conditions, M_∞, Re_m, and q_∞, are the same in the tunnel and in flight.

12. The analysis of transitional and turbulent Preston-tube data may not be used to calculate ΔR_{eff} since vorticity fluctuations in the boundary layer make it insensitive to background noise. The derived ΔR_{eff}'s from these data do not calibrate the tunnel's flow quality, but rather reflect the effect of internal vorticity fluctuations on P_p measurements, Chapter IV, p. 77.

13. Vorticity and pressure fluctuations in transitional boundary layer flow are larger in flight than in the 11-TWT for similar freestream conditions, Chapter IV, p. 91.

14. A traversing Preston tube is insufficient, by itself, to calibrate the effects of transonic wind-tunnel noise on skin-friction. The Preston-tube data must be supplemented with direct measurements of skin friction if this objective is to be achieved.

CHAPTER VI

RECOMMENDATIONS

The calibrating procedure described in this report may be used to calibrate environments in other transonic wind tunnels, especially those tunnels where the AEDC cone was tested.

The author recommends that skin friction be measured directly and used in conjunction with Preston-tubes in future wind tunnel and flight tests. This will permit the described calibration procedure to reveal the effects of noise, if any, on skin friction drag.

Care should be taken in measuring Preston-tube pressure in future experiments. Every effort to prevent probe twisting and lifting will reduce experimental errors especially in the flight tests. The gain factor and the reference pressure for the transducer should be accurately recorded.

REFERENCES

1. Dougherty, N. S., Jr. and Steinle, F. W., Jr., "Transition Reynolds Number Comparisons in Several Major Transonic Tunnels," AIAA Paper No. 74-627, July 1974.

2. Reed, T. D., Pope, T. C., and Cooksey, J. M., "Calibration of Transonic and Supersonic Wind Tunnels," NASA CR-2920, Nov. 1977.

3. Pope, A. and Harper, J. J, Low-Speed Wind Tunnel Testing, Wiley, 1966, Chapter 3.

4. Miller, D. G. and Bailey, A. B., "Sphere Drag at Mach Numbers from 0.3 to 2.0 at Reynolds Numbers Approaching 10^7", Journal of Fluid Mechanics, Vol. 93, 1979, pp. 449-464.

5. Treon, S. L., et al., "Further Correlation of Data from Investigation of a High-Subsonic-Speed Transport Aircraft Model in Three Major Transonic Wind Tunnels," AIAA Paper No. 71-291, March 1971.

6. Jones, B. M., "Flight Experiments on the Boundary Layer," First Wright Brothers' Lecture, Dec. 17, 1937, reprinted in Astronautics and Aeronautics, Feb. 1981, pp. 39-42, 75.

7. Dougherty, N. S., Jr. and Fisher, D. B., "Boundary Layer Transition on a 10-Degree Cone: Wind Tunnel/Flight Data Correlation," AIAA Paper No. 80-0154, Jan. 1980.

8. Reed, T. D. and A. Abu-Mostafa, "Study of Boundary-Layer Transition Using Transonic-Cone Preston Tube Data," Final Report, NASA/Ames Research Grant Number NSF-2396, July 1982.

9. Preston, J. H., "The Determination of Turbulent Skin Friction by Means of Pitot Tubes," Journal of Royal Aeronautical Society, Vol. 58, 1954, pp. 109-121.

10. Stephens, A. V. and Haslam, J. A. G., "Flight Experiments on Boundary Layer Transition in Relation to Profile Drag," Aeronautical Research Council, R & M No. 1800, Aug. 1938.

11. Patel, V. C., "Calibration of the Preston-Tube and Limitations on its Use in Pressure Gradients," Journal of Fluid Mechanics, Vol. 23, 1965, pp. 185-208.

12. Quarmby, A. and Das, H. K., "Measurement of Skin Friction Using a Rectangular Mouthed Preston Tube," Aeronautical Journal of the Royal Aeronautical Society, Vol. 73, 1969, pp. 288-330.

13. McMillan, F. A., "Experiments on Pitot Tubes in Shear Flow," Aeronautical Research Council, R & M No. 3028, 1957.

14. Allen, J. M., "Reevaluation for Compressible-Flow Preston Tube Calibrations," NASA TM X-3488, 1977.

15. Sommer, S. C. and Short B. J., "Free-Flight Measurements of Turbulent-Boundary-Layer Skin Friction in the Presence of Severe Aerodynamic Heating at Mach Numbers from 2.8 to 7.0," NACA TN 3391, 1955.

16. Allen, J. M., "Evaluation of Compressible-Flow Preston Tube Calibrations," NASA TN D-7190, 1973.

17. Allen, J. M., "Experimental Study of Error Sources in Skin-Friction Balance Measurements," ASME Journal of Fluids Engineering, March 1977, pp. 197-204, and NASA TN D-8291, October 1976.

18. Allen, J. M., "An Improved Sensing Element for Skin-Friction Balance Measurements," AIAA Journal, Vol. 18, No. 11, Nov. 1980, pp. 1342-1345.

19. Prozorov, A. G., "Determination of the Skin Friction in the Boundary Layer with a Small Pitot Probe," Fluid Mech. Soviet Research, Vol. 5, No. 6, 1976.

20. Wu, J-M and Lock, R. C., "A Theory for Subsonic and Transonic Flow Over a Cone - With and Without Small Yaw Angle," U.S. Army Missle Command, Redstone Arsenal, Alabama, Tech. Report RD-74-2, Dec. 1973.

21. Dhawan, S. and Narasimha, R., "Some Properties of Boundary Layer Flow During the Transition from Laminar to Turbulent Motion," Journal of Fluid Mechanics, Vol. 3, pp. 418-436, 1958.

22. Narasimha, R., "On the Distribution of the Intermittency in the Transition Region of a Boundary Layer," Journal of Aeronautical Science, Vol. 24, pp. 711-712, 1957.

23. Emmons, H. W., "The Laminar-Turbulent Transition in a Boundary Layer - Part I," Journal of Aeronautical Science, Vol. 18, pp. 490-498, 1951.

24. Whitfield, J. D. and Dougherty, N. S., "A Survey of Transition Research at AEDC," AGARD Conference Proceedings No. 224.

25. Mabey, D. G., "Boundary Layer Transition Measurements on the AEDC 10° Cone in Three RAE Wind Tunnels and Their Implications," Aeronautical Research Council, R & M No. 3821, June 1976.

26. Becker, H. A. and Brown, A. P. G., "Response of Pitot Probes in Turbulent Streams," Journal of Fluid Mechanics, Vol. 62, Part 1, pp. 85-114, 1974.

27. NASA/Ames 11-Ft Transonic Wind Tunnel Preston-Tube Measurements, NASA/Ames Research Center, Moffett Field, California, March 1975.

28. Crawford, M. E. and Kays, W. M., "STAN5 - A Program for Numerical Computation of Two-Dimensional Internal/External Boundary Layer Flows," Dept. of Mech. Eng., Stanford University, Stanford, California, Report No. HMT-23, Dec. 1975.

29. Abu-Mostafa, A. S., "Correlation of Theoretical Laminar Skin Friction with Preston-Tube Measurements on a Subsonic Cone," M.S. Report, School of Mech. and Aero. Eng., Oklahoma State University, May 1980. Also included in the Semiannual Progress Report, Jan.-June 1980, NASA/Ames Research Grant No. NSF-2396.

30. Steinle, F. W., Jr., Private Communication.

31. White, F. M., Viscous Fluid Flow, McGraw-Hill, 1974.

32. Tetervin, N., "A Transformation Between Axisymmetric and Two-Dimensional Turbulent Boundary Layers," AIAA Journal, May 1970, pp. 985-987.

33. Musker, A. J., "Explicit Expression for the Smooth Wall Velocity Distribution in a Turbulent Boundary Layer," AIAA Journal, Vol. 17, No. 6, pp. 655-657, 1979.

34. Weeks, D. J., and Hodges, J., "An Experimental Investigation Into the Influence of Acoustic Disturbances on the Development of a Turbulent Boundary Layer," R & M No. 3825, London, 1978.

35. Raghunathan, S., Coll, J. B., and Mabey, D. G., "Flat Plate Turbulent Boundary Layers Subject to Large Pressure Fluctuations," AIAA Journal, Vol. 17, No. 1, January 1979.